

SURFACE TILTS
FROM A MASSIVE HYDROFRACTURE
AND
FROM GROUNDWATER TRANSIENTS

by

Philip F. Johnston

CLOSED RESERVE

ARTHUR LAKES LIBRARY
COLORADO SCHOOL of MINES
GOLDEN, COLORADO 80401

ProQuest Number: 11016568

All rights reserved

INFORMATION TO ALL USERS

The quality of this reproduction is dependent upon the quality of the copy submitted.

In the unlikely event that the author did not send a complete manuscript and there are missing pages, these will be noted. Also, if material had to be removed, a note will indicate the deletion.



ProQuest 11016568

Published by ProQuest LLC (2019). Copyright of the Dissertation is held by the Author.

All rights reserved.

This work is protected against unauthorized copying under Title 17, United States Code
Microform Edition © ProQuest LLC.

ProQuest LLC.
789 East Eisenhower Parkway
P.O. Box 1346
Ann Arbor, MI 48106 – 1346

A thesis submitted to the Faculty and the Board of Trustees of the Colorado School of Mines in partial fulfillment of the requirements for the degree of Master of Science, Geophysics.

Signed: Philip F. Johnston
Philip F. Johnston

Golden, Colorado

Date: 7 May, 1979

Approved: Maurice W. Major
Maurice W. Major
Thesis Advisor

Golden, Colorado

Date: _____, 1979

Approved: George V. Keller
George V. Keller
Head of Department of Geophysics

Golden, Colorado

Date: _____, 1979

ABSTRACT

Stekettee's and Maruyama's works are followed in justifying the modelling of a hydrofracture as a dislocation in an elastic half space. Maruyama's expression for the vertical component of displacement at the earth's surface does not include the source dilatation term. Including this term and taking spatial derivatives gives expressions for surface tilt.

Maps generated from these expressions suggest that: 1) Tilts as large as 3.3×10^{-7} radians may result from a large (vol. = 10^3 m^3), shallow (depth = 1 km) hydrofracture; and 2) the shape of the tilt field strongly reflects the fracture orientation.

An attempt to determine fracture azimuth with tiltmeters was made at an Amoco well located in Sec. 20, T4N, R65W, Weld County Colorado, which was fractured on August 28, 1978. Four tiltmeters, each deployed approximately 400 m from the well, produced six tilt channels of records. One channel showed a tilt of 7×10^{-7} radians probably associated with the hydrofracture, on 5 channels the hydrofracture signal was hidden by noise in the period range 1 to 24 hours.

Tilts associated with the filling of an irrigation ditch located within 50 m of 2 sites introduced noise

episodes having amplitudes as great as 2×10^{-5} radians. A hydrologic equation was used to model these transient tilts in terms of the parameters A_{\max} , the maximum amplitude, t_o , the onset time, and a function which involves the aquifer properties permeability, void ratio, and height of water table. These three parameters can be determined graphically from the tilt data.

Experimental parameter analysis shows: 1) shallow vaults with foam insulation limit diurnal noise to 1μ radian, which could be further reduced by recording vault temperature to 0.1°C ; 2) more data could be recorded by implementing automatic instrument rezeroing, deploying more tiltmeters, and leveling of recorder boxes; 3) site specific noise arises from irrigation ditches within 100 m, vehicles within 25 m, and people within 5 m of the tiltmeters; and 4) better inductors and provision for internal inspection would simplify operation of the particular tiltmeters used.

TABLE OF CONTENTS

	page
ABSTRACT	iii
LIST OF ILLUSTRATIONS	vii
ACKNOWLEDGEMENTS	ix
INTRODUCTION	1
MODELLING OF SURFACE TILTS	6
The Hydrofracture Tilt Model	6
the hydrofracture geometry	7
mathematical treatment of a hydro-	
fracture dislocation	11
Surface Tilts from a Ditch Leaking Water	35
possible mechanisms	36
modelling the surface tilt	36
EXPERIMENTAL PARAMETERS	44
Introductory Discussion	44
Instrument Sites	46
site selection	46
site description	47
Tiltmeter Vaults	50
site preparation	50
instrument installation	52
Instrumentation	52
tiltmeters	52
thermometers	57
System Response and Operational Summary	59
DATA ANALYSIS	62
Field data	62
Rejection of Noisy Data	62
Improving Signal to Noise Ratio	72
discussion of noise	72
sites 2 and 4	72
sites 1 and 3	74
Results	87
SUGGESTIONS FOR FUTURE OPERATIONS	92

CONCLUSIONS	95
APPENDICIES	99
Surface Displacement Program	99
Surface Tilt Program	105
Fracturing program data	111
REFERENCES	119

LIST OF ILLUSTRATIONS

	Page
1-1 Probable hydrofracture geometry	9
1-2 Hydrofracture model	10
1-3 Physically acceptable and unacceptable dislocations	14
1-4 Double force at P giving displacement at Q	20
1-5 Point force combinations which describe a hydrofracture dislocation	22
1-6 Comparison of image force problem and $\frac{1}{2}$ space problem	25
1-7 Geometric representation at terms in Maruyamas' equation	27
1-8 Hypothetical hydrofracture tilt maps	32-34
1-9 Cross sectional view of an idealized leaky ditch	38
1-10 Family of hydraulic transient curves	41
2-1 Map showing location of study area	45
2-2 Map of study area showing site locations	48
2-3 Schematic cross section of a tiltmeter vault	51
2-4 Schematic diagram of a tiltmeter	54
2-5 Schematic diagram of tiltmeter calibration mechanism	56
2-6 Sample calibration	58
2-7 Operational summary chart	61
3-1 Field data 26-27 Aug.	63

	page
3-2	Field data 28-29 Aug. 64
3-3	Field data 30-31 Aug. 65
3-4	Field data 1-2 Sept. 66
3-5	Field data 3-4 Sept. 67
3-6	Channel 2 data - diurnal signal removed 75
3-7	Channel 4 data - diurnal signal removed 76
3-8	Channel 1 data - diurnal signal removed 78
3-9	Channel 3 data - diurnal signal removed 79
3-10	Graphic determination of A_{\max} 81-83
3-11	Graphic determination of $x/\sqrt{4\alpha t}$ 84-86
3-12	Residual curves, channels 1 and 3 88
3-13	Collection of tilt traces during pumping interval 89
3-14	Channel 4N and fracture volume during pumping interval. 90

ACKNOWLEDGEMENTS

I would like to thank the members of my committee, Dr. Major, Dr. White, and Dr. Yeatts, for the many hours which they invested in advising this work. I would particularly like to thank Dr. Major for the enormous amount of time which he unselfishly contributed to this project. His active participation in all phases of this project, from the initial feasibility study and instrument modification to the field exercise and the reduction and interpretation of the data, is sincerely appreciated. Without his contribution this project could never have been completed. I would also like to thank Dr. Yeatts for patiently guiding me to an understanding of dislocation theory, a substantial chore since I started with no exposure at all to this subject.

I am grateful for the financial assistance in the form of a research assistantship which was provided my first year by the Geophysics Department and my second year by the sponsors of the Integrated Geophysics Project. Dr. Kim and Mr. Christianson of the Amoco Production Company provided critical information and assistance which made the field exercise possible.

Further, I am indebted to Neal Fausset for the time he contributed to modifying the tiltmeters, to Tom

Guttinger for his role in preparing and carrying out the field experiment, and particularly to John Graves, whose help modifying the tiltmeters, reducing the data and carefully reading parts of this work was invaluable.

INTRODUCTION

No method has yet been developed for adequately determining the azimuth of a massive hydrofracture. This is despite an interest which has been sufficient to prompt workers to investigate the applicability of several geophysical methods to this problem. It has been suggested by Wood (1976) that a massive hydrofracture might set up a measurable tilting of the earth's surface, and further, that by measuring this tilting, the orientation of the hydrofracture might be determined.

This work is in part an attempt to determine the orientation of a massive hydrofracture, via a modelling study and a field experiment. Additionally, this work includes a study of surface tilting caused by leakage from an irrigation ditch. Addressing this second subject became necessary when ditch tilts interfered with the tilt caused by the hydrofracture, the target signal in the field experiment. Since the technique developed for treating ditch tilts may have application beyond its use in this hydrofracture experiment, it is discussed with the hydrofracture tilt modelling technique in a chapter devoted to the modelling of surface tilts caused by these two sources.

The hydrofracture modelling is done according to a scheme developed by Volterra for determining how much an

arbitrary point P in an elastic body is displaced, following a dislocation on some surface within that body. In the case of a hydrofracture, the two sides of the induced fracture surface are "dislocated" as fluid is injected, causing displacement of the surface of the earth.

Volterra's method has seen considerable application in geophysics, primarily in modelling earthquake faulting, and as a result, the equations which describe the surface displacements of an idealized earth due to various types of dislocations are available in the literature. Maruyama (1965) gives a particularly complete listing of these equations, including the equation which treats the dislocation appropriate for modelling a hydrofracture.

In this study, Maruyama's equation was used to generate maps of the displacement fields set up by hypothetical hydrofractures having various dimensions. Surprising results led to an examination of the development of this equation, and it was found that a term had been dropped in its derivation. After including this term, spatial derivatives of the displacement equation were taken to obtain tilt equations, which were then used to generate tilt maps. Examination of these tilt maps showed that for a hydrofracture at a depth of 1000 m having a volume of 10^3 m^3 , tilt values as large as 0.3μ Radians should result. These results suggested that a field exercise might be fruitful,

provided the hydrofracture chosen for study were both large and shallow by present industry standards.

During August and September of 1978 a field experiment was carried out, in which four two-component tiltmeters were deployed at distances of approximately 400 m from an Amoco Production Company well. This well underwent a fracture treatment on the 28th of August, and records were collected for a total of 10 days, both before, during, and after the fracture day.

This field experiment was far from trouble free, as might be expected, since it involved deploying recently modified tiltmeters in a new location. The problems encountered were of two types; equipment shortcomings and high noise levels. From what was learned in the course of this experiment, a number of suggestions are made for minimizing these problems in future field experiments.

One of the most serious sources of noise in this exercise was surface tilting associated with the flooding of a previously dry irrigation ditch, which passed near two of the 4 sites. Since this event occurred at the same time as the pumping, and had an amplitude approximately 50 times the anticipated hydrofracture signal, it was necessary to carefully approximate and remove the source of noise before the signal could be estimated. Assuming that surface

tilting due to the ditch filling is proportional to the tilt of the groundwater table allows a hydrologic equation to be used in approximating this tilt. The equation, developed by Glover (1974), expresses groundwater table tilt in terms of several hydrologic parameters. By approximating these parameters from the field records, the ditch tilt can be approximately removed from the data.

After also approximating the diurnal signal on each channel and removing this approximate signal from the data, values can be chosen for the tilt or for the upper limit of tilt at each site. The best determined tilt value is 0.7μ Radians of North down tilt at site 4, the most noise free site in the experiment.

Comparing the magnitude of this tilt to the hypothetical tilt maps which were generated suggests that the actual tilts from a hydrofracture are at least as large, and possibly larger than the modelled tilts. Also, this experiment indicates that under favorable field conditions these tilts are measurable. Since field conditions were far from ideal at several of the sites occupied in this experiment, the orientation of the hydrofracture cannot be determined, although certain orientations can be dismissed as unlikely, based on the data which was collected. The prospect of improving the field experiment to the point

that enough tilt values can be determined to fix the orientation of the hydrofracture seems good enough to warrant another field effort.

MODELLING OF SURFACE TILTS

In this chapter, methods are developed for modelling tilting of the earth's surface caused by two sources: 1) a hydrofracture, and 2) a linear ditch leaking water into an aquifer. The hydrofracture tilt model is discussed first in section A, the ditch tilt model is discussed in section B.

In the following section, a review of the contributions made by many workers to the field of modelling dislocations is undertaken. This is not intended to be a claim to originality, but rather is intended to demonstrate the applicability of the method to the problem of modelling a hydrofracture. Hopefully this approach will reveal the important assumptions made in arriving at the final equations, and will show the nature of a minor correction which was made to an expression presented by Maruyama.

A.) HYDROFRACTURE MODEL

The theory of elasticity provides equations for calculating the displacement, stress, strain, and rotation fields in an elastic body which are caused by a dislocation on some surface within that body. By considering a hydrofracture to be a dislocation on some surface within the earth, these equations can be used to calculate the

displacement and tilt fields resulting from the hydrofracture. In order to express the equations for these fields in a tractable form, however, a model of the hydrofracture geometry must be found which strikes an acceptable compromise between being geologically accurate and having a simple mathematical description.

1.) The Hydrofracture Geometry

Several pieces of information suggest that a hydraulically induced fracture will follow a vertically oriented plane. Hubbert (1957) indicates that fractures created in an isotropic medium by the injection of pressurized fluids should be approximately perpendicular to the least principal stress axis. In tectonically relaxed areas, the greatest principal stress in the earth's crust is vertical, which restricts the orientation of the least principal stress axis to the horizontal plane. This implies the fracture should be vertical. Further, since it is unlikely that the stress state of the earth's crust will vary appreciably in the small volume of crust which contains a hydrofracture, the orientation of the least principal stress axis should be relatively constant, and the strike of the fracture should in turn be nearly constant, giving a vertical planar surface.

Experimental evidence also supports the model of a vertical planar fracture. Several researchers from Sandia

Laboratories created a small scale hydrofracture in a uniform ash-tuff in order to study fracture geometry (Tyler and Vollendorf, 1975). The fracture was propped open with a colored grout, so it could be easily traced, and the fracture was mapped by mining it out. The results of mapping two separate hydrofractures showed fracturing to be nearly vertical and nearly planar in each case.

A diagram of the probable hydrofracture geometry is shown in figure 1-1. Figure 1-2 is a diagram of the hydrofracture model chosen to approximate this geometry. In this model, the fracture is assumed to lie along a vertically oriented planar surface, the edges of which are vertical and horizontal, forming a rectangular surface. As fluid is injected during the fracturing operation, the two sides of the fracture are pried apart, and sand is transported into the fracture to prop it open. This results in the sides of the fracture being displaced, or dislocated, from one another by some distance, shown as Δx in figure 1-2. For simplicity we assume that Δx is constant over the entire fracture area. The dimensions L , W , and Δx are chosen such that the volume of the rectangular slab used in the hydrofracture model approximates the volume of fluid injected in the actual hydrofracture.

Having now arrived at a model for the geometry of a hydrofracture, equations can be used to generate maps of

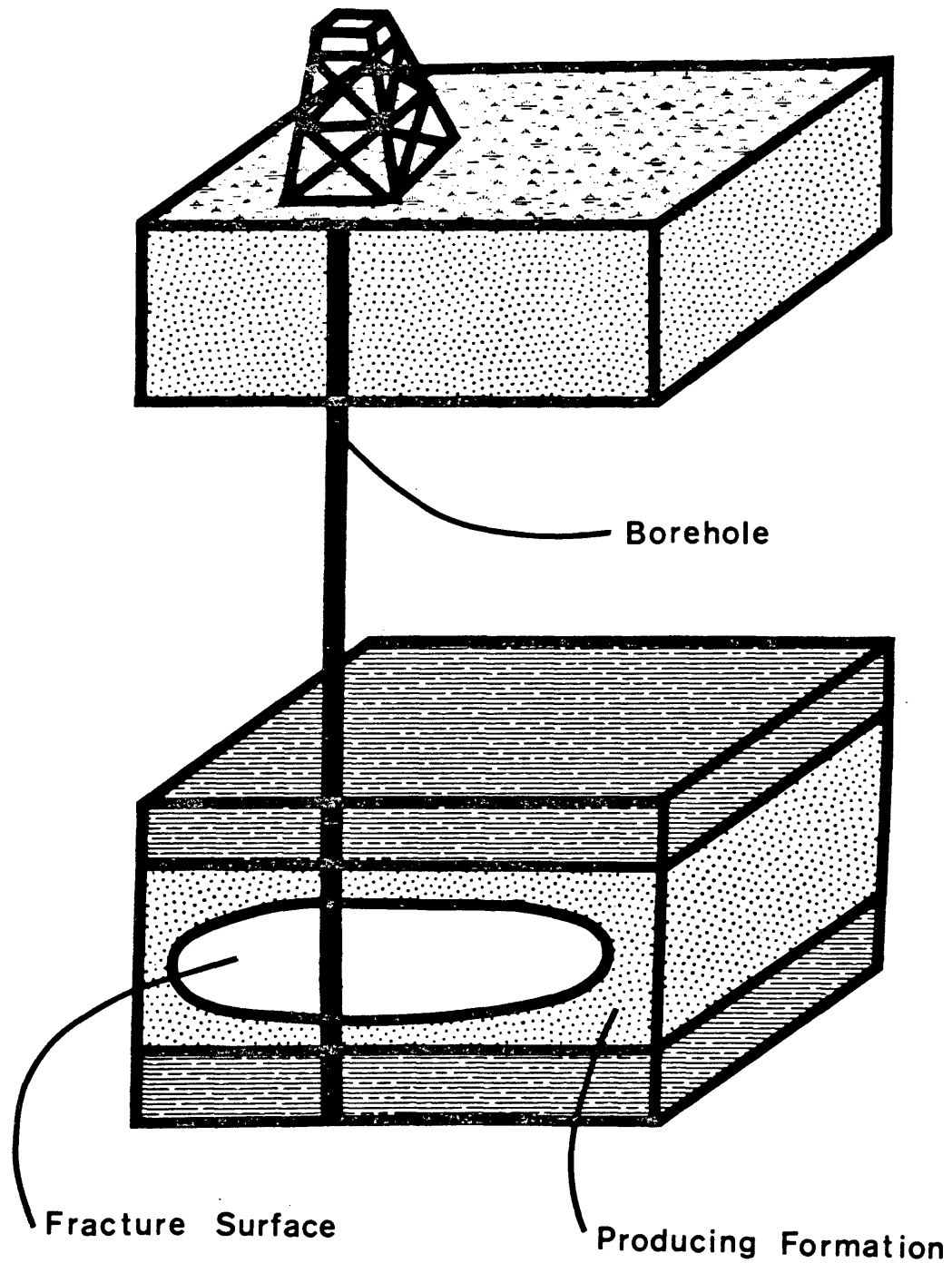


Figure 1-1

The probable hydrofracture geometry, idealized and shown in cross section. The cross section is taken in such a way that it includes the fracture surface (after Shuck, 1974).

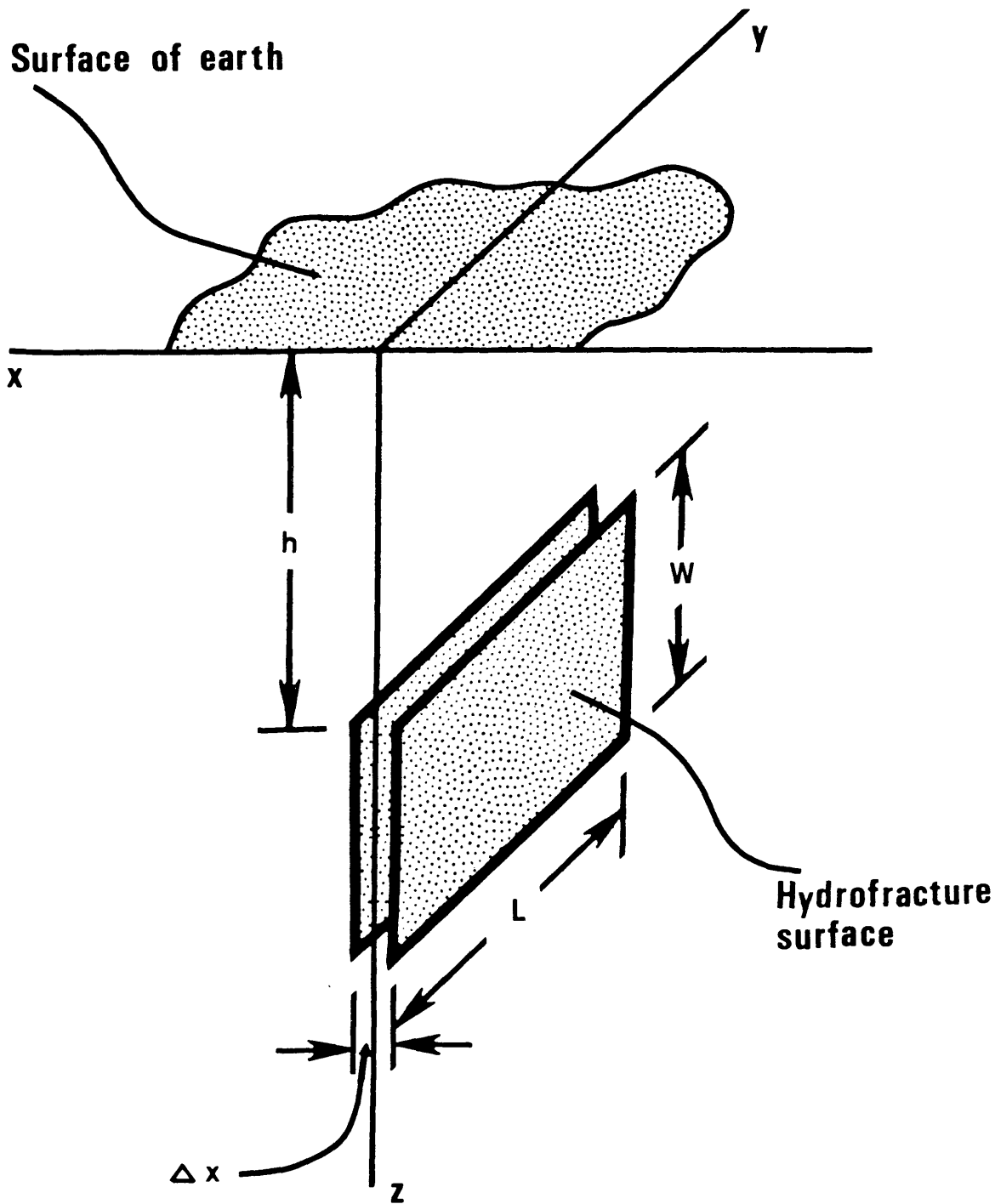


Figure 1-2

The geometry of the model used to represent the hydrofracture.

the displacement and tilt fields at the surface of the earth which should result from a hydrofracture having this assumed geometry.

2.) Mathematical Treatment of a Hydrofracture Dislocation

a.) Development of Volterra's Equation

Following work done by Volterra, Stekettee and others, Maruyama (1964) has developed equations which can be used directly to calculate the displacement field at the earth's surface due to a dislocation having the geometry shown in figure 1-2. For the purpose of relating the physics of the problem to the equations which will be used for numerical calculations, a brief review of the contributions made by various workers in developing these equations seems appropriate.

Volterra was able to develop an equation which gives the displacement at some point in a medium resulting from a dislocation on some surface in that medium. Volterra's equation is a general one: it applies to any medium geometry, any dislocation surface geometry, and yields the displacement at any point in the medium.

Volterra's equation is developed from Betti's reciprocal theorem, so we are adopting any assumptions made in arriving at this theorem. Betti assumes in his derivation

that the superposition principle holds, which means a body subject to two sets of forces and stresses, F_1, τ_1 , and F_2, τ_2 , will be deformed into a shape which does not depend on the order in which the two sets are applied. This assumption is valid provided that the strains in the body are infinitesimal.

By making the assumptions that no stresses act on the free surface and that there are no body forces, Volterra's equation can be gotten from Betti's theorem. Volterra's equation is given below, after Maruyama (eq. 1.1).

$$U_m(Q) = \int_{\Sigma} \Delta U_k(P) T_{kl}^m(P,Q) \gamma_l(P) d\Sigma \quad (1.1)$$

where summation over the three spatial dimensions is implied by repeated indices.

b.) Physical Meaning of Terms in Volterra's Equation

Volterra has expressed the desired quantity, the m th component of displacement at point Q , $U_m(Q)$, in terms of $\Delta U_k(P)$, $T_{kl}^m(P,Q)$, $\gamma_l(P)$ and Σ . In this equation P represents a point on the dislocation surface and Q represents a point elsewhere in or on the body at which the displacement is desired. $\Delta U_k(P)$ is the amount of dislocation in the k direction which exists between the two side of the

dislocation surface at point P. Σ is the dislocation surface, and $d\Sigma$ is the infinitesimal element of that surface located at point P. $\gamma_1(P)$ is a unit normal vector, giving the direction cosines between the dislocation surface normal and the coordinate axes l at point P. The remaining term in equation 1.1, $T_{k1}^m(P,Q)$, is the k - l component of the stress tensor which is set up at point P by the application of a unit point force in the m direction at point Q.

In order to get numerical results for $U_m(Q)$, expressions for $\Delta U_k(P)$, $\gamma_1(P)$, Σ , and $T_{k1}^m(P,Q)$ which are appropriate for the model shown in figure 1-2 must be substituted into equation 1.1. The expressions for these terms are arrived at in the next section.

c.) Specialization of Volterra's Equation to Hydrofracture Geometry

Each element of equation 1.1 is treated separately, in the order $\Delta U_k(P)$, $\gamma_1(P)$, Σ , and $T_{k1}^m(P,Q)$.

$$\underline{\Delta U_k(P)}:$$

Volterra's equation (1.1) is an integral equation for displacement U_m ; the displacement appears both inside the integral and as the left side of the equation. Solving this equation is difficult, and not all displacement functions are acceptable solutions. Figure 1-3 shows a

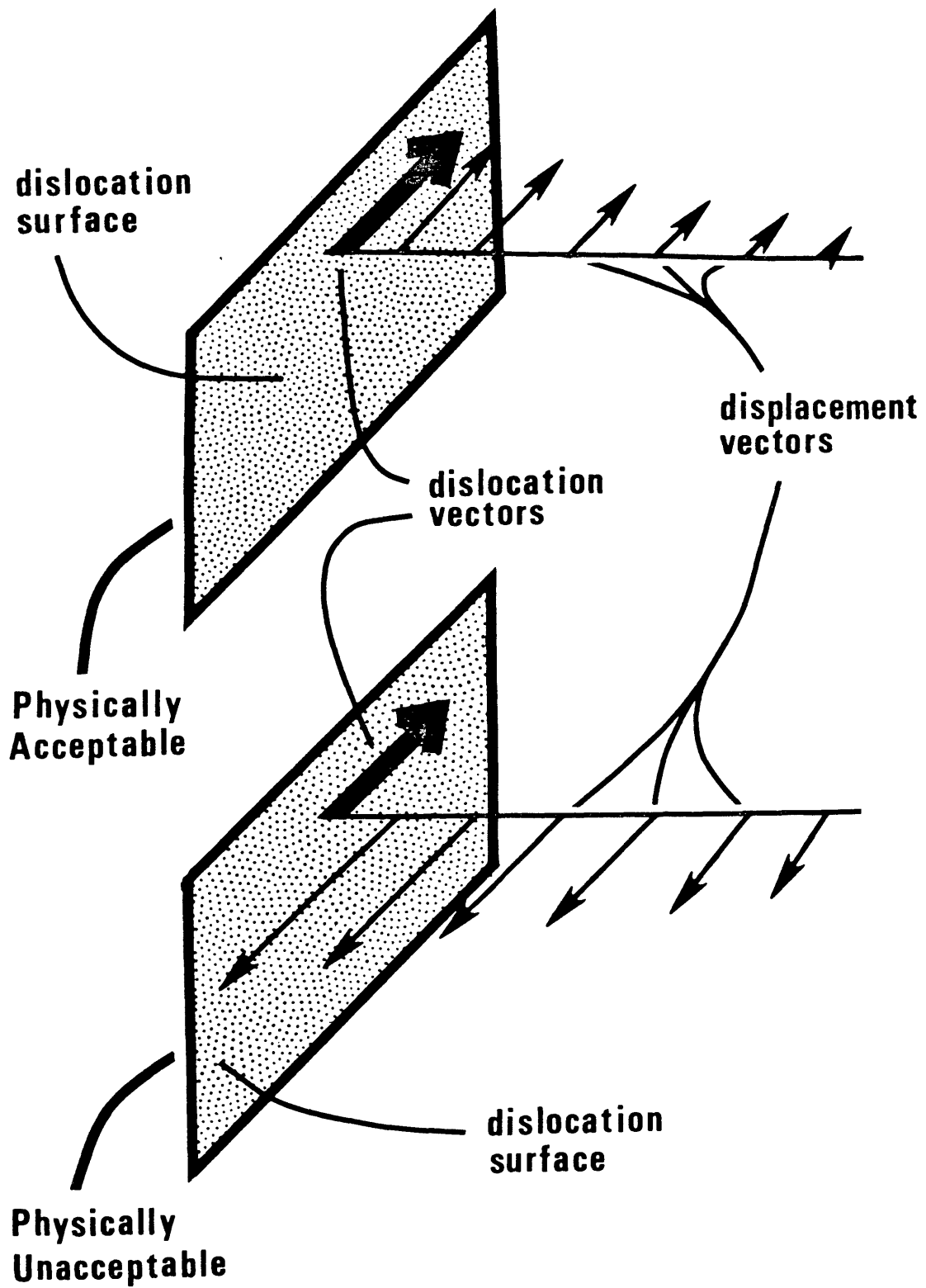


Figure 1-3

The displacement vector at a field point must approach the dislocation vector at a source point as the field point approaches the source point.

dislocation function which satisfies the integral equation and another dislocation which does not. Weingarten was able to show that by choosing the correct type of dislocation, Volterra's equation reduces from an integral equation to a simpler integration problem. The Weingarten relation, given by Stekette (1958), requires that the two dislocation surfaces move with respect to one another as if they were rigid bodies. Since the motion of two originally coincident planes directly away from one another is of this type, the hydrofracture dislocation model shown in figure 1-2 does satisfy the Weingarten relation. This type of dislocation leads to singularities in stress and strain at the edges of the dislocation surface, however. Physically this is unreal, but considering the mathematical simplification it yields, it is a good approximation. From figure 1-2 then, ΔU_k for the hydrofracture is given by equation 1.2 below.

$$\Delta U_1(P) = \Delta x \quad (1.2)$$

$$\Delta U_2(P) = 0$$

$$\Delta U_3(P) = 0 \quad \text{for all points } P.$$

$$\underline{\gamma_1(P)}:$$

Since 1 is a repeated index in equation 1.1, it is summed from 1 to 3. γ_1 is the cosine of the angle between

the hydrofracture surface normal and the x_1 axis. Since the surface is normal to this axis, $\gamma_1 = 1$ (see fig. 1-2). The other axes are perpendicular to the surface normal, so $\gamma_2 = \gamma_3 = 0$.

Σ :

Σ , the dislocation surface, is a vertically oriented rectangular surface of dimensions L and W , located a distance h below the earth's surface, as shown in figure 1-2. Σ is normal to the x axis.

$T_{kl}^m(P,Q)$:

Finding an expression for $T_{kl}^m(P,Q)$ is the most difficult step in solving Volterra's equation, and the solutions given by Maruyama and others rest on certain simplifying assumptions. For most geophysical problems, including this one, it is assumed that the medium is homogeneous, isotropic, and described by Lamé' coefficients λ and μ .

The first step in finding an expression for $T_{kl}^m(P,Q)$, the stress at point P due to a unit force at point Q , is to find an expression for the displacement at point P which results from a force at point Q . In a homogeneous isotropic whole space, the Somigliana tensor is just such an expression, giving the k th component of displacement at

point P due to the mth component of force at point Q. The Somigliana tensor, S_{ij} , is given in equation 1.3 below.

$$U_k^m(P,Q) = S_{km} = \frac{F}{8\pi\mu} (\delta_{km} r_{,nn} - \alpha r_{,mk}) \quad (1.3)$$

$$\alpha = \frac{\lambda + \mu}{\lambda + 2\mu},$$

r is a vector from point P to point Q

where repeated indicies imply summation over the spatial dimensions, as before, and indicies following a comma indicate differentiation with respect to that spatial variable.

The fact that this is the expression for displacement in a whole space and we desire the solution of equation 1.1 in a half space is not a problem, as will become evident later.

By using the appropriate Somigliana tensor components as expressions for both the k and the l components of displacement due to the mth component of force, and by differentiating these expressions, we obtain the k-l component of strain at P due to the force at Q. Again following Maruyama's notation,

$$e_{kl}^m(P,Q) = \frac{1}{2}(U_k^m(P,Q)_{,l} + U_l^m(P,Q)_{,k}) \quad (1.4)$$

where $e_{kl}^m(P,Q)$ is the kl component of strain at P due to a unit force in the m direction at Q , and $U_k^m(P,Q)_{,1}$ is the derivative with respect to x_1 of the k component of displacement at P due to a unit force in the m direction at Q .

By assuming that the medium exhibits Hookean behavior, we can use the Lamé coefficients of the medium to express the desired stresses in terms of the above strains. Doing so yields equation 1.5, below.

$$T_{kl}^m(P,Q) = \lambda \delta_{kl} e_{nn}^m(P,Q) + 2\mu e_{kl}^m(P,Q) \quad (1.5)$$

As before, repeated indicies indicate summation. This expression for $T_{kl}^m(P,Q)$ is in terms of the elastic moduli of the medium and the coordinates of the points P and Q only. Equation 1.5 is a Green's function, and consequently, certain symmetries exist among its subscripts. As a result of the symmetries, it can be shown (Stekettee, 1958) that $T_{kl}^m(P,Q)$ correctly describes two different physical situations which turn out to be mathematically equivalent. $T_{kl}^m(P,Q)$ can represent the stress at P due to a force at Q , which is the case introduced into Betti's theorem, or $T_{kl}^m(P,Q)$ can represent the displacement at point Q which results from a combination of forces acting at point P . The latter interpretation seems to be physically more relevant, since it involves force combinations

acting at the dislocation causing displacements elsewhere in the body.

The type of force combination which acts at each source point P depends on the type of dislocation being modelled. In order to find what kind of force combination represents the dislocation shown in figure 2, equations 1.4 and 1.5 can be combined to give equation 1.6

$$T_{kl}^m(P,Q) = \lambda \delta_{kl} U_{n,n}^m + \mu (U_{k,l}^m + U_{l,k}^m) \quad (1.6)$$

in which $U_{k,l}^m$ is the l-derivative of the k-m component of the Somigliana tensor with respect to x_l . Maruyama (1964) shows that a spatial derivative of the Somigliana tensor can be thought of as an expression for the displacement at Q due to a double force applied at P. Specifically,

$$U_{k,l}^m(P,Q) = \lim_{\Delta x_l \rightarrow 0} \frac{U_k^m(P + \Delta x_l, Q) - U_k^m(P - \Delta x_l, Q)}{2\Delta x_l} \quad (1.7)$$

Where $U_k^m(P + \Delta x_l, Q)$ and $-U_k^m(P - \Delta x_l, Q)$ each represent the displacement at Q from one force removed from P by either + or - Δx_l . This situation is shown in figure 1-4.

Equation 1.6 can now be used to show what combination of point forces corresponds to a dislocation of the type

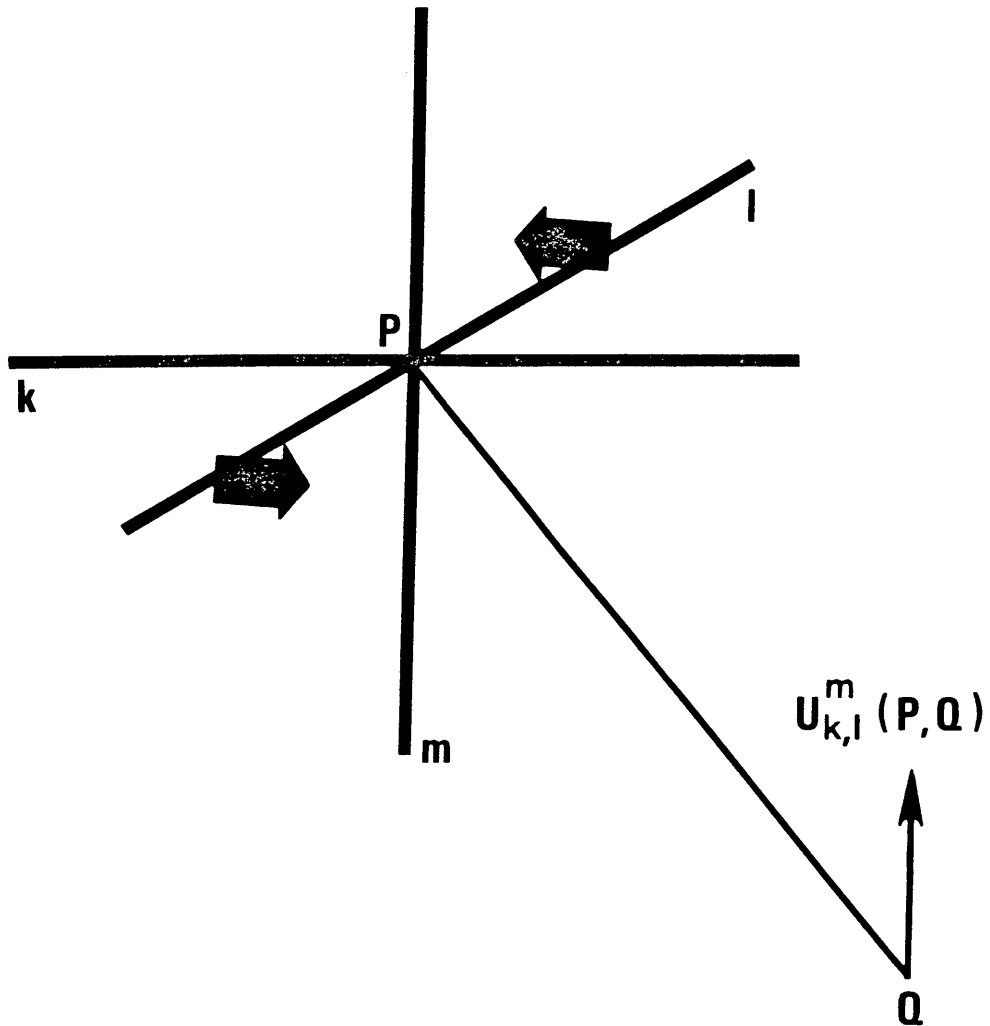


Figure 1-4

A double force at the source point P results in a displacement $u_{k,l}^m$ at the field point Q .

used in modelling a hydrofracture. Substituting the desired 1,1,3 for k,l,m gives

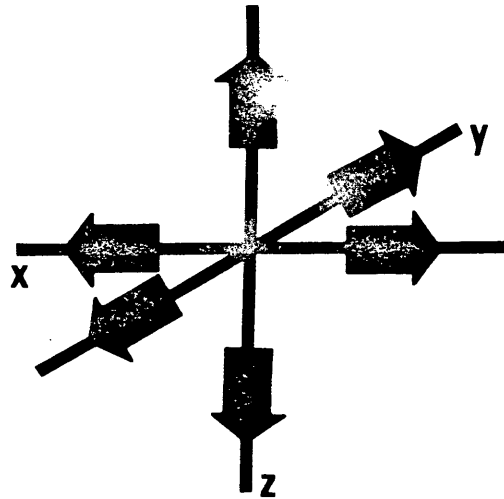
$$T_{11}^3(P,Q) = \lambda \underbrace{(U_{1,1}^3 + U_{2,2}^3 + U_{3,3}^3)}_a + 2\mu \underbrace{U_{1,1}^3}_b \quad (1.8)$$

Referring to figure 1-4, we can see that $T_{11}^3(P,Q)$ gives the displacement at Q due to the two sets of point forces shown as a and b in figure 1-5, and which correspond to the Somigliana tensor derivatives labeled a and b in equation 1.8.

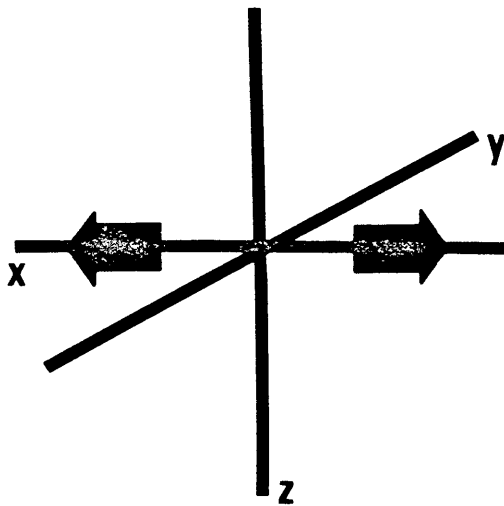
The set of forces shown in figure 5a is called a center of dilatation, and gives the response due to the volume change associated with the hydrofracture. The pair of forces shown in figure 5b is called a double force without moment, and gives the response due to the dislocation of the two surfaces.

d.) Half-Space Solution

Since the displacement due to a point force is not the same in a half space as in a whole space, it would seem that a new, more complicated expression for displacement, equivalent to equation 1.2 but valid in the half space, must be developed. This expression could then be used to solve for the appropriate $T_{kl}^m(P,Q)$ for the half



a.) Center of Dilatation



b.) Double Force Without Moment

Figure 1-5

These two point force combinations represent a dislocation of the type used to model a hydrofracture.

space. In order to find such an expression, workers have introduced a modified image method, which has a known solution. This method, as discussed by Stekettee and Maruyama, involves working the problem with the whole space expressions, and examining the boundary values. If they do not match the boundary values required for the half space problem, forces are added to the whole space problem as necessary to make the boundary values correct. When the boundary conditions are met, the solution of the image force problem in the whole space is identical to the solution of the half space problem involving the original forces.

The boundary conditions for the half space are as follows: 1) All stresses vanish on the free surface $x_3 = 0$, and 2) the stresses and displacements are differentiable everywhere, and vanish at infinity. Examination of the contribution to the stresses at $x_3 = 0$ made by the force combination which acts at one source point $P(x_1, x_2, x_3)$, on the dislocation surface in the whole space shows that the stresses $\tau_{31}(x_3 = 0)$, $\tau_{32}(x_3 = 0)$, and $\tau_{33}(x_3 = 0)$ are in general non-zero. Symmetry in the stress expression (obtained by taking spatial derivatives of equation 1.8 and substituting into Hooke's law) is helpful, however. As a result of the symmetry, an image force combination at a position $P'(x_1, x_2, -x_3)$, (the image

point of P with respect to the plane $x_3 = 0$), will cause the tangential stress components to vanish for all points on the $x_3 = 0$ plane, and will cause the normal component of stress to be doubled. By adding a third set of forces, a distribution of forces acting normally on the free surface, we can exactly cancel the normal stress caused by the original and image force combinations, producing a stress free surface $x_3 = 0$. The methods for finding the fields due to a distributed normal load are well known (Love, 1944). Figure 1-6 compares the image force whole space problem to the actual half space problem, for one source point on the dislocation surface.

Maruyama has solved for the various half space equivalents of $T_{kl}^m(P,Q)$ by carrying the necessary mathematics through the steps which have been outlined above. As Maruyama develops this half space solution, he changes the variable $T_{kl}^m(P,Q)$, which is used to represent the displacement at Q due to the force combination of P in the whole space, to $W_{kl}^m(P,Q)$, which represents the half space displacement. At the free surface $x_3 = 0$, these expressions take a particularly simple form, and $W_{11}^3(P,Q)_{x_3=0}$, the solution which is appropriate for the hydrofracture model, is written below (from Maruyama).

$$W_{11}^3(P,Q)_{x_3=0} = \frac{1}{4\pi} \frac{1}{r^2} \left[B + \frac{x_1^2}{r^2} E \right] \quad (1.9)$$

HALF SPACE PROBLEM

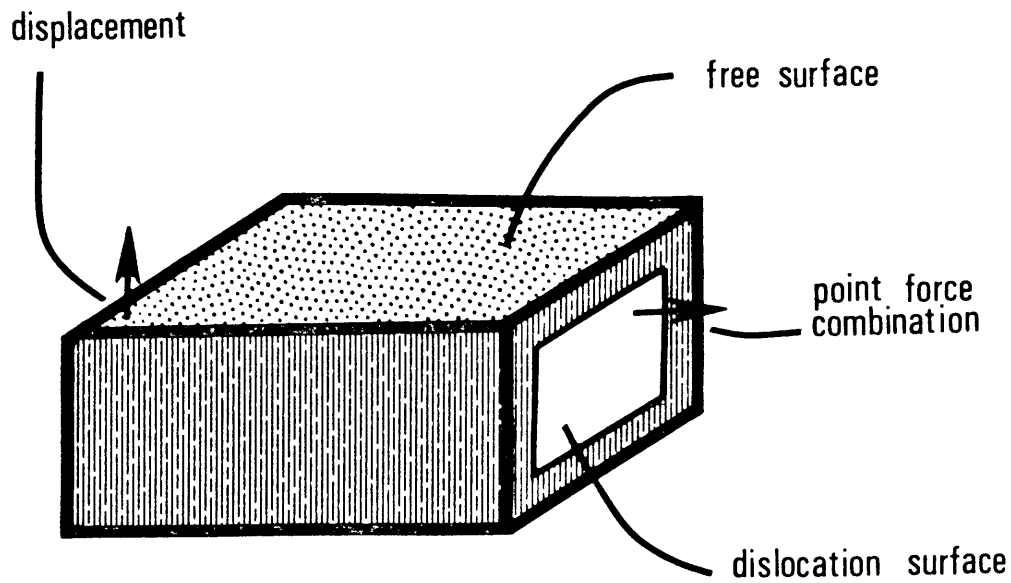


IMAGE FORCE SOLUTION

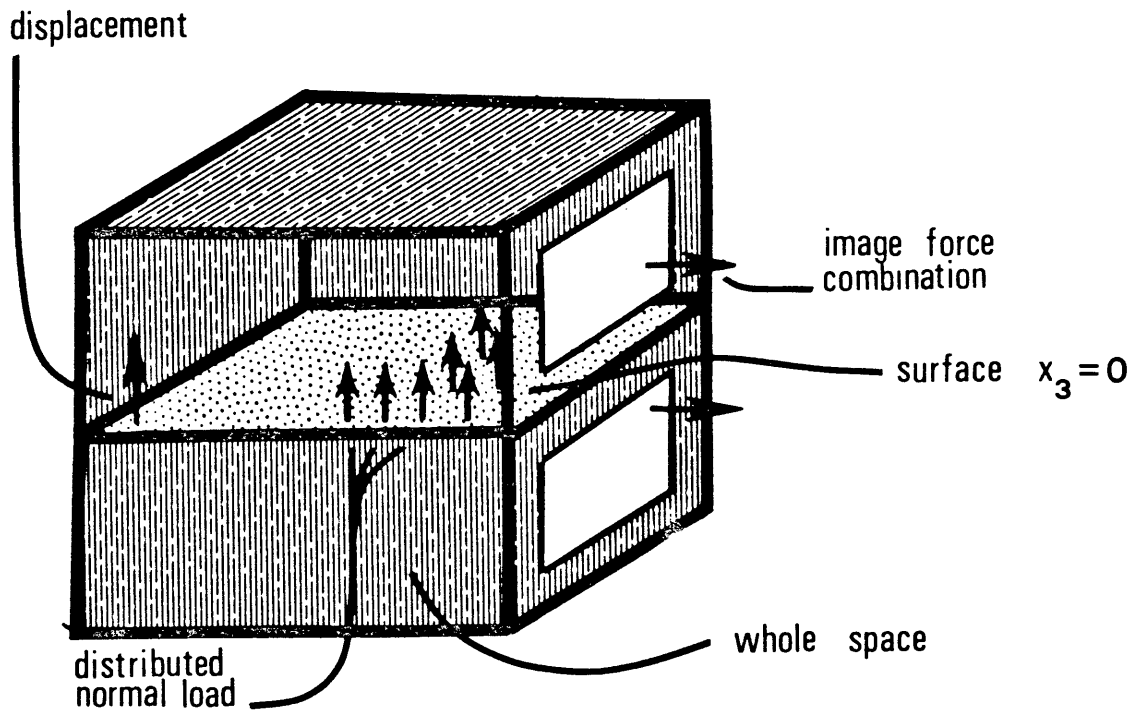


Figure 1-6

The half space problem for which a solution is desired is shown above, the technique for obtaining a solution is shown below. (In the lower figure, two faces are transparent to show the surface $x_3 = 0$).

with

$$B = -1 + 2 \zeta - \zeta^3,$$

$$E = 2 - 9 \zeta + 13 \zeta^3 - 6 \zeta^5,$$

$$\zeta = \xi_3 / \rho$$

$$\rho = (x_1^2 + x_2^2 + \xi_3^2)^{1/2}, \text{ and}$$

$$r = (x_1^2 + x_2^2)^{1/2}.$$

The variable used in this expression are labelled in figure 1-7.

It can be shown by differentiation of equation B-1 from Mindlin and Cheng's (1950) paper, or more easily, by differentiation of equation 32 from Yeatts (1973) paper, that Maruyama's expression for $W_{11}^3(P,Q)_{x_3=0}$, equation 1.9 above, does not include the dilatation term shown in figure 1-5. After modifying his equation to include this term, the correct expression for W_{11}^3 is obtained, given by equation 1.10 below.

$$W_{11}^3 = \frac{1}{4\pi} \frac{1}{r^2} \left[B + \frac{x_1^2}{r^2} E \right] \quad (1.10)$$

$$B = -\zeta(\zeta^{-1} + 1)^{-1}$$

$$E = 2 - 9 \zeta + 13 \zeta^3 - 6 \zeta^5$$

ζ defined as before

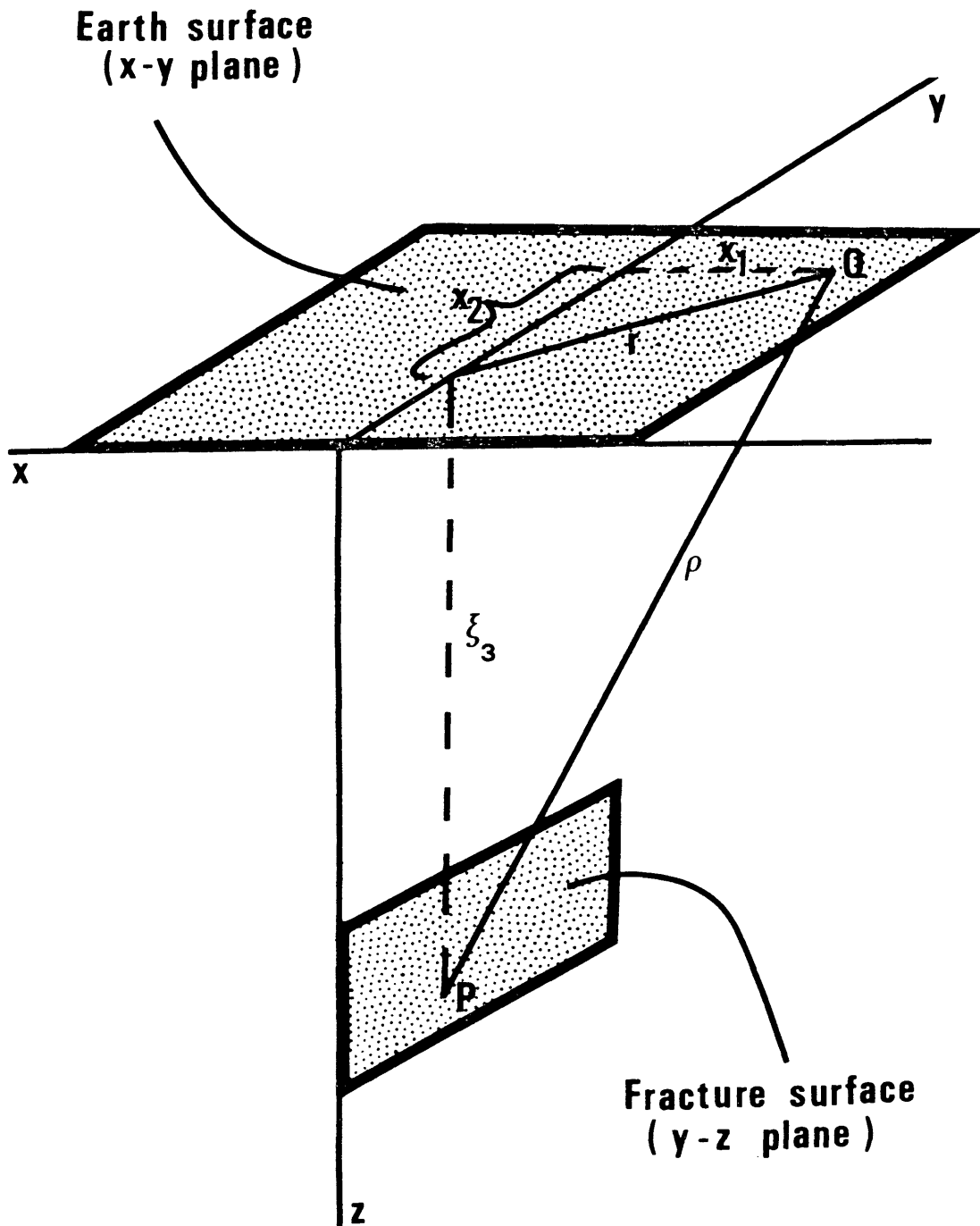


Figure 1-7

This shows the relation of the variables used by Maruyama to the hydrofracture geometry (After Maruyama, 1964).

Equation 1.10 can now be substituted into equation 1.1, along with the previously determined $v_1(P)$ and $\Delta U_k(P)$, giving

$$U_3(Q) = \int_{\Sigma} \Delta x \ W_{11}^3(P,Q) \ d\Sigma. \quad (1.11)$$

This expression can now be numerically integrated over the dislocation surface to give the displacement at one field point Q, caused by the entire dislocation. This procedure can then be repeated for many field points Q, resulting in a map of the sampled displacement field.

Obviously, the generation of such a map involves so many computations that a computer program is necessary. Dr. F.R. Yeatts (of the Colorado School of Mines Physics Department) has written a program to generate surface displacement maps for model earthquake dislocations, a problem which differs from that of generating hydrofracture displacement maps only in that the $W_{k1}^3(P,Q)$ of equation 1.11 are not the same for the two types of dislocations. By substituting $W_{11}^3(P,Q)$ into this program, we obtain the desired tool for making maps of the surface displacement to be expected from a hydrofracture with the geometry of figure 1-2. Dr. Yeatts was kind enough to provide a copy of his program for this purpose, as well as instruction for the proper modification and for the use of

this program. A copy of this modified program, which has been documented, is given in appendix 1. Instructions for the use of this program are also given in appendix 1.

Equation 1.10 may alternatively be written in the form

$$W_{11}^3 = \left(\frac{2G}{U}\right)^2 \left[-AB + \left(\frac{x_1}{U}\right)^2 A^3 - AB^2 - 6A^5 \right]. \quad (1.12)$$

This is a more efficient form for computational purposes, and is the form used in the displacement program.

e.) The Rotation Field

The expression for the rotation field in an elastic body is

$$\omega_{ij} = 1/2 (U_{i,j} - U_{j,i}) \quad (1.13)$$

This expression can be simplified at the free surface $x_3 = 0$, since the stress must vanish at the free surface, that is,

$$\tau_{ij} = \lambda \delta_{ij} \theta + \mu (U_{i,j} + U_{j,i}) = 0. \quad (1.14)$$

For $i \neq j$, this implies $U_{i,j} = -U_{j,i}$. Substituting this result into equation 1.13 yields

$$\omega_{ij} (x_3=0) = U_{i,j}. \quad (1.15)$$

This expression can be used to calculate the rotation at a field point Q caused by the hydrofracture dislocation. The rotation about the x_2 axis at point Q caused by the force combination at point P is simply the derivative of W_{11}^3 with respect to x_1 , since W_{11}^3 is the only element of equation 1.11 which contains the variable x_1 . Integrating $W_{11}^3(P,Q)_{,1}$ over the dislocation surface gives the total rotation at Q due to the dislocation, just as the integration of W_{11}^3 over Σ yielded the total displacement. Similarly, the rotation about the x_1 axis at Q is the derivative of W_{11}^3 with respect to x_2 , integrated over Σ .

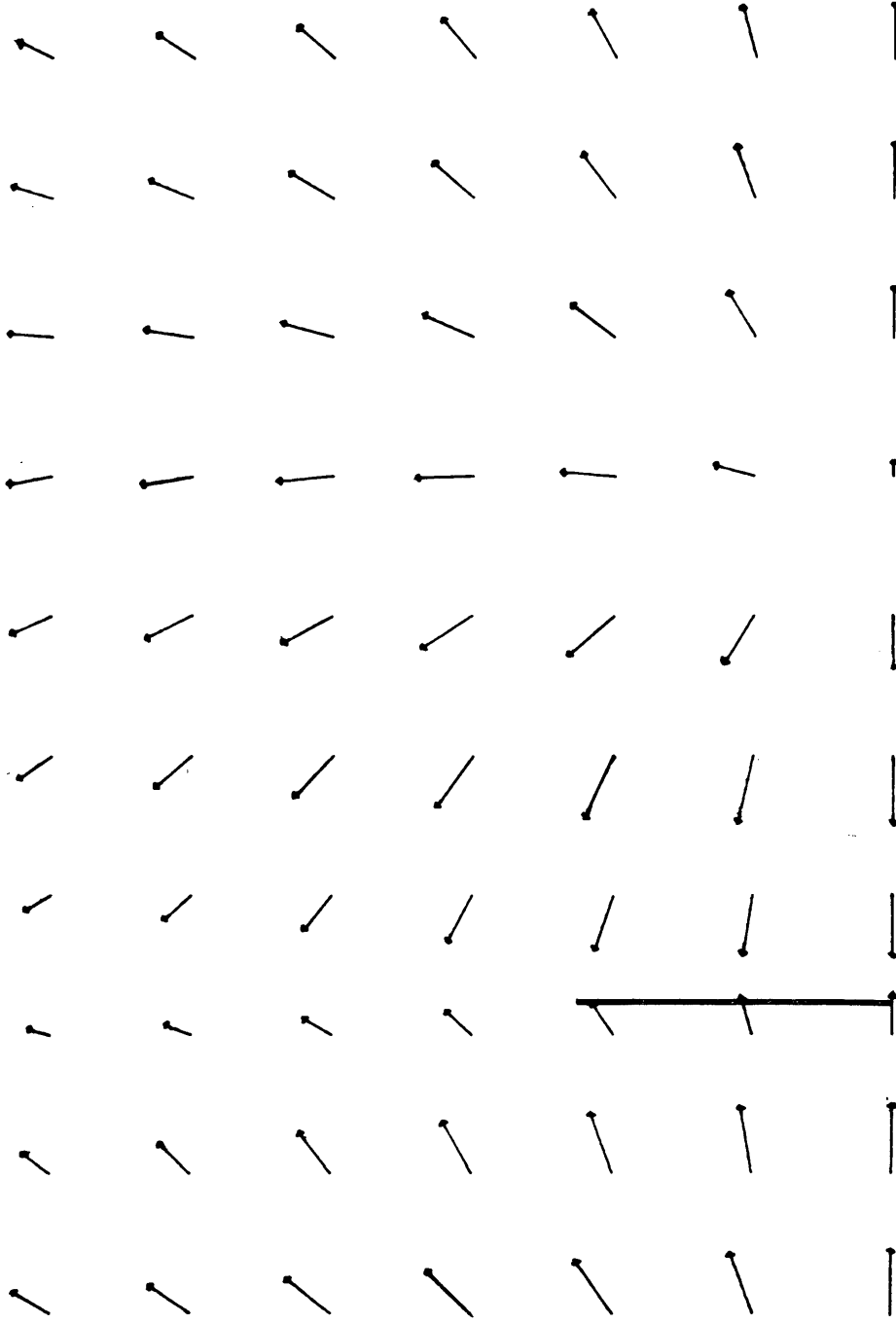
The rotations at Q about the x_1 and x_2 axes can be considered as components of a tilt vector. These components can be composed into a vector at each field point $Q(x_3 = 0)$, which points in the direction of tilting, and which has a length proportional to the magnitude of the tilting. By computing such a vector for a number of field points Q, a map of the tilt field due to the assumed hydrofracture dislocation can be constructed. A program has been written to generate such maps, and a copy of this program, including documentation, is given in appendix 2. The necessary derivatives of W_{11}^3 , $W_{11,1}^3$ and $W_{11,2}^3$, are arrived at from equation 1.12, also in this appendix.

4.) Feasibility Study

By generating maps for hydrofracture models having various dimensions, we can evaluate the feasibility of; A) Measuring with field instruments the tilting caused by an actual hydrofracture event; and, B) of using these tilt measurements to determine the approximate azimuth of the hydrofracture. Maps which were made for this purpose are shown below in figure 1-8.

By comparing the maximum value of the tilt on each map with the sensitivity of the tiltmeters, we can see whether or not measurable tilts might be expected from hydrofractures having dimensions comparable to those of the models. Since the tiltmeters are capable of resolving tilts of $\sim 1 \times 10^{-7}$ radians, the maximum values shown in figure 1-8 suggest that if the hydrofracture is either small or deep, measurable tilts will probably not result. If the hydrofracture event is both large and shallow however, it may be possible to record tilting. Furthermore, the shape of the hypothetical tilt fields reflect the dislocation orientation, suggesting that if a number of tilt values could be measured, some statement might be made about the orientation of the fracture.

On the basis of the modelling, it was decided that if a large, shallow hydrofracture operation were to be available for study, a field experiment would be in order.



FRACTURE DIMENSIONS (meters)

$l = 10^3$ $h = 10^3$

$w = 2 \times 10^2$ $\Delta x = 10^{-2}$

MAP PARAMETERS

1 km. = 3.3 in.

area = 2.0×1.5 km.

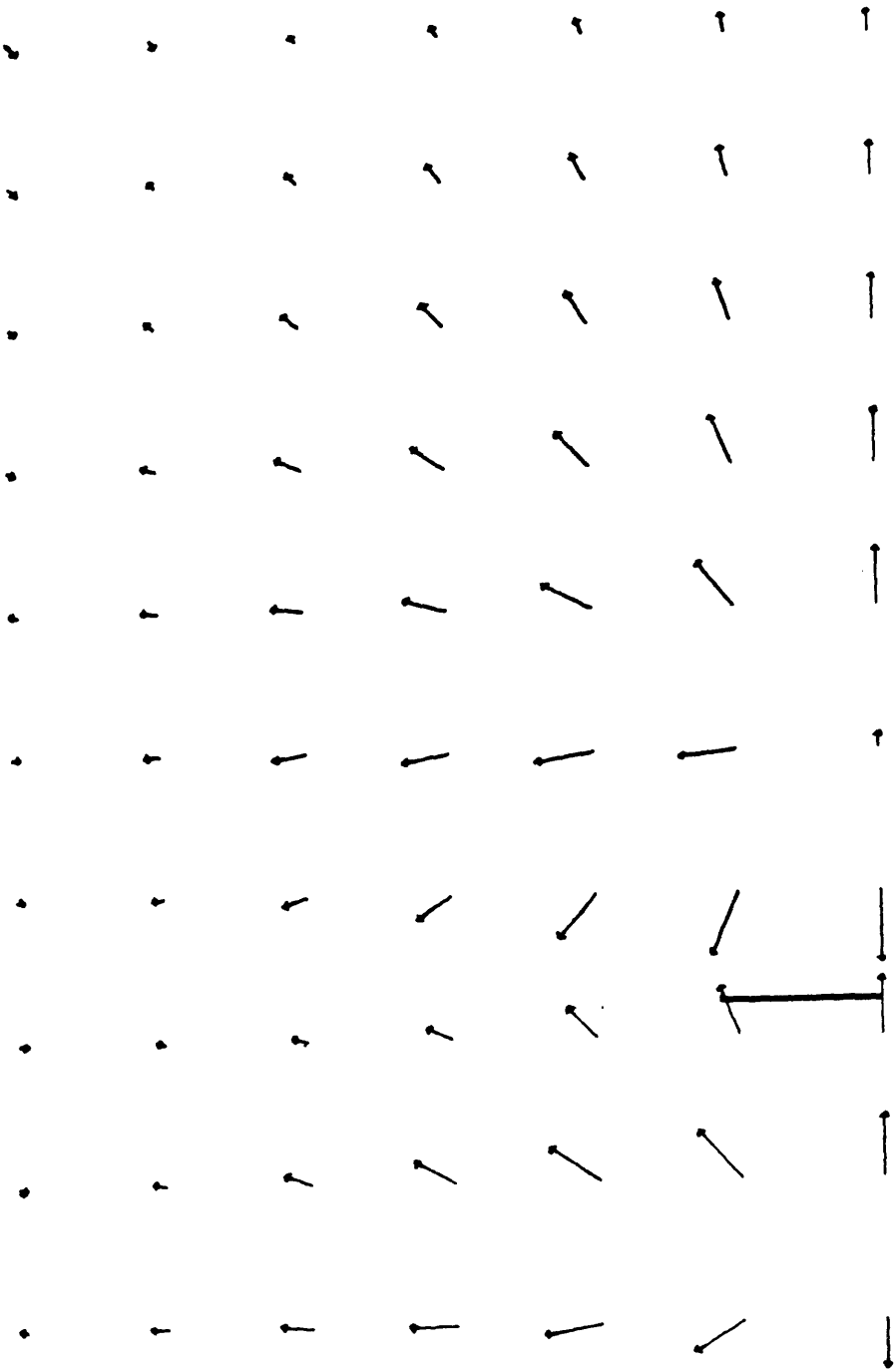
RESULTS

max tilt =

3.25×10^{-7} radians

Figure 1-8a

The modelled tilt field for a large, shallow, hydrofracture. The projection of the fracture on the map surface is shown in black. Half of the fracture projects beyond the map border.



FRACTURE DIMENSIONS (meters)

$l = 5 \times 10^2$ $h = 10^3$
 $w = 10^2$ $\Delta x = 10^{-2}$

MAP PARAMETERS

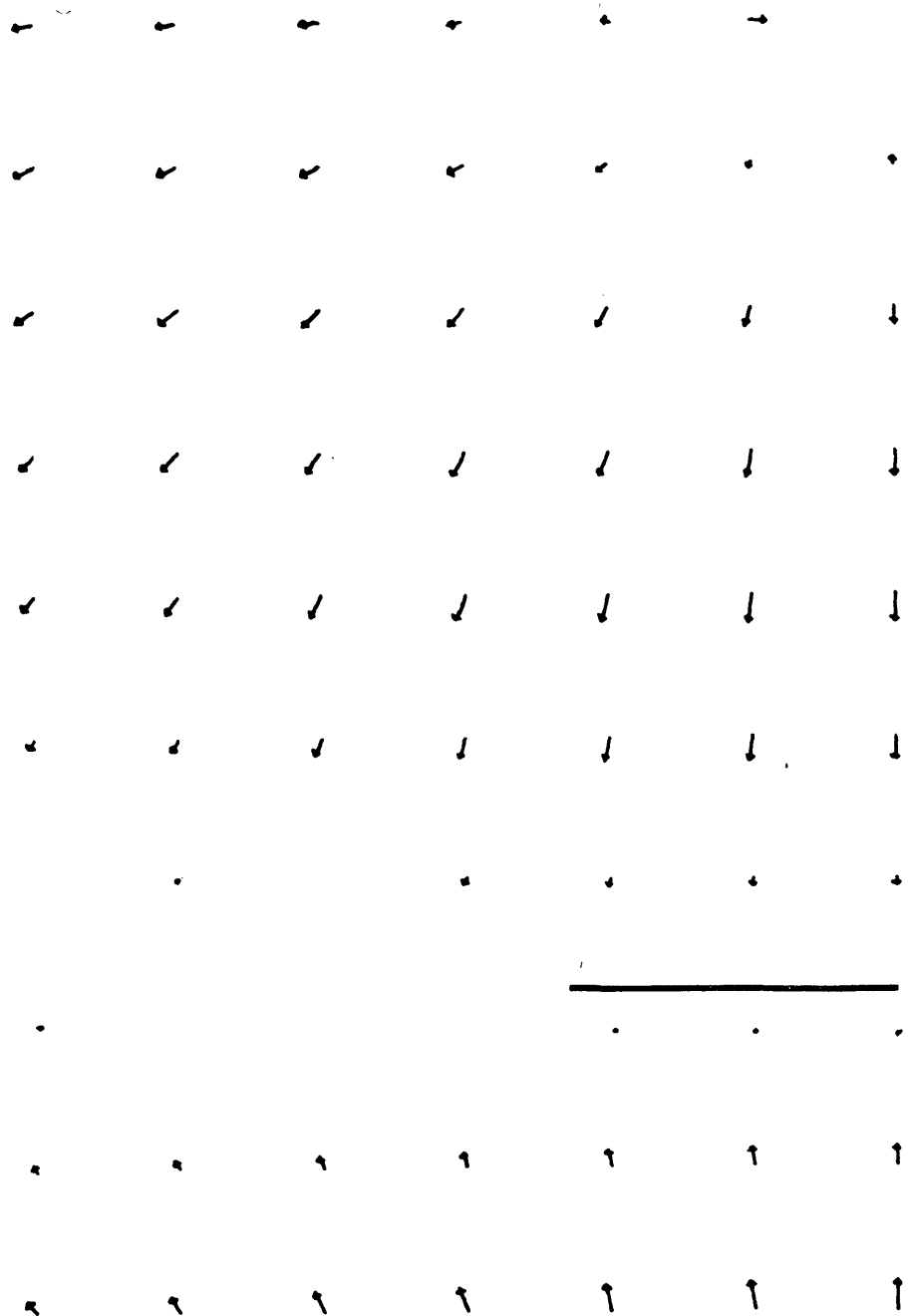
1 km. = 3.3 in.
 area = 2.0×1.5 km.

RESULTS

max. tilt = 1.02×10^{-7} radians

Figure 1-8b

The modelled tilt field for a small, shallow, hydrofracture. The projection of the fracture on the map surface is shown in black. Half of the fracture projects beyond the map border.



FRACTURE DIMENSIONS (meters)

$l = 10^3$ $h = 2 \times 10^3$
 $w = 2 \times 10^2$ $\Delta x = 10^{-2}$

MAP PARAMETERS

1 km. = 3.3 in.
 area = 2.0 x 1.5 km.

RESULTS

max. tilt = 4.9×10^{-8} radians

Figure 1-8c

The modelled tilt field for a large, deep, hydrofracture. The projection of the fracture on the map surface is shown in black. Half of the fracture projects beyond the map border.

Fortunately, we were able to conduct a field experiment in August and September of 1978, at the site of a fracturing program which was large, shallow, and was conveniently close to Golden, Colorado. Our participation in this fracturing program was made possible in large part due to the efforts of Dr. Dan Kim of Amoco. The field experiment which was conducted is discussed in detail in the next chapter.

B.) SURFACE TILTS FROM A DITCH LEAKING WATER

During the course of the field experiment which was designed to detect surface tilts caused by a massive hydrofracture, a number of tilt episodes were recorded at sites located near an irrigation ditch. These tilt episodes corresponded to changes in the water level of the ditch; particularly dramatic tilting occurred when the ditch was filled with water after having previously been dry. One ditch tilt episode occurred simultaneously with the fracturing program, obscuring any hydrofracture tilt. In an effort to approximate the ditch tilt so it could be subtracted from the record in order to better expose the hydrofracture tilt, a method for modelling the ditch tilt was devised. This method is described below.

1.) Possible Mechanisms

It has been hypothesized that the ditch related tilt may have resulted from one or both of the following mechanisms. 1.) As the groundwater table rose beneath the ditch following its flooding, an additional volume of soil became saturated. Individual grains in this volume were buoyed up by the fluid, resulting in a decrease in the amount of compaction of the soil. This effect would be greatest where the water-table was highest, producing a tilt away from the ditch, as observed. 2.) Alternatively, since a moving water table implies there is fluid flow which requires that a pressure gradient exist in the saturated section, the surface tilt may have resulted from forces acting on material in the aquifer as a result of this pressure gradient. If either or both of these mechanisms are responsible for the surface tilt, then it is reasonable to expect that at any given location, the tilting of the earth's surface caused by the ditch being filled will be proportional to the tilt of the groundwater table directly beneath that location.

2.) Describing Groundwater Table Tilt

Conveniently, an equation is given by Glover (1974), which describes as a function of time the tilt of the groundwater table near a ditch leaking water into an

aquifer. This equation treats an initially dry ditch which is filled at time $t_0 = 0$, and thereafter leaks water at a constant rate q . The equation applies in the case of an infinite straight ditch on the surface of an aquifer having constant porosity and permeability. Furthermore, the surface of the water table must initially be horizontal and a distance D above the base of the aquifer. This situation is shown in cross section in figure 1-9.

For ditches which satisfy these constraints, Glover's equation, 1.16 below, can be used to describe tilt transients.

$$-KD \frac{\partial h}{\partial x} = \frac{q}{2} \left[1 - \frac{2}{\sqrt{\pi}} \int_0^{\frac{x}{\sqrt{4\alpha t}}} e^{-U^2} dU \right] . \quad (1.16)$$

$\frac{\partial h}{\partial x}$ = slope of groundwater table

q = rate of leakage

K = permeability

D = thickness of aquifer

$\alpha = KD/V,$

V = void ratio

Solving for the slope of the groundwater table is trivial, giving equation 1.17,

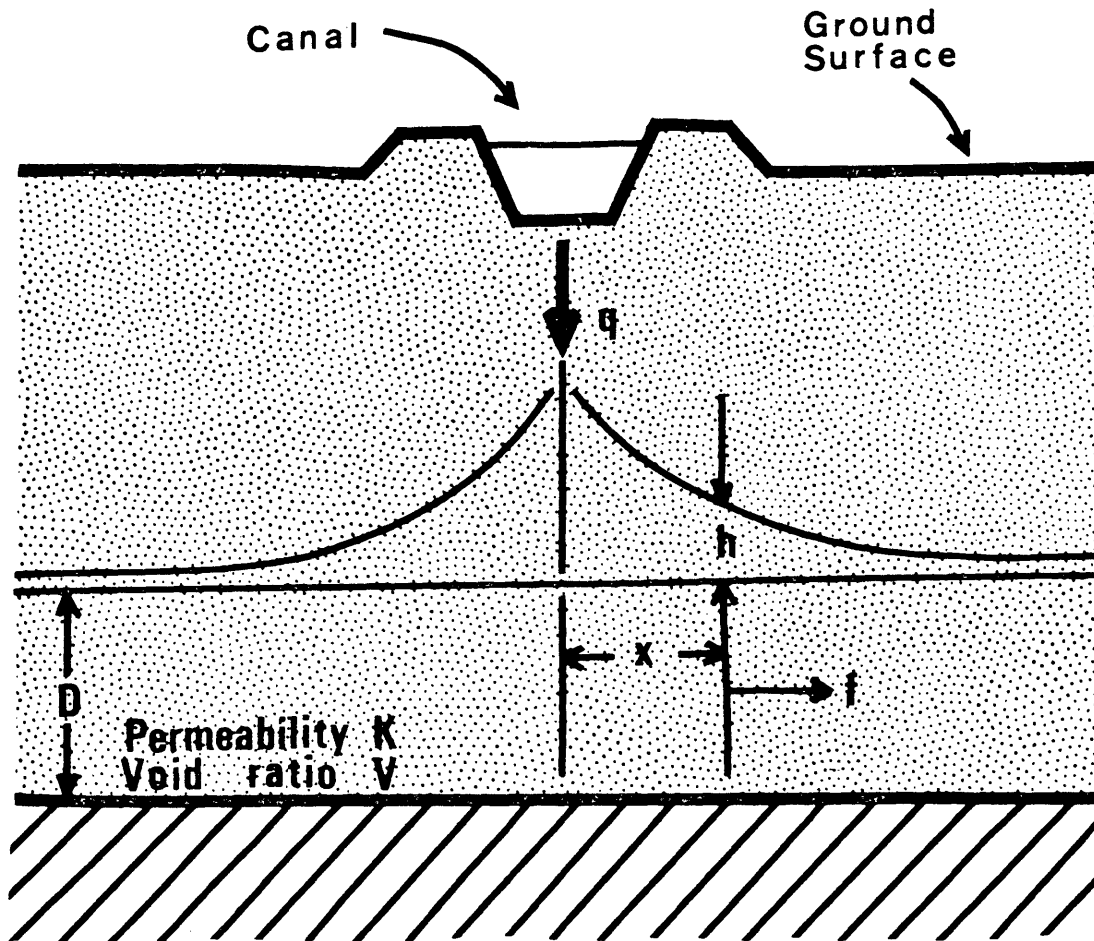


Figure 1-9

View in cross section of the geometry described by Glover's equation 1.16, wherein q is leakage per unit length, f is flow per unit length, h is height of the addition to the water table, and x is the horizontal distance from the ditch (After Glover, 1974).

$$\frac{\partial h}{\partial x} = \frac{-q}{2KD} \left[1 - \frac{2}{\sqrt{\pi}} \int_0^{\sqrt{\frac{x}{4\alpha t}}} e^{-U^2} dU \right]. \quad (1.17)$$

We have hypothesized that surface tilt is proportional to ground water table tilt, that is, surface tilt = $B \frac{\partial h}{\partial x}$, B being a constant of proportionality. Since neither B , q , K , or D are known, they can collectively be replaced by $A_{\max} = Bq/2KD$, a constant which can be determined from the data. Since the real disturbance we are trying to approximate starts at t_0 rather than at zero, the limits of integration must be changed from $x[4\alpha t]^{-1/2}$ to $x[4\alpha(t - t_0)]^{-1/2}$.

These substitutions yield the following expression for surface tilt T , equation 1.18.

$$T = A_{\max} \left[1 - \frac{2}{\sqrt{\pi}} \int_0^{\sqrt{\frac{x}{4\alpha(t - t_0)}}} e^{-U^2} dU \right]. \quad (1.18)$$

From equation 1.18, it can be seen that to specify a particular groundwater transient tilt curve, 3 parameters must be fixed: 1) the time of onset of the disturbance, t_0 ; 2) the parameter $x[4\alpha]^{-1/2}$, which sets the upper limit of integration for any time t ; and 3) the maximum amplitude of the disturbance, A_{\max} .

If field tilt records have been collected which contain transient tilts related to the filling of a ditch, these three parameters can be determined from the records

in the following manner. t_o , the time at which the ditch was flooded, is determined by comparing the records from all tilt channels located near the ditch. If the disturbance hits all channels at nearly the same time, this common time can be taken as t_o . If the ditch is used for irrigation purposes, information regarding the onset of flooding might be obtained from the operator of the irrigation system. (As was done in this experiment.)

Attempting to find A_{\max} directly from the records is unfortunately a riskier prospect than determining t_o . This is because the amplitude of the disturbance may not approach its maximum value until several days after onset; this length of time is large enough that gradual drift and later noise events can become superimposed on the tilt transient, complicating the shape of the record in the region of maximum amplitude. Certain properties of equation 1.18 make it possible to infer the value of A_{\max} from the shape of the curve shortly after the onset of the disturbance, however, allowing A_{\max} to be estimated in spite of the above limitations.

Figure 1-10 shows equation 1.18 plotted on a logarithmic time scale. A family of curves is shown, each curve representing a different value of the parameter $x[4\alpha]^{-1/2}$. Examination of this figure shows that each curve in the family has exactly the same shape as any other curve.

HYDRAULIC TRANSIENT TILT CURVES

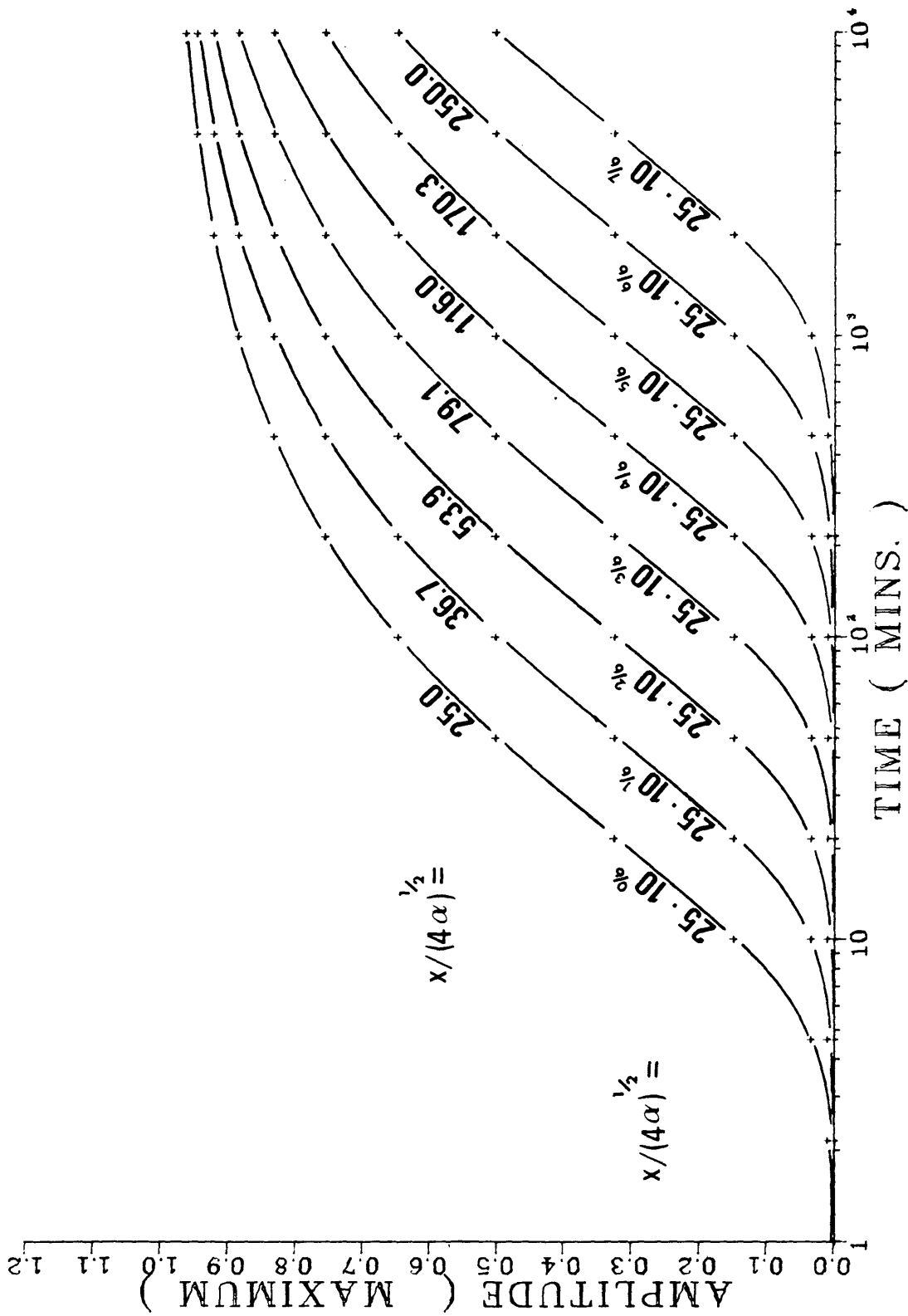


Figure 1-10

Family of curves of equation 1.18 for different values of $x/(4\alpha)^{1/2}$.

This means that the shape of the curve, and therefore the slope at any particular fraction of A_{\max} , is independent of the parameter $x[4\alpha]^{-1/2}$. Another observation which can be made from the figure is that the slope m is nearly constant between values of 0.2 and 0.45 A_{\max} , and has a value in this region given by

$$m = \frac{A_2 - A_1}{\log(t_2 - t_0) - \log(t_1 - t_0)} \quad (1.19)$$

where A_2 has an amplitude of 0.45 A_{\max} and occurs at time t_2 , and A_1 has an amplitude of 0.20 A_{\max} and occurs at time t_1 . Dividing each side of equation 1.19 by A_{\max} and using values picked from the first curve in figure 1-11 gives

$$\frac{m}{A_{\max}} = \frac{.25}{\log(37.2) - \log(12.6)}, \quad \text{or}$$

$$\frac{m}{A_{\max}} = .533 \quad (1.20)$$

By plotting the record of ditch tilt on a logarithmic time scale, identifying the region of constant slope, evaluating the value of the slope, and substituting into 1.20, the value of A_{\max} for the ditch transient on that particular tilt channel can be computed. Note from figure 1-10

that the region of constant slope contains the only inflection point on the curve - this helps to identify the correct segment of the real data.

Having determined t_o and A_{\max} , it is now possible to determine the final parameter required to specify a particular ditch transient, $x[4\alpha]^{-1/2}$. First, the observed tilt values are converted to fractional values of A_{\max} , and the data plotted logarithmically, in a fashion similar to figure 1-10. Next, a number of curves showing equation 1.8 for varying values of $x[4\alpha]^{-1/2}$ are plotted. These curves are members of the family shown in figure 1-10, and the value of $x[4\alpha]^{-1/2}$ which produces a curve giving the best match with the actual record is the desired quantity.

Once values have been determined for the three parameters t_o , A_{\max} and $x[4\alpha]^{-1/2}$, they can be substituted into equation 1.18. Evaluating this equation for different values of t then gives an approximation of the tilt caused by the ditch transient. This technique proved useful in approximately removing the ditch tilts from the tilt records collected during the hydrofracture field experiment. In chapter 3 the application of this method to the real data is discussed.

EXPERIMENTAL PARAMETERS

A.) INTRODUCTION

As a result of the feasibility study which was described in the last chapter, a field experiment was designed and later conducted to investigate the tilt field caused by an actual hydrofracture. In this chapter, the parameters of the field experiment will be described, including a discussion of the instrument sites which were selected, the vaults constructed at each site, the instruments which were used, and comments on the system response and the site noise encountered.

1.) Location and duration of the experiment

This investigation was undertaken at the Amoco Production Company Hemple #2 well, located at the center of the SW/4 of Sec. 20, T4N R65W in Weld County, Colorado. This location is shown on figure 2-1, which is a reproduction of part of the Army Map Service "Greely" Sheet, (NK 13-11).

The Hemple #2 underwent a fracture treatment on August 28, 1978, and data was collected from August 26 through September 4, 1978.

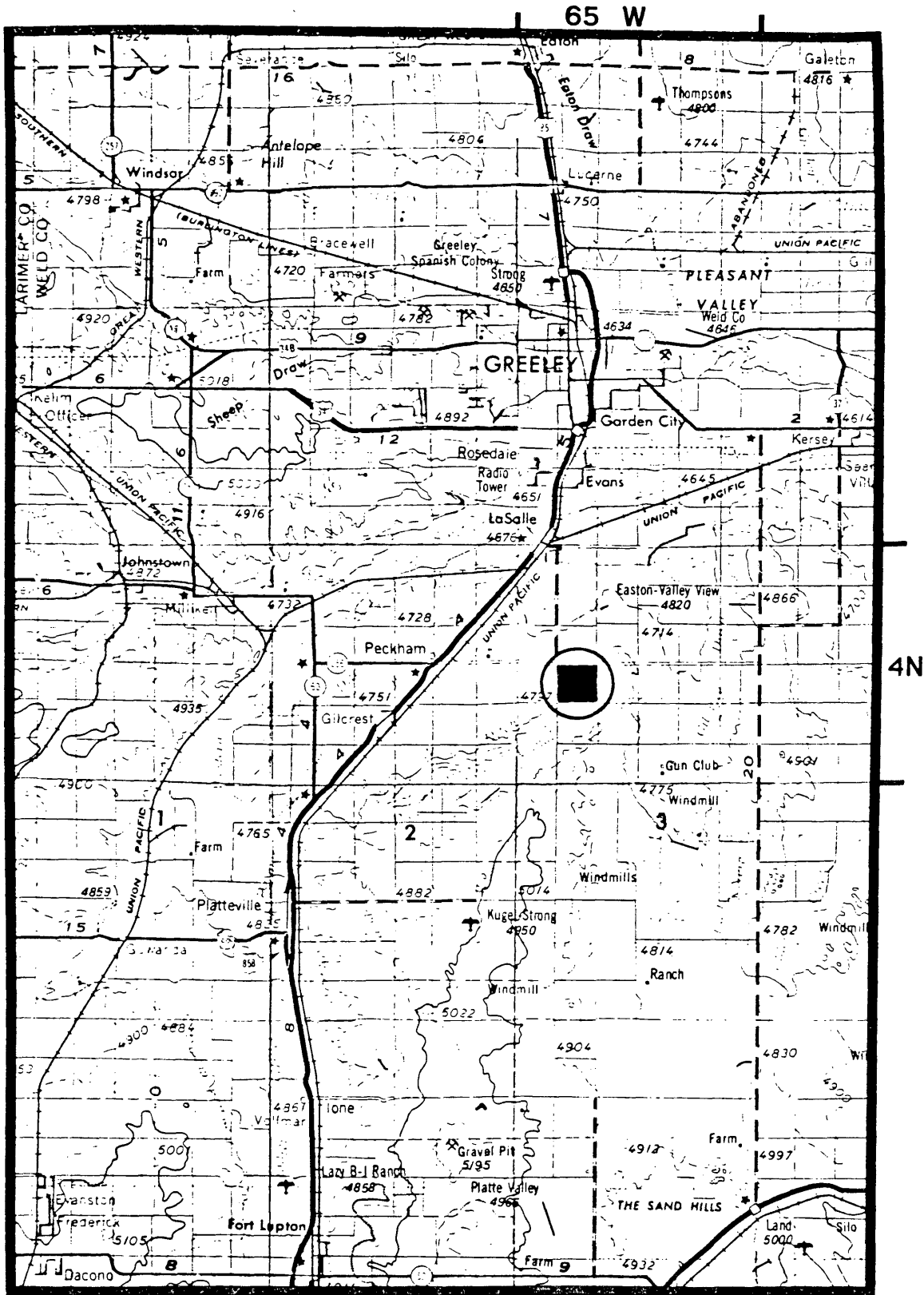


Figure 2-1

Army map service "Greely" sheet, showing location of study area T4N R65W sec.20 to Greeley Colorado, and Fort Lupton Colorado. Section 20 is circled.

2.) Past experience

The instruments used in this experiment were previously used in a tilt experiment in the Las Vegas vicinity, and several experimental parameters were chosen on the basis of experience gained during the Las Vegas experiment. Specifically, instrument modifications were made in order to allow the tiltmeters to be calibrated while running at the sensitivity necessary to see a signal of the anticipated magnitude, and the instruments were housed in insulated vaults in order to reduce the large diurnal signal encountered in Las Vegas. These improvements will be discussed in greater detail later in this chapter.

B.) INSTRUMENT SITES

1.) Site Selection

Having four tiltmeters available, it was decided to deploy all four at approximately the same distance from the borehole, all equally spaced from one another. A hypothetical tilt map, using appropriate source dimensions, suggested an optimum distance from the borehole at which the tiltmeters could be deployed. Several factors prevented this ideal configuration from being implemented, however. Since hand carrying of the instruments and vault materials a large distance would be a formidable chore, the sites all had to be accessible with vehicles. Also,

being guests on cultivated private property, we had to avoid occupying sites which would cause excessive damage to the owner's crops. Figure 2-2 is a map of the study area, showing the site locations ultimately chosen and the location of the well which was fractured.

Each site which was selected had some unique problems, which are described, by site, below.

2.) Description of Sites

a.) Site 1

Site 1 was located approximately 220 m N of the borehole in a recently mowed hay field. The selection of the site was unfortunate in two respects. First, it was located approximately 16 m from an irrigation ditch. The effect of the ditch on the data will be discussed in the next chapter. Secondly, a crew laying the pipeline for the well was operating near the site on the day of the fracture and their equipment left an undesirable signature on the tilt records.

b.) Site 2

Site 2 was located approximately 440 m E of the borehole, in a hay field which was mowed during the course of the experiment. This site was just off a well travelled access road, and pieces of farm equipment were occasionally parked near enough to the instrument to disturb the

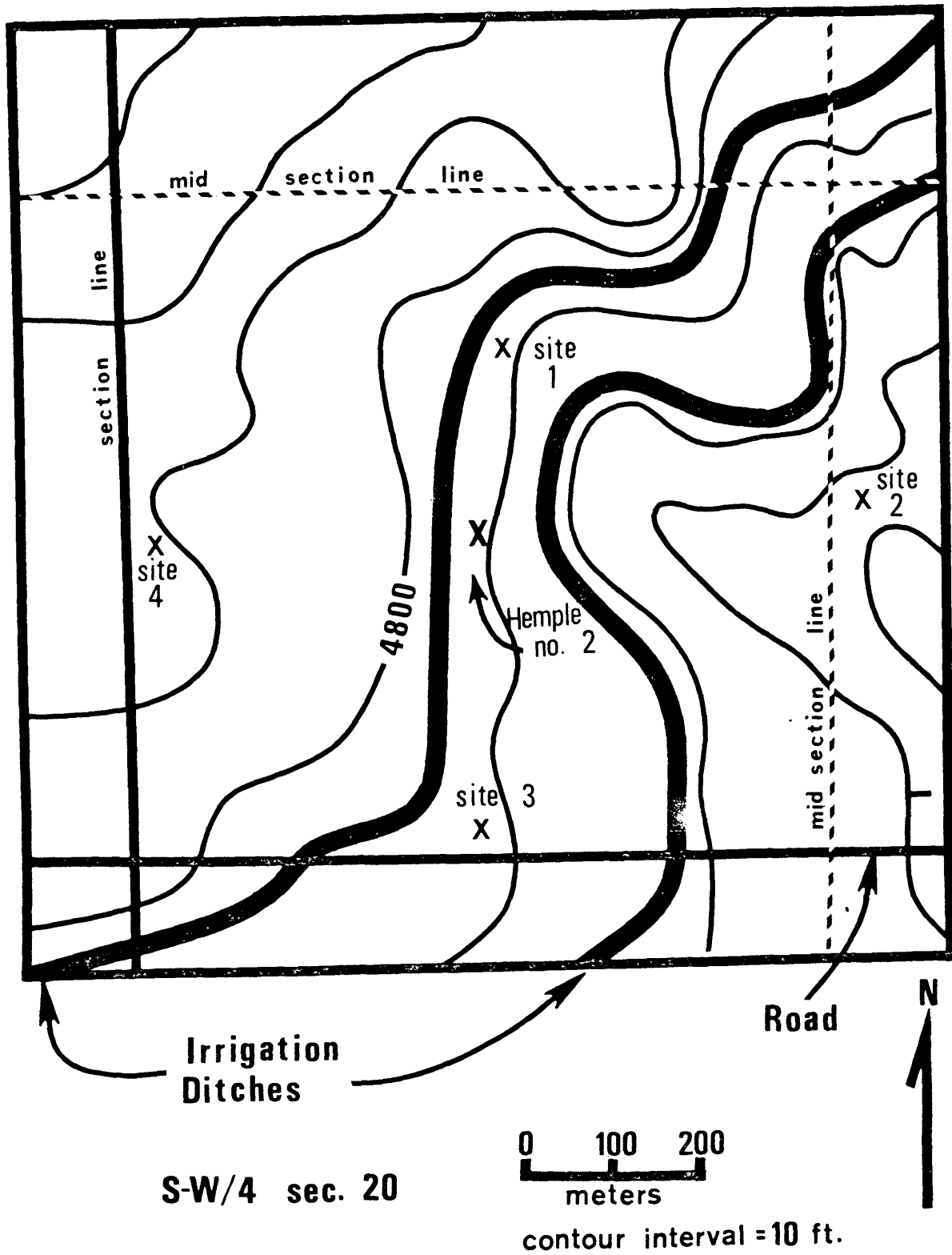


Figure 2-2

Map of study area showing well and tiltmeter locations.

record. The hay was irrigated by a mechanical sprinkler system which slowly moved over the field. The sprinkler system moved over the site during the afternoon of August 29, the day after the hydrofracture operation. This disturbed the record and prevented meaningful comparison of the tilts of these two days.

c.) Site 3

Site 3 was located approximately 340 m S of the borehole, near the same ditch which was mentioned in the description of site 1. This ditch also "contaminated" the site 3 record, again discussed later. An additional problem at this site was the high water table, which was only 1.3 m below the surface. This necessitated elevating the vault slightly, and packing dirt around the sides, rather than having a completely buried vault as at the other sites.

d.) Site 4

This site, located approximately 370 m W of the borehole was fortunately free of the problems encountered at the other sites, and provided a consistently good record.

The manner in which the sites were prepared and the instruments installed is discussed next.

C.) TILTMETER VAULTS

Records obtained during a 1976 tiltmeter experiment in Las Vegas showed diurnal tilts associated with air temperature variations of $1-2 \times 10^{-5}$ radians (Major, 1976). In order to reduce the magnitude of this diurnal signal, insulated vaults were constructed at each of the four sites discussed in the last section.

1.) Site Preparation

At each site, a pit was dug of approximately the dimensions 1.5 m deep, 2 m wide and 3 m long. In each pit a plywood and styrofoam vault was constructed, open on the bottom and with a roof slightly below ground level. Each vault had a hatch large enough for a person to climb through, which opened several inches above ground level. The vaults were then covered with earth, flush with ground level, and a styrafoam plug was placed in the hatchway to improve the thermal insulation. Figure 2-3 is a schematic diagram of this type of vault.

These shallow buried vaults worked well. Figures 3-4 and 3-5 show the diurnal signal recorded in this experiment to be approximately 1×10^{-6} radians. This is only 1/20 of the amplitude observed in Las Vegas, when the tiltmeters were mounted on uninsulated concrete slabs.

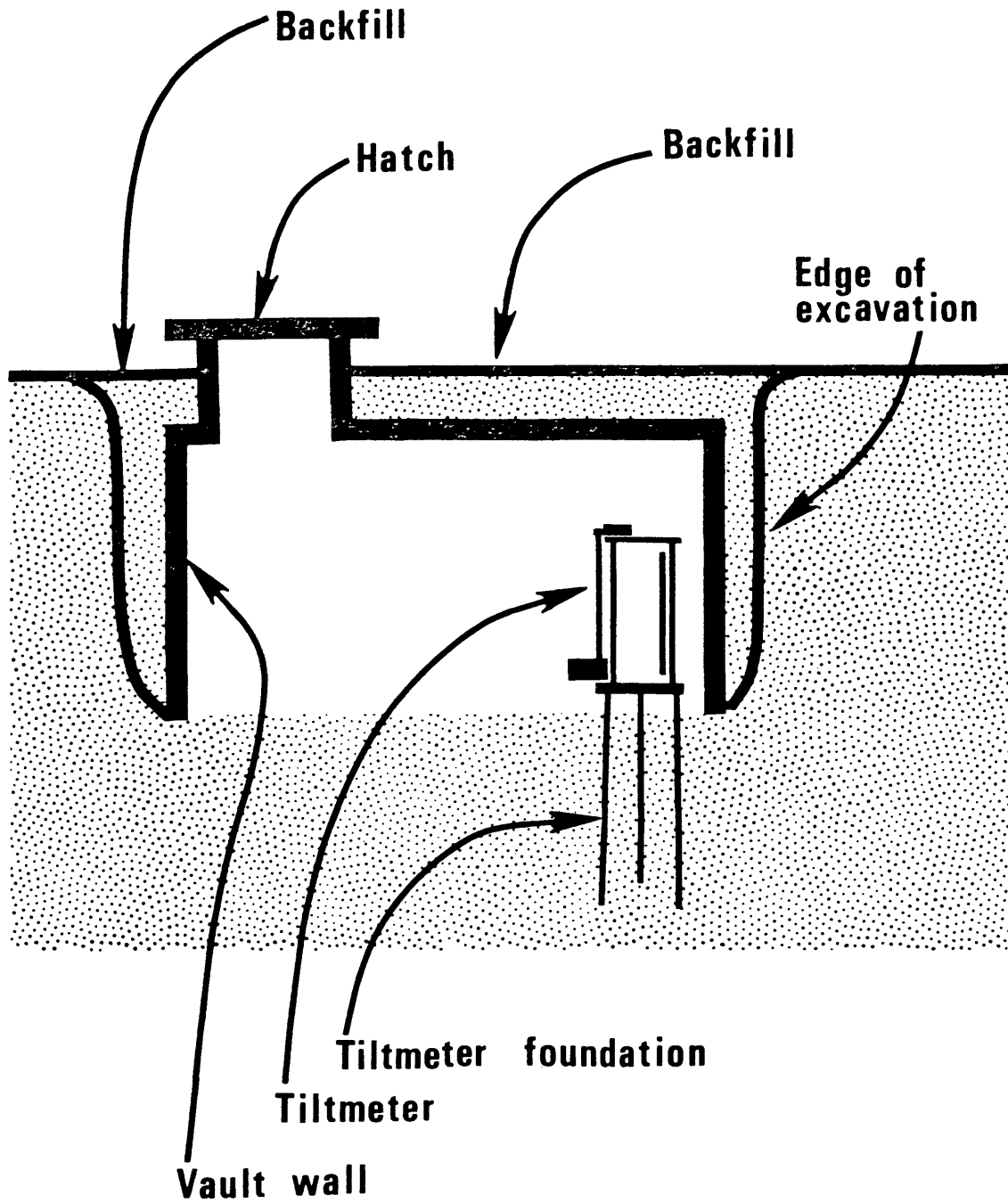


Figure 2-3

Tiltmeter vault shown in cross section. Heaviest lines are plywood and styrofoam walls.

2.) Instrument Installation

In each vault, three threaded rods were pounded into the ground, and collectively served to couple the tiltmeter to the earth's surface; the tiltmeter base being bolted to each rod. The electronics package for each tiltmeter was also placed in the vault, as were the batteries which supplied power to the electronics and to the micrometer screw motors. Signal and motor control wires were run from the vault approximately 25 m to an operator's station. This allowed the instruments to be monitored, calibrated, and rezeroed without having to approach the sites, either in vehicles or on foot, closely enough to produce measurable tilts from surface loads. At the operator's station two Easterline-Angus chart recorders and the switches for motor control were mounted inside plywood boxes. Four two component tiltmeters and two temperature recording devices were used in this study, these instruments are described in the section which follows.

D.) INSTRUMENTATION

1.) Tiltmeters

The tiltmeters used were constructed in 1967 for the Colorado School of Mines Geophysics Department, and have subsequently undergone several modifications to improve their performance. The tiltmeter outputs were recorded on

Easterline-Angus wind up strip chart recorders, which inked an analog signal at either of two speeds, 1.5 in./hr. or 1.5 in./min.

a.) Principle of Operation

The tiltmeters operate according to the principle described below, and shown schematically in figure 2-4.

The tiltmeter housing is rigidly fixed to the surface of the earth, and a mass is suspended from the top of this housing by wires, in such a manner that it is free to move under the influence of gravity, acting as a pendulum. If the surface of the earth tilts, the mass will move with respect to the side of the housing by an amount which is proportional to the tilt (for small angles). By monitoring the distance between the pendulum and the tiltmeter housing, in two perpendicular directions, the magnitude and direction of tilting can be established.

Obviously, to resolve small tilts requires that the distance between the pendulum and the housing be known accurately. By attaching parallel capacitor plates to the pendulum and to the housing, an air gap capacitance is established, this capacitance being inversely proportional and quite sensitive to air gap distance. Incorporating this capacitor in a resonant circuit, the response of which is inversely proportional to capacitance yields an

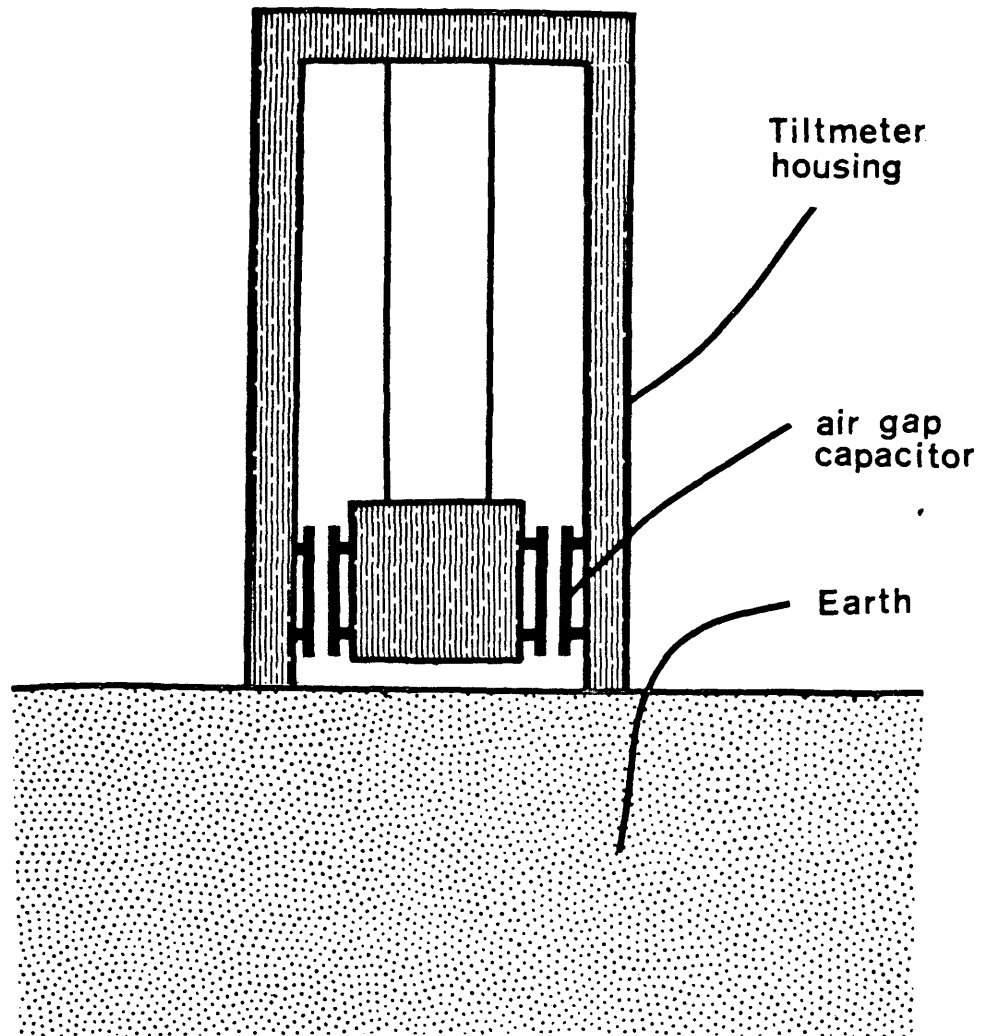


Figure 2-4
Schematic diagram of a tiltmeter.

output voltage which is, at least ideally, proportional to tilt. After rectification, this signal is used to deflect the pen on a strip chart recorder. Since not all the constants which relate air gap distance to capacitance, capacitance to output voltage, and output voltage to pen position are well known, it is necessary to calibrate each channel of each tiltmeter individually, in order to recover tilt values from the field records. The calibration system, which was modified just prior to this experiment, is described below.

b.) Calibration

By changing the distance between the pendulum and the tiltmeter housing by a known amount, the effect of a known tilt on the system can be duplicated. Taking the ratio of the recorder response to this known tilt yields the sensitivity of the channel. The pendulum-housing distance is changed by translating the suspension point of the pendulum with respect to the housing. This adjustment is made with a micrometer screw, which is operated remotely via a servo motor. The micrometer screw bears on a motion reducing lever, permitting the pendulum to be moved in increments proportionally smaller than the increments obtainable directly from the micrometer screw itself. A schematic representation of the calibration mechanism is given in figure 2-5.

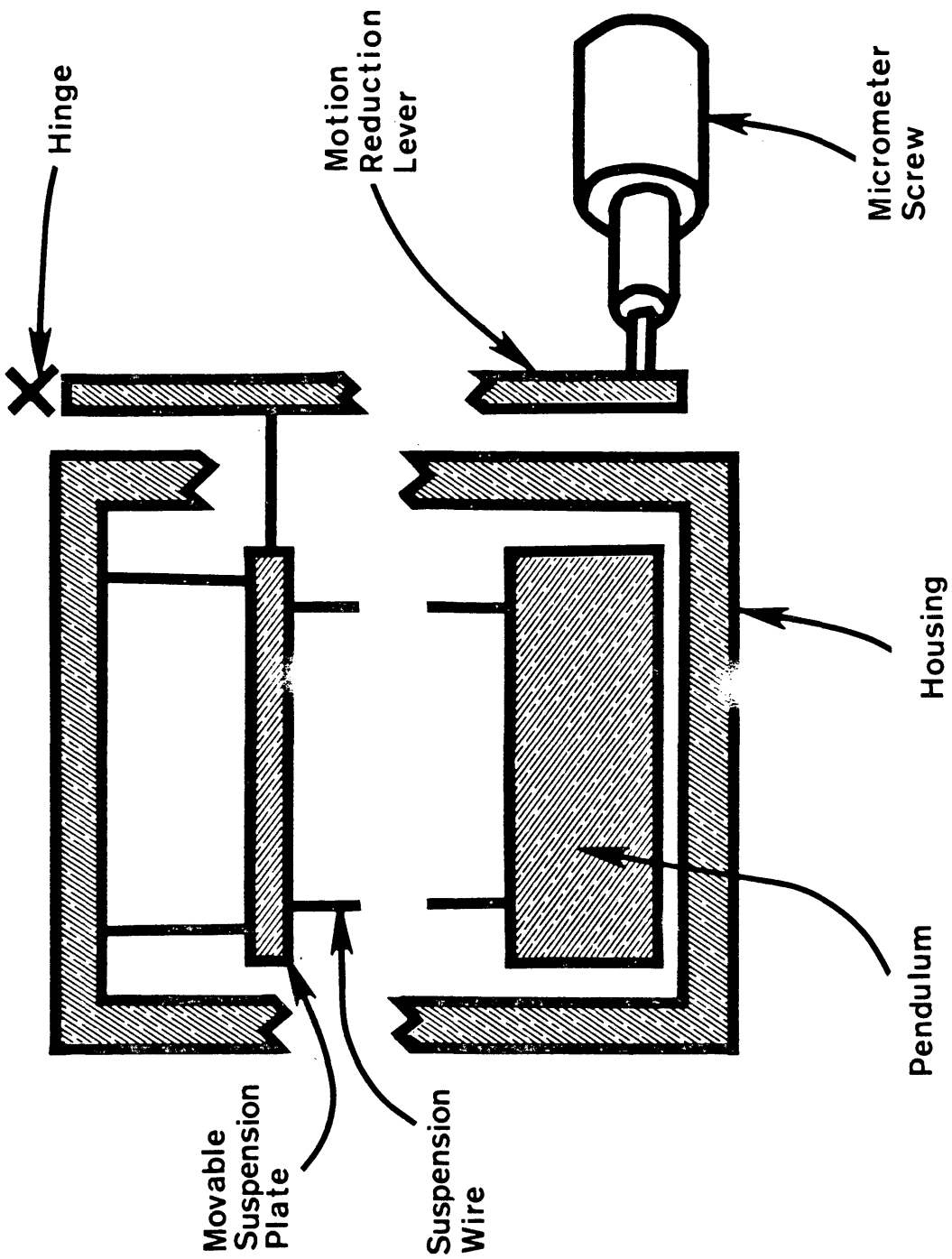


Figure 2-5

Mechanism employed for calibrating tiltmeters at sensitivities of 10^{-6} radians.

Every 1/10 of the micrometer screw revolution, a switch is briefly closed, which grounds the output circuit. This provides a record on the field trace of how far the pendulum was moved, allowing the sensitivity to be calculated. A sample calibration of one channel is shown in figure 2-6, and sensitivity values for all channels are given on the operational summary chart, figure 2-7.

2.) Thermometers

If a relation between the diurnal tilt and temperature could be found, any tilt signal from the hydrofracture would be easier to identify, since much of the "background" signal could be accounted for. In hopes of finding such a relation, two recording thermometers were used in this experiment, one to monitor the temperature of air at ground level near site #1, the other to monitor the temperature inside the tiltmeter vault at site #1.

a.) Air Temperature

The instrument for measuring air temperature was an old bimetallic strip type thermometer, which required refurbishing for the field. This refurbishing necessitated recalibrating the thermometer. Calibration was done in a rather crude manner, and the temperature values recorded may be in error by as much as 3°C. Since the goal of the

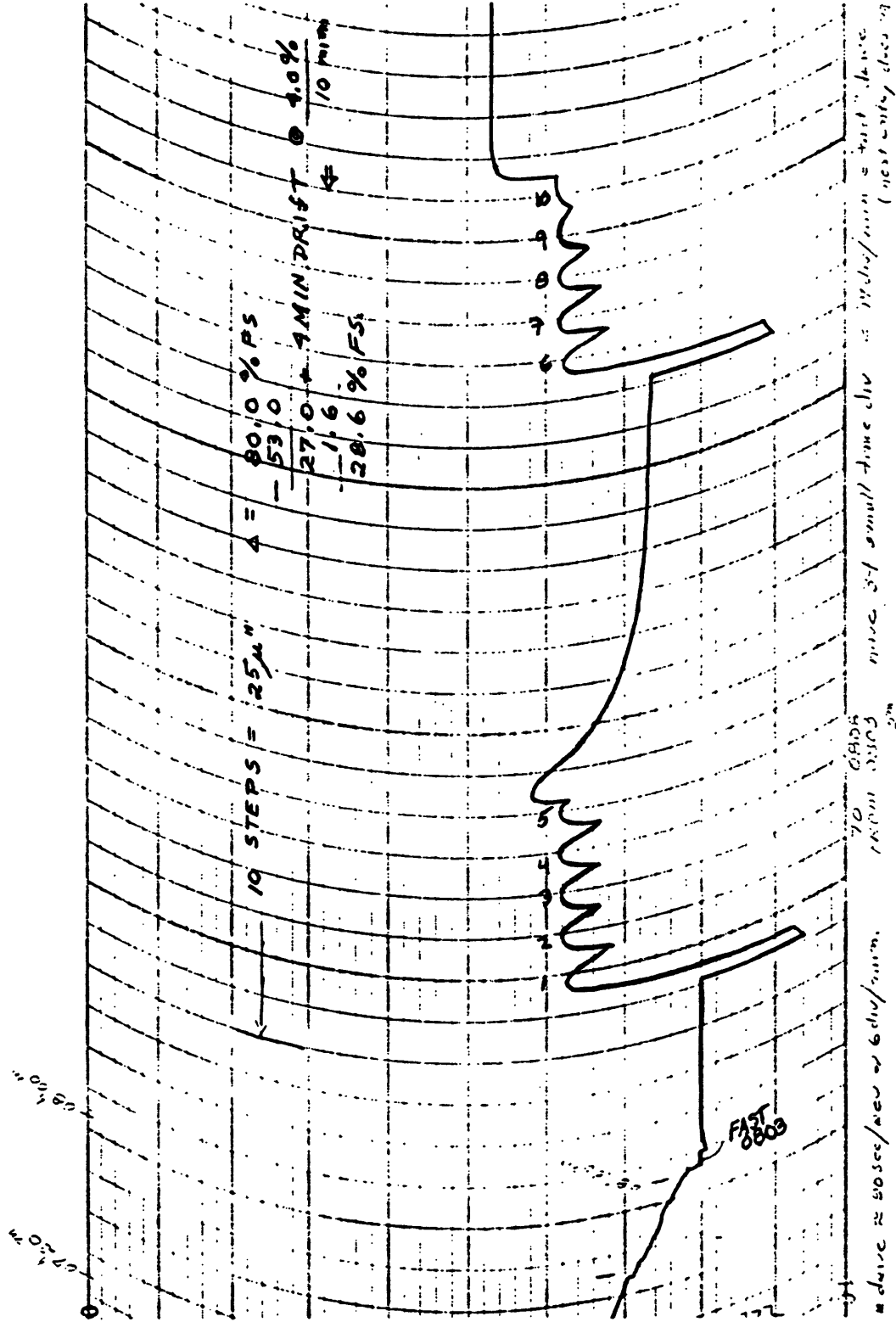


Figure 2-6

Sample record showing calibration. Paper feed rate changed from 1.5 in./hr. to 1.5 in./min. at 0803 local time.

temperature study was to establish curve shapes for comparison with the tilt records, this inaccuracy is unimportant. This thermometer was placed approximately 25 m from site #1, approximately 10 cm off the ground, and inside a plywood box with one side missing. This arrangement provided continual shade, without creating stagnant air around the thermometer.

b.) Vault Temperature

The temperature within the vault was monitored on a Rustrak strip chart recorder, the needle of which was deflected by a Radio Shack electronic thermometer kit. This system was also calibrated in a crude fashion, and recorded values may vary from actual values by as much as 3°C. As before, the absolute temperature value is not what we desire, and this inaccuracy is unimportant. Unfortunately, this device did not function as expected. The Rustrak meter drained the power battery quickly, and the system only operated for several hours before requiring a new battery. Since the site was usually inspected only twice per day, the vault temperature record is very incomplete.

E.) SYSTEM RESPONSE AND OPERATIONAL SUMMARY

The fracturing program at the Hemple #2 involved approximately six hours of fluid injection. Thus, the dominant frequency of the target signal should be in the

period range of approximately six hours. A 100 sec. filter in the electronics and hand smoothing during digitization reduced the high frequency noise content. Important sources of noise had dominant frequencies near to that of the target signal, specifically the diurnal signal, which had an amplitude of approximately 1μ radian, and the hydraulic ditch transient, with amplitudes of approximately 20μ radians.

As might be expected, not all the instruments which were deployed yielded continuous records. Instruments occasionally went off scale, required mechanical adjustment, did not ink properly, or had other problems which interrupted the record. Information on when each instrument was recording satisfactorily and when each instrument was "down" is presented in the operational summary chart, figure 2-7.

OPERATIONAL SUMMARY CHART

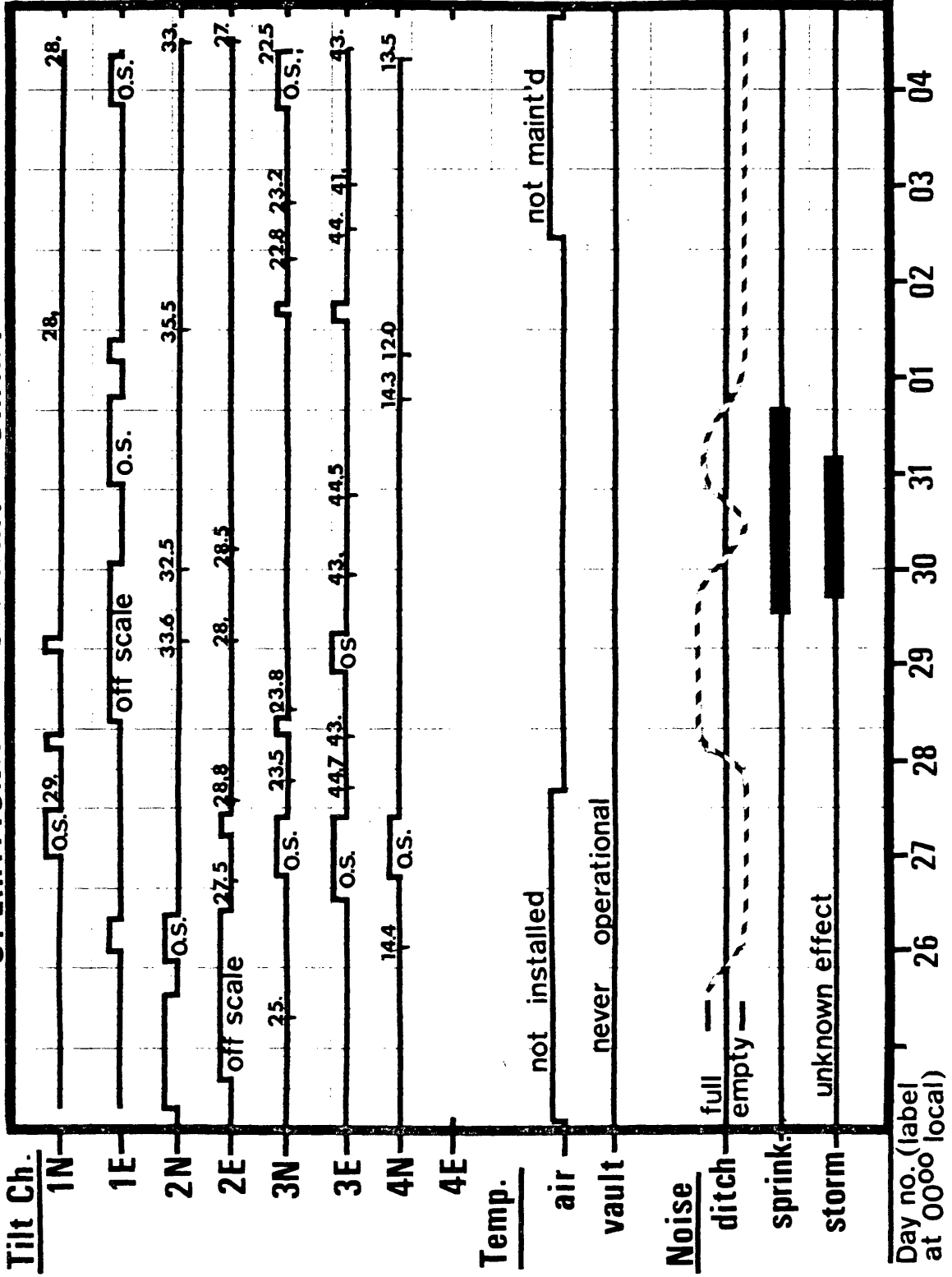


Figure 2--7

Record of instrument operation including important sources of noise.

DATA ANALYSIS

A.) FIELD DATA

Figures 3-1 through 3-5 show the data which was collected in the field. Tiltmeter data is only shown for the intervals during which the instruments were running at high gain. Some obviously contaminated data is not shown. (For example, if a tiltmeter vault was entered on a particular day, that day's record is considered to be contaminated.) All traces have been sampled at a 20 min. interval, and tears in the data resulting from the micrometers being driven to rezero the traces have been removed. The records have been converted from units of scale divisions to units of tilt, in micro-radians, by multiplication of the data for each channel by the appropriate sensitivity factor.

Note that no data from the E/W channel at site 1 is shown, despite the fact that this channel ran at high gain for many days. (See operational summary chart, figure 2-7.) This data has not been considered because the record was off scale during the entire pumping interval; no information about the hydrofracture is present on this channel.

B.) REJECTION OF NOISY DATA

Many of the days of data presented in figures 3-1 through 3-5 contain noise events which can be identified.

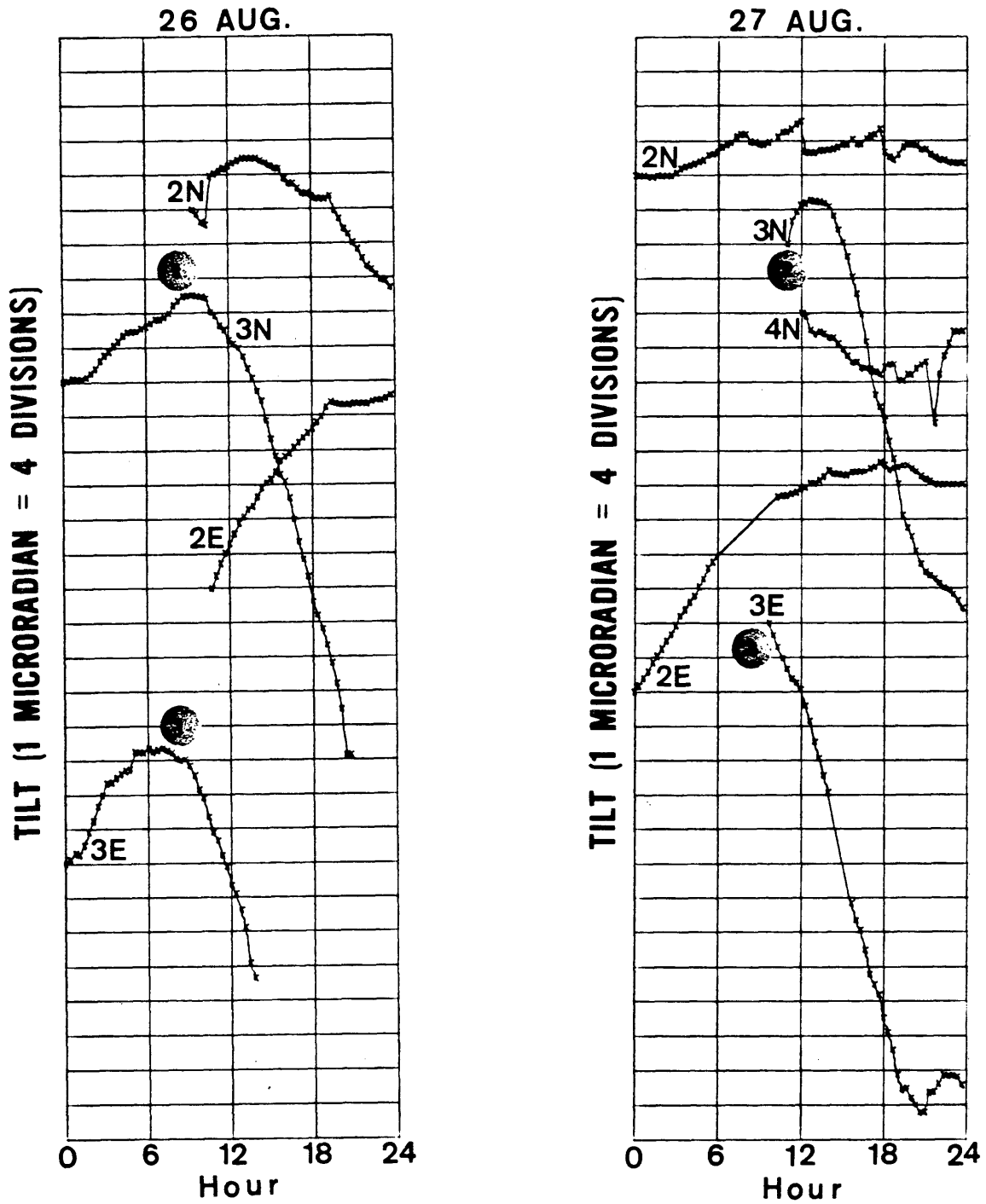


Figure 3-1

Tilt records collected on 26 and 27 August, from 00⁰⁰ m to 24⁰⁰ m local time.

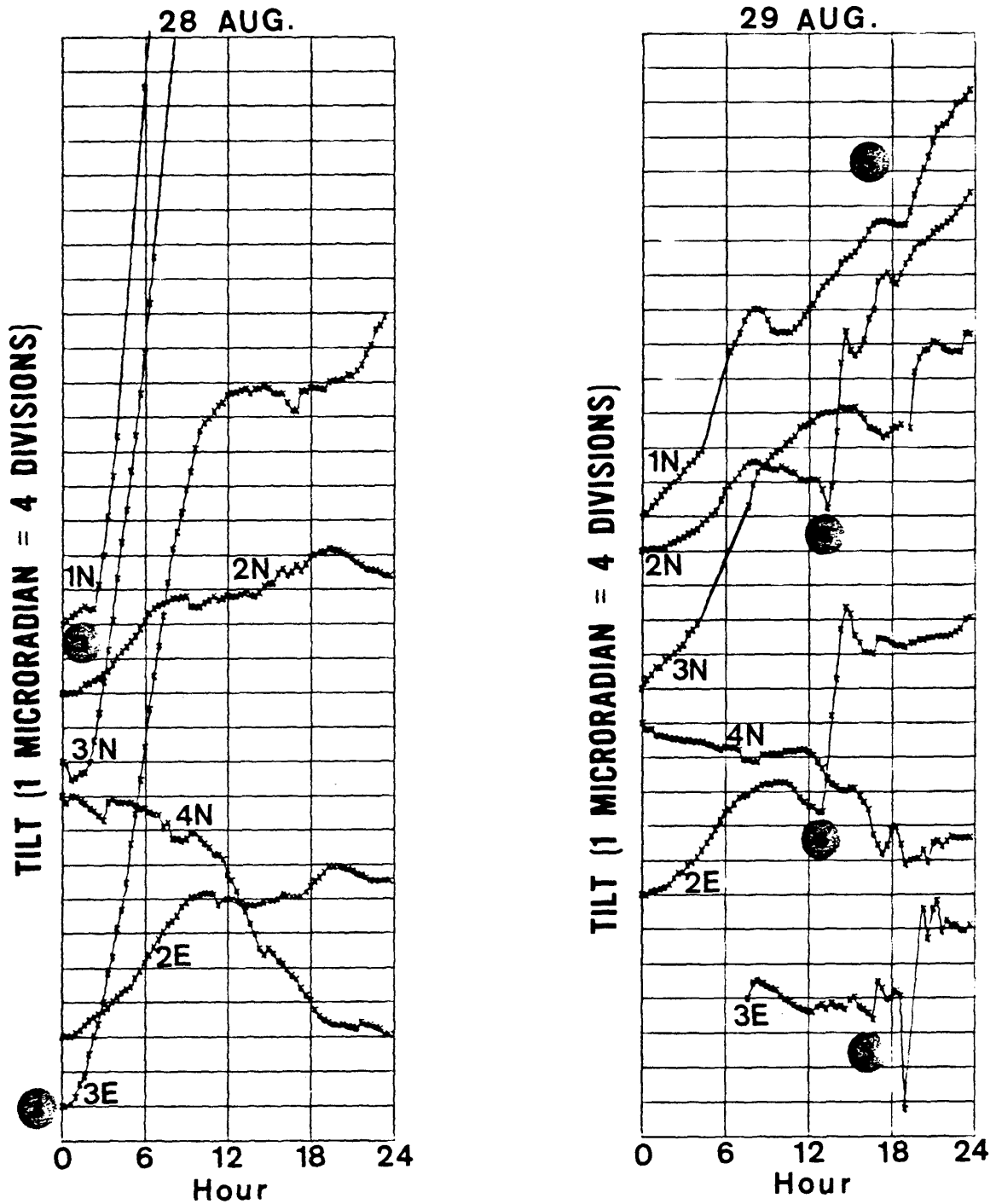


Figure 3-2

Tilt records collected on 28 and 29 August from 00⁰⁰ m to 24⁰⁰ m local time.

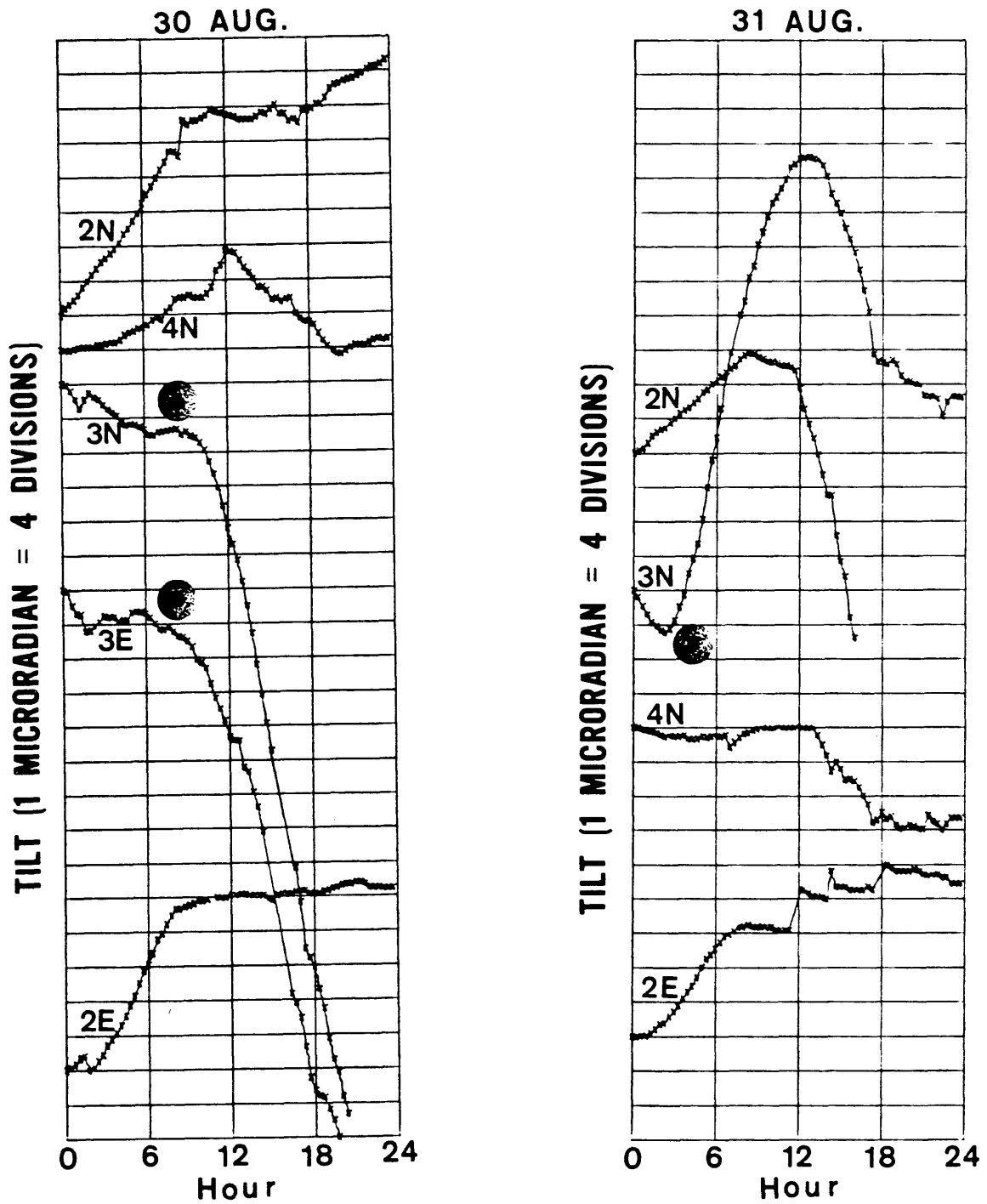


Figure 3-3

Tilt records collected on 30 and 31 August from 00⁰⁰ m to 24⁰⁰ m local time.

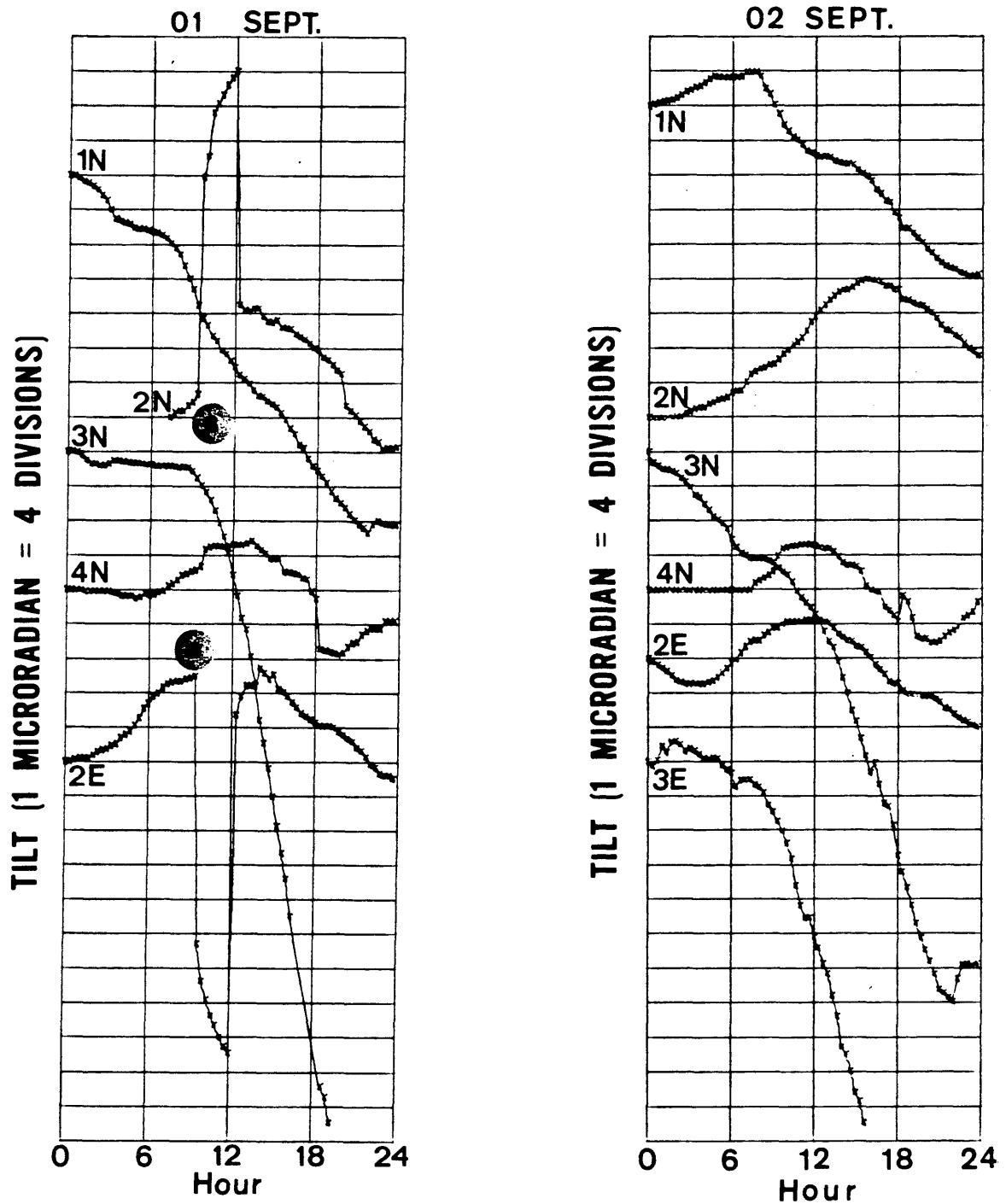


Figure 3-4

Tilt records collected on 01 and 02 September from 00⁰⁰ m to 24⁰⁰ m local time.

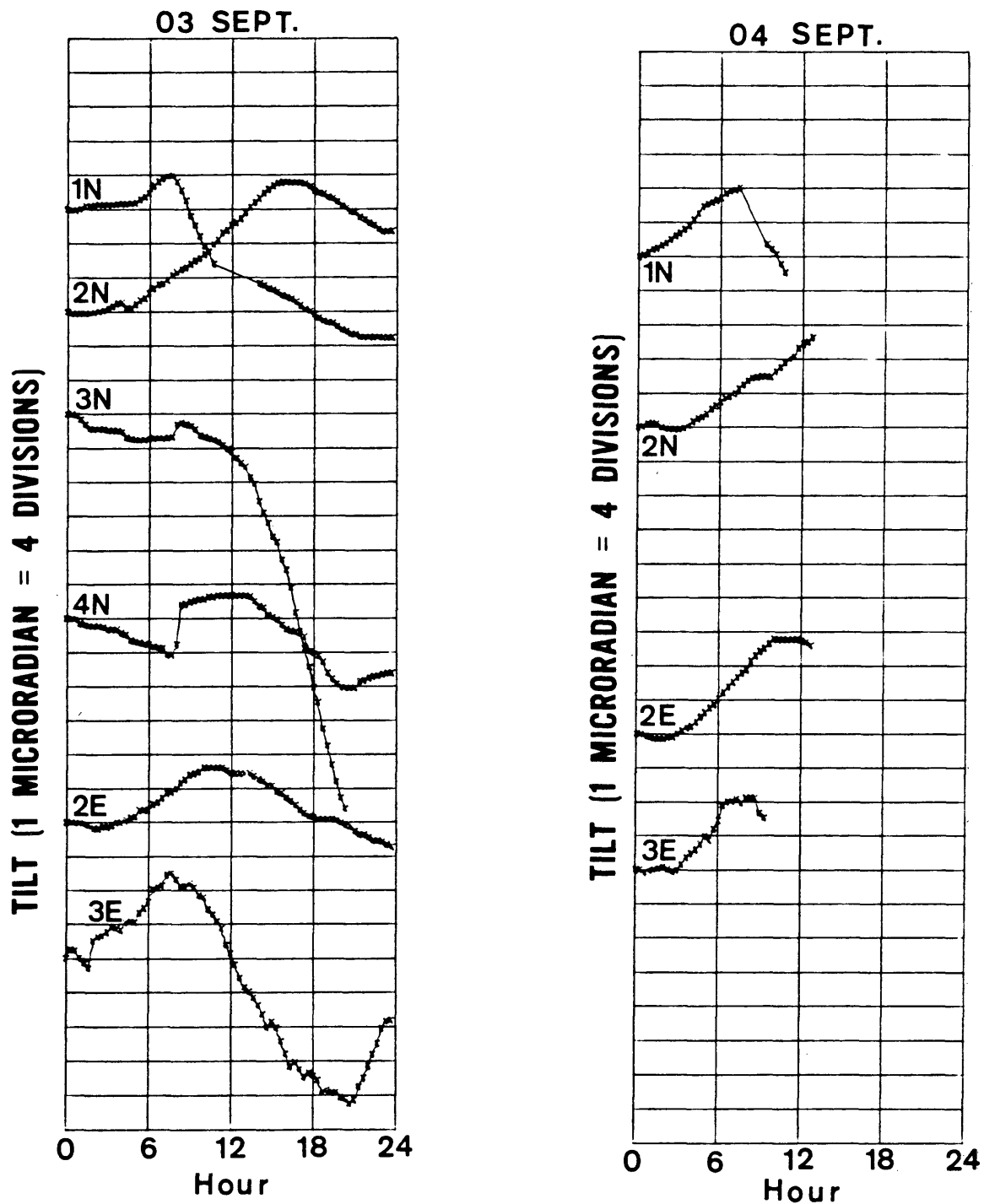


Figure 3-5

Tilt records collected on 03 and 04 September from 00⁰⁰ m to 24⁰⁰ m local time.

If a particular record segment is badly disturbed, and the cause of the disturbance is well known, that segment is of no use and can be discarded. An exception to the rule is that no data from the pumping day may be discarded, regardless of the presence of noise.

All data which contains such identifiable noise, and which will not be considered further, is marked on figures 3-1 through 3-5 with a number near the affected trace, at the approximate time of onset of each noise episode. For such episode so labelled, the nature of the disturbance will be discussed below. If a particular noise episode disrupts more than one site, the same number will be put near each trace so affected at the approximate onset time.

1.) On the morning of August 26 at approximately 0800 local time the irrigation ditch passing near sites 1 and 3 was observed to be dry, having been full on the previous day. Drying of this ditch consistently caused West down and North down tilting which continued for several days, while filling of the ditch consistently resulted in East down and South down tilting which also continued for many days. This particular ditch-drying tilt episode lasted until the ditch was again filled, on the 28th of August.

2.) At approximately 1030 local time on August 27 the vault was entered at site 3. This disturbance caused the North-South component of the tilt record to briefly reverse direction, but after several hours this effect died out, and was overpowered by the gradual North down tilting which started on August 26.

3.) At approximately 0150 local time on August 28 the ditch was flooded, causing a rapid tilting to the South and East. The tilt rate gradually decreased with time, but tilting continued until the ditch dried up again on the 30th.

4.) Between 1200 and 1730 local time on August 29 an automatic sprinkler irrigation system passed over site 2, drenching the site. This caused rapid South down and East down tilting. The North-South component did not recover from this drenching until the 31st of August. It is not clear when the East-West component recovered. The different response of the two channels could possibly be due to the anisotropy of ground cover at the site; the site was located near an East-West trending road which separated a corn field from a hay field. Alternatively, some other condition which was not observed might have caused the difference between channel responses.

5.) On the 29th of August, a storm passed through the area, with rain starting to fall at approximately the

time marked 5 on all traces. What effect the storm had on the records is not known, so consequently no data has been rejected. The possibility exists, however, that the records were complicated to some extent by this storm.

6.) Another tilt episode caused by a drying of the ditch begins on August 30. The ditch was observed to be drying up at the time marked 6, but may have started to dry prior to this time. The resultant North down, West down tilt continues until the ditch fills again, on the 31st of August.

7.) At 0700 local time on the 31st of August the ditch was full, but by 1800 on that same day had begun to dry out. This produced a short period of South down tilting followed by the North down tilt characteristic of a drying episode. This drying lasted until the end of data collection.

8.) The sudden South down, West down tilt at site 2 on the 1st of September and the sudden return several hours later were almost certainly caused by a piece of farm equipment being parked near to the vault.

Based on the previous discussion of noise events, the following channel-days of data are considered to be polluted with noise, and will not be used further.

At site 1, August 26, 27, 30, 31, and September 1.

At site 2, August 30, 31, and September 1.

At site 3, August 26, 27, 30, 31, and September 1 and 2.

At site 4, no data is rejected.

A quick examination of the remaining data shows that on a typical day, excursions in the recorded tilt of 1 micro-radian or more are common. Furthermore, on several traces tilt events exist which have amplitudes of many micro-radians. Since the maximum tilt amplitude expected from the hydrofracture is less than a micro-radian, it is evident that an effort to understand these daily excursions and occasional high amplitude events is necessary. Ideally, such an understanding would enable these noise events to be removed from the records, leaving only the hydrofracture's tilt signature. Practically, an improvement in the signal to noise ratio is possible (Where "noise" is defined as everything except the tilt caused by the hydrofracture.)

The method employed to improve the signal to noise ratio and the resultant data are presented in the next section.

C.) IMPROVING SIGNAL TO NOISE RATIO

1.) Nature of Remaining Noise

Examination of the data on the pumping day, August 28, shows that large deflections begin slightly after the start of the day at sites 1 and 3, but that no such deflections occur at sites 2 or 4. These large tilts were caused by the flooding of the irrigation ditch which passed near sites 1 and 3 only, and which was previously dry. It is unfortunate that this disturbance occurred in a time window which included the pumping interval, since it pushed one record completely off scale (channel 1 E/W), and super-imposed on 3 of the remaining 6 channels a tilt approximately 50 times the anticipated tilt from the hydrofracture.

As a result of the disturbance, two separate schemes for processing the data are necessary, one scheme for the sites not affected by the filling of the ditch (sites 2 and 4), and one scheme for the sites near the ditch (sites 1 and 3). The scheme for sites 2 and 4 is discussed first.

2.) Sites 2 and 4

Examination of figures 5-2 through 5-5 shows a similarity between the records from the 2nd, 3rd, and 4th of September at site 2, and at site 4 a similarity of the

records from August 29, 30, and 31, and September 1, 2, and 3; these being the most noise free days available for study at each site (see fig. 2-7). This similarity suggests that there is some remaining diurnal signal on each channel, which possibly can be removed. Attempts were made to find a relationship between this diurnal tilt signal and the temperature data which was collected, without success. Either temperature is not the principal cause of the diurnal tilt, or the vault temperature curves have a noticeably different shape than the air temperature curves. If the latter is the case, careful monitoring of vault temperature in future experiments might allow the diurnal tilt to be accurately accounted for.

In either event, a more approximate method must be used to treat the diurnal signal in this experiment, starting with the assumption that the physical parameter or parameters which cause the observed tilt vary in a similar manner every day, resulting in daily tilt records which deviate only slightly from some average daily tilt. An approximation of this average daily signal is calculated for each tilt channel in the following manner. Referring to figure 2-7, days for which the record is incomplete and days which are known to contain noise are rejected. Point by point averaging of the remaining days yields an average day, in which the diurnal signal is

emphasized and fluctuations not common to all days are de-emphasized. This approximate diurnal signal is then subtracted from every daily trace, leaving only each day's deviation from the average day.

The residual traces from sites 2 and 4, after removal of the average day, are shown in figures 3-6 and 3-7. Also shown in these figures are the calculated average days; the days used in calculating each average day are indicated next to each average day trace.

3.) Sites 1 and 3

In trying to recover the tilt signal from the hydrofracture at sites 1 and 3, we must not only attempt to approximate and remove the diurnal signal, but must also attempt to approximate and remove the tilt which resulted from the irrigation ditch being filled.

a.) Treating the diurnal tilt

The diurnal effect is treated in the same manner as with sites 2 and 4, the only difference being an increase in the number of days rejected due to noise, since changes in the ditch's water level constitute noise, and unfortunately, occur fairly frequently. In fact, at site 3 the only day used in estimating the diurnal signal is the 3rd of September, because all other days are either incomplete or are closely preceded by a change in the water level of

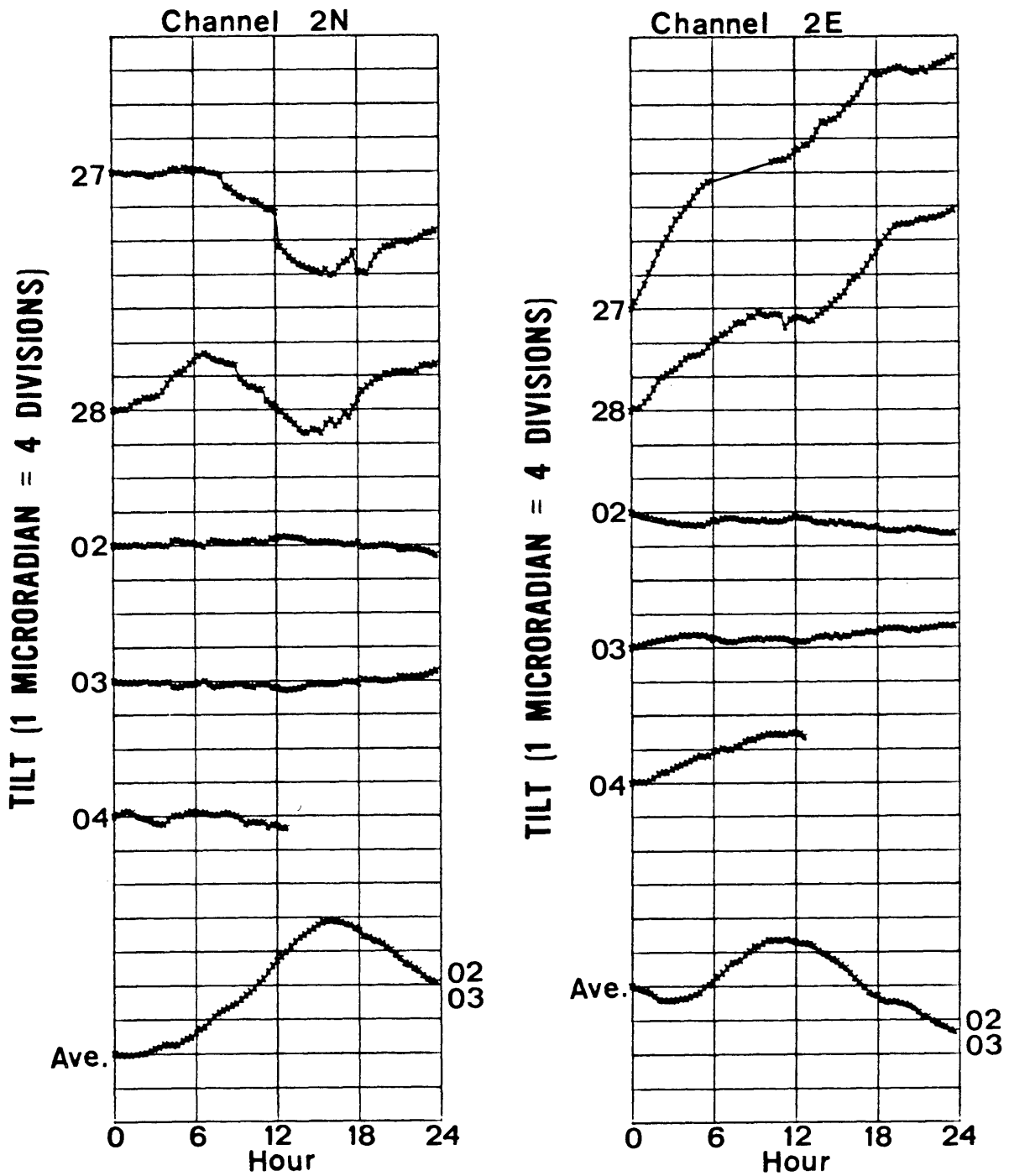


Figure 3-6

Tilt records from site 2 after removal of an average diurnal tilt from every trace.

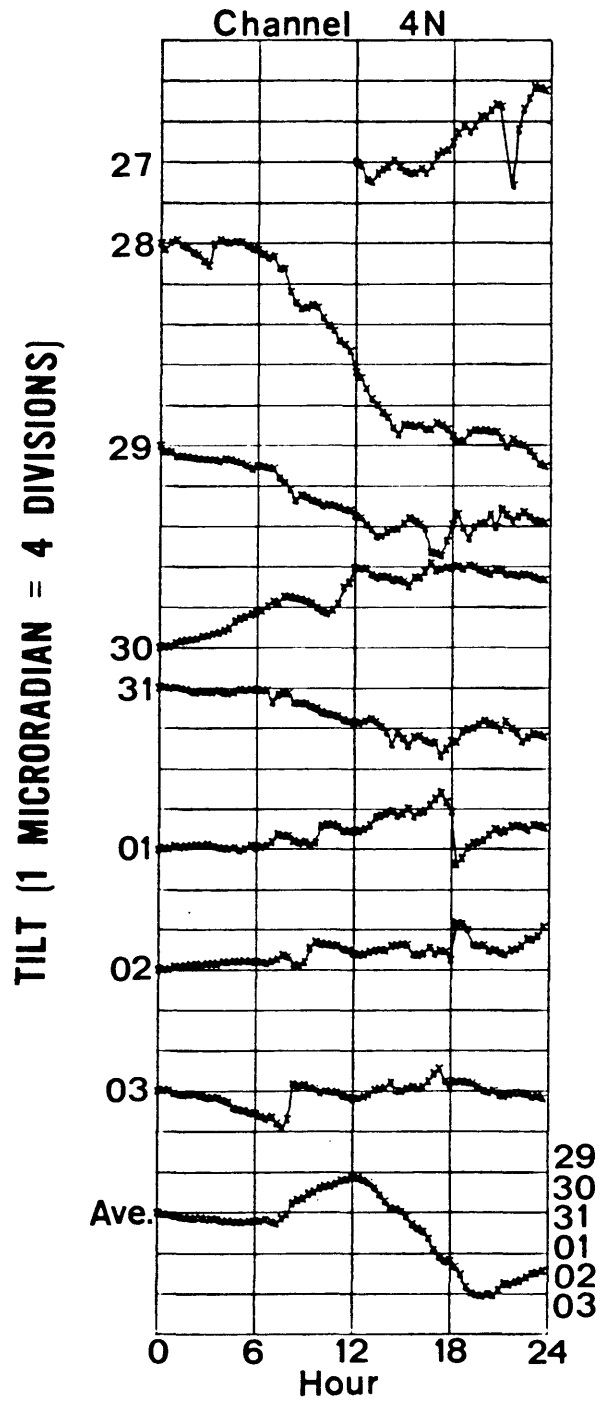


Figure 3-7

Tilt records from site 4 after removal of an average diurnal tilt from every trace.

the ditch. At site 1, the record for the 3rd of September is not complete, so the 2nd of September is used instead. This data is slightly closer to the last preceding time of ditch emptying, however, and thus probably contains slightly more drift than the 3rd. The tilt data, after removal of this diurnal estimate, is shown in figures 3-8 and 3-9.

b.) Treating the irrigation ditch tilt

When the irrigation ditch was filled on August 28 the instruments recorded tilting away from the ditch. This ditch tilt is modelled using the technique presented in the second section of the first chapter. For each tilt channel, a model tilt curve is calculated which represents the best approximation of the portion of the record which is due to the hydraulic transient. Subtracting this model tilt curve from the data should leave an approximation of the tilt which would have existed had the hydraulic transient not occurred.

To calculate the model tilt curve for a particular channel, the parameters t_0 , A_{\max} and $x[4]^{-1/2}$ must be determined, as discussed in chapter 1. t_0 should be common to all records, and the disturbance does appear to strike all channels at approximately 0150 local time. Agreement between channels seems to be a better indicator of t_0 than

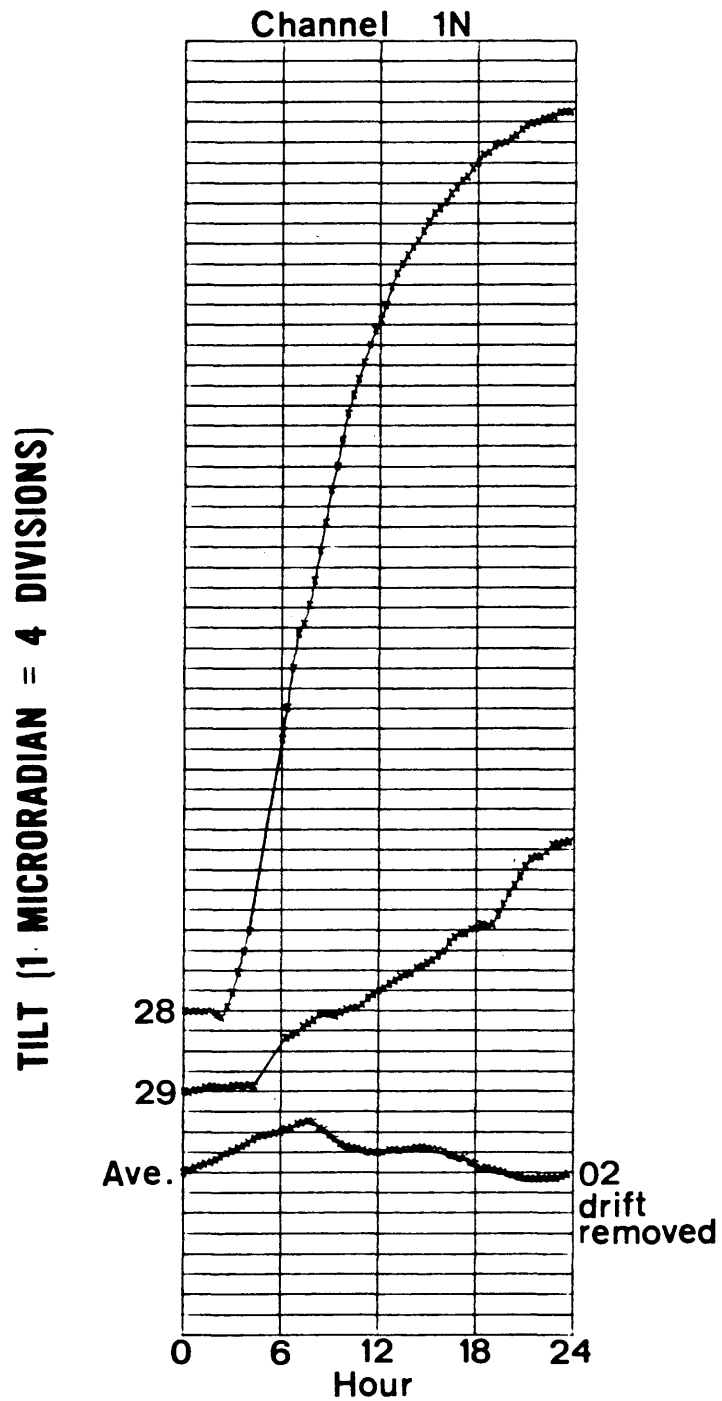


Figure 3-8

Tilt records from site 1 after removal of an average diurnal tilt from every trace.

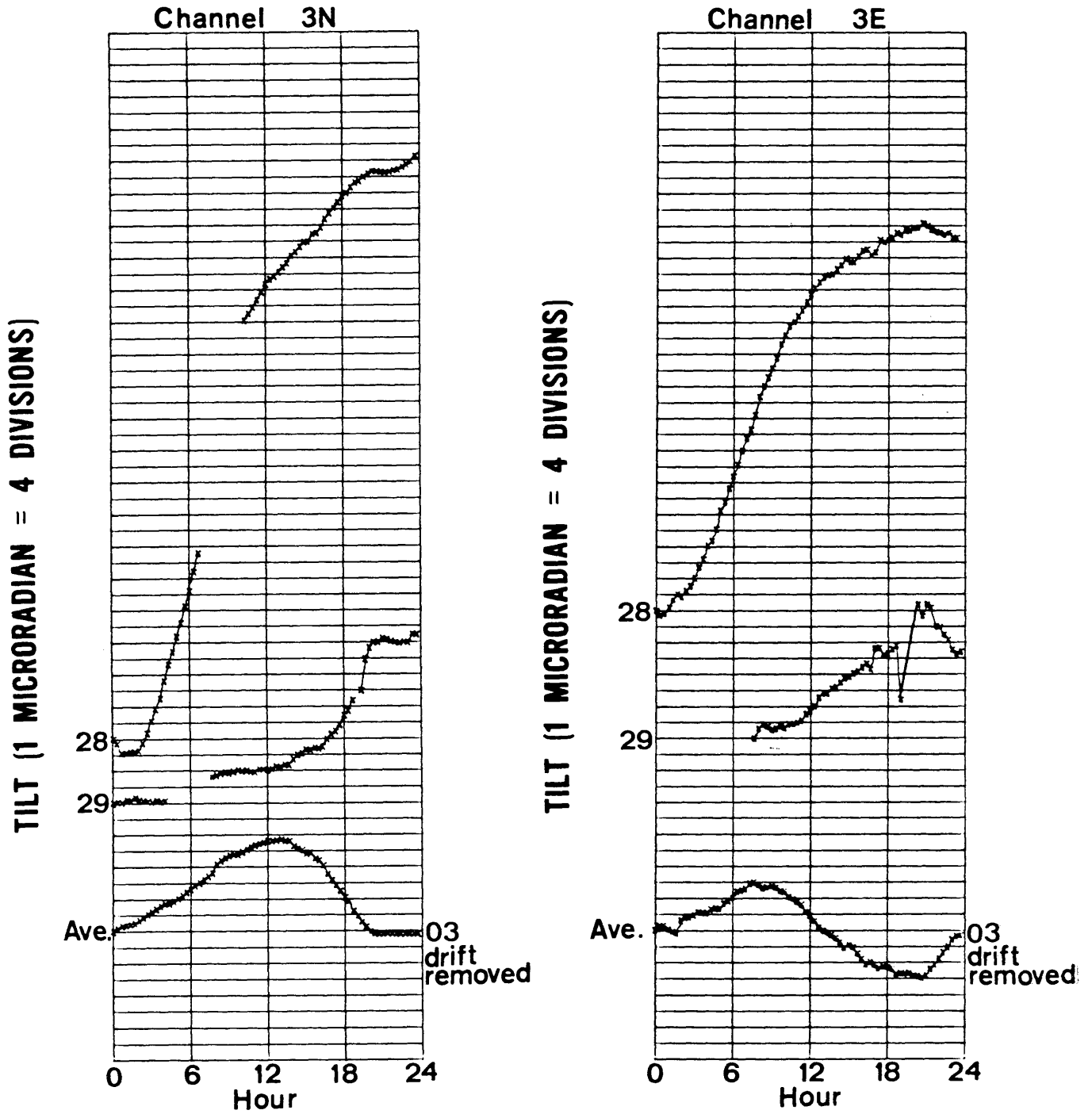


Figure 3-9

Tilt records from site 3 after removal of an average diurnal tilt from every trace.

information provided to the landowner by the operator of the irrigation system regarding the time of day when water was turned into the ditch. (About midnight of the night of August 27-28.)

The values of A_{\max} for each channel are determined in figure 3-10, according to the method described in chapter 1. The values of $x[4\alpha]^{-1/2}$ are determined for each channel in figure 3-11, again following the method described in chapter 1. The parameters t_o , A_{\max} , and $x[4\alpha]^{-1/2}$ for each channel are presented in table 3-1.

		<u>t_o</u>	<u>A_{\max}</u>	<u>$x[4\alpha]^{-1/2}$</u>
1	N/S	01 ⁵⁰	22.5	125
3	N/S	01 ⁵⁰	16.9	118
3	E/W	01 ⁵⁰	13.0	130

Table 3.1

Now that t_o , A_{\max} , and $x[4\alpha]^{-1/2}$ have been determined, the ditch tilt for each component can be estimated by substituting these values into equation 1.18 and calculating tilt values as a function of time from the equation.

These approximate hydraulic tilt transients can now be subtracted from the data shown in figures 3-7 and 3-8,

MAXIMUM AMPLITUDE DETERMINATION
CHANNEL 1N

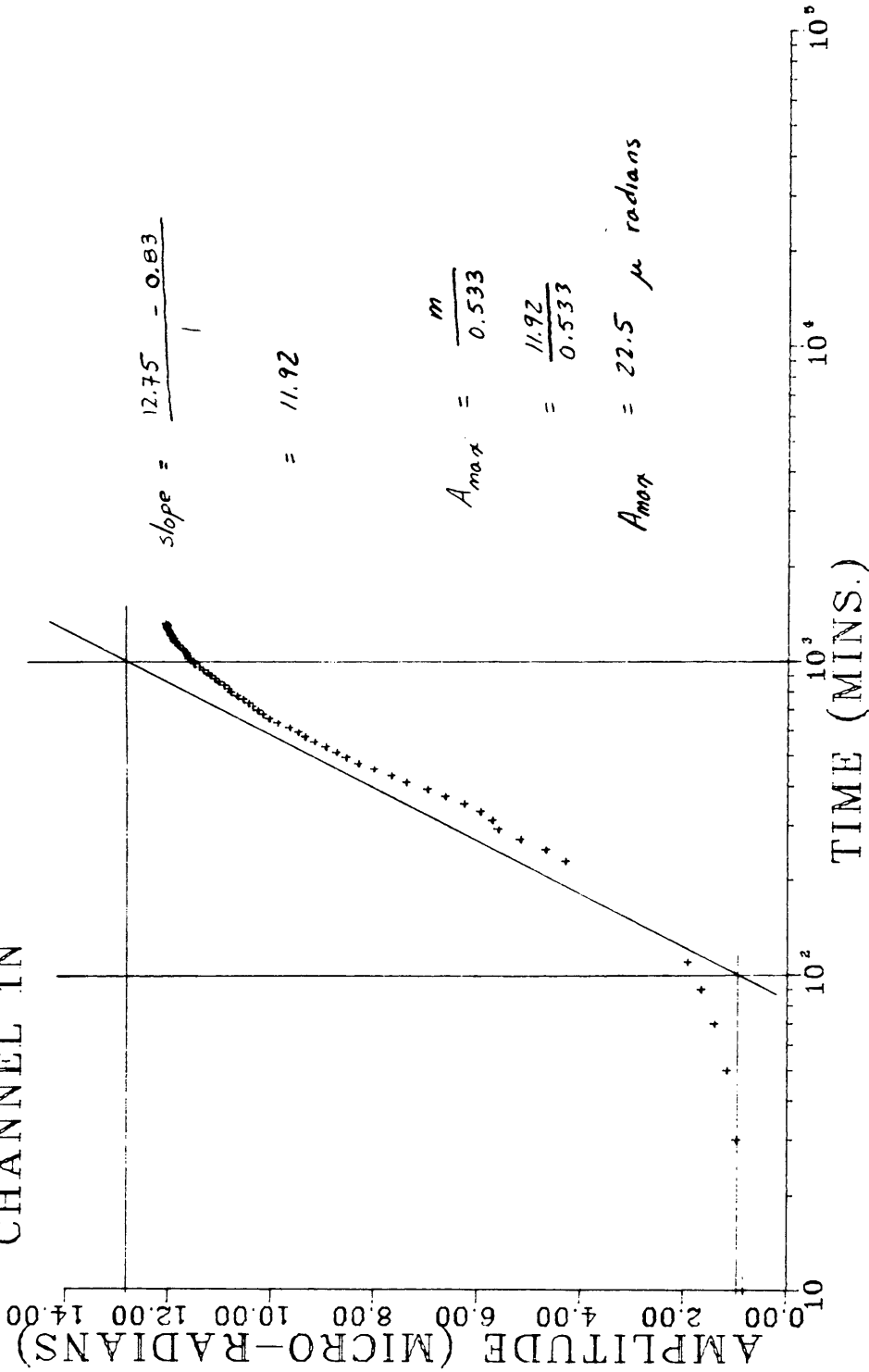


Figure 3-10a

Determination of the hydrologic parameter A_{max} for channel 1N.

MAXIMUM AMPLITUDE DETERMINATION
CHANNEL 3N

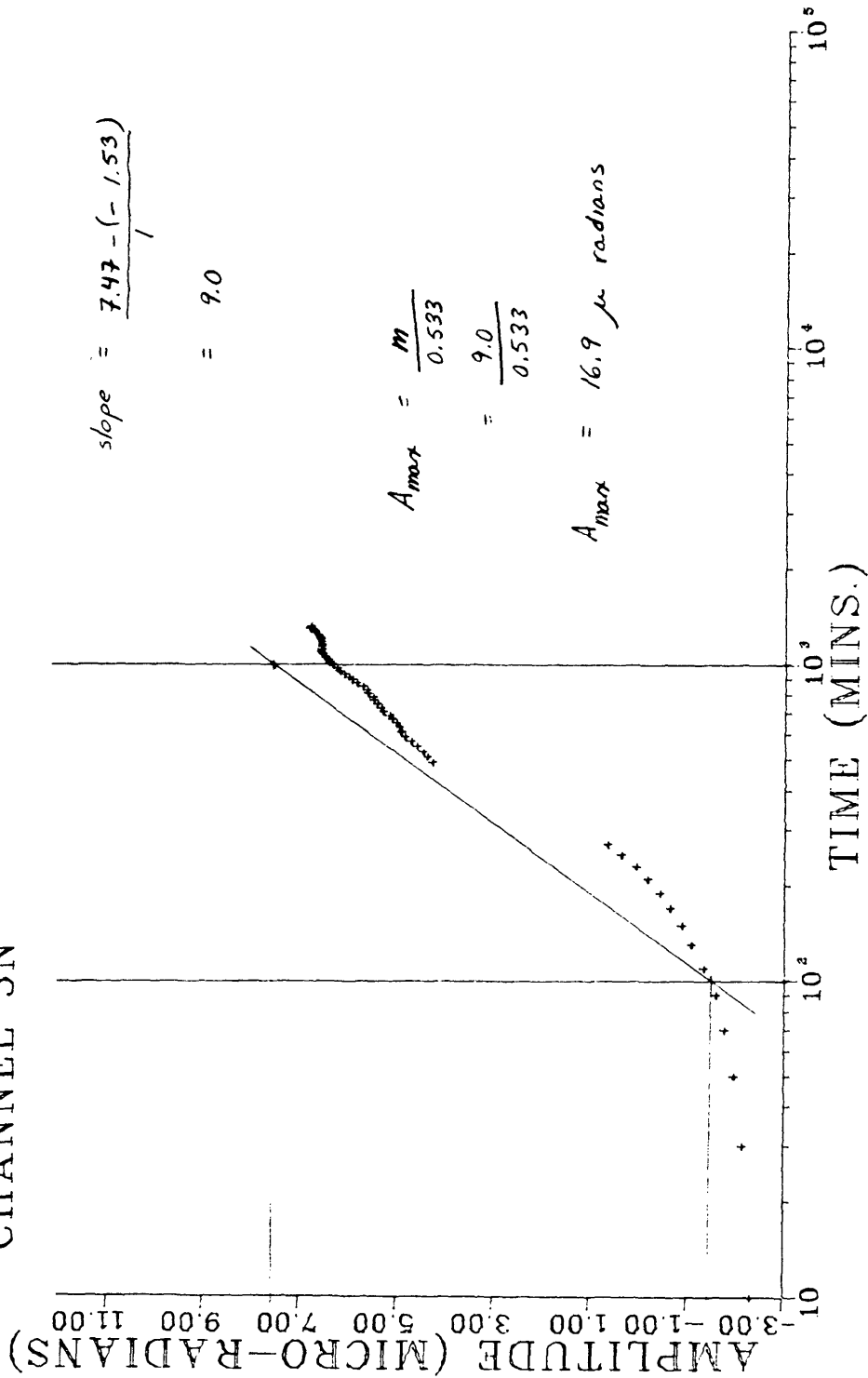


Figure 3-10b

Determination of the hydrologic parameter A_{max} for channel 3N.

MAXIMUM AMPLITUDE DETERMINATION
CHANNEL 3E

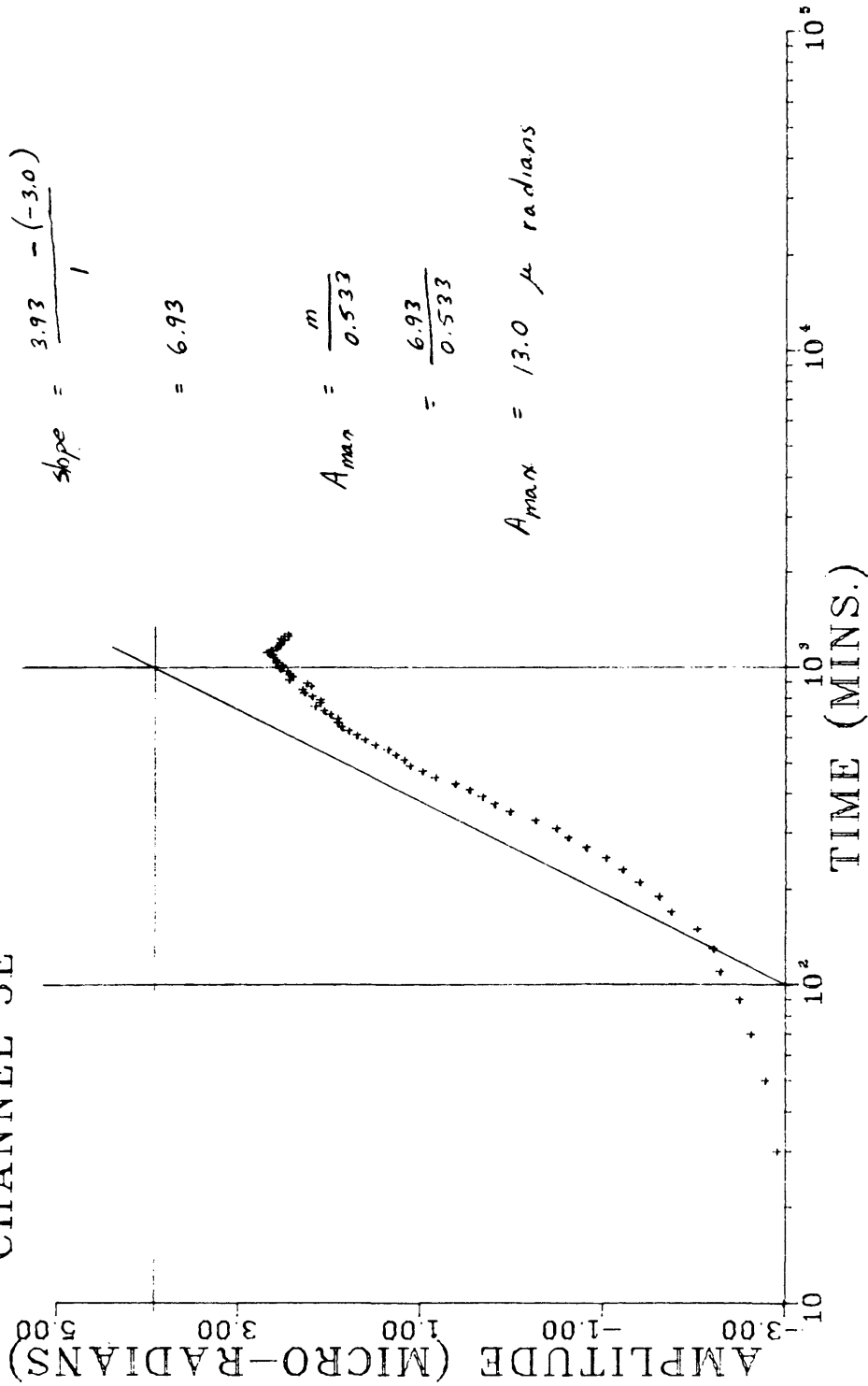


Figure 3-10c

Determination of the hydrologic parameter A_{max} for channel 3E.

NORMALIZED TILT DATA 28-29 AUG.
CHANNEL 1N

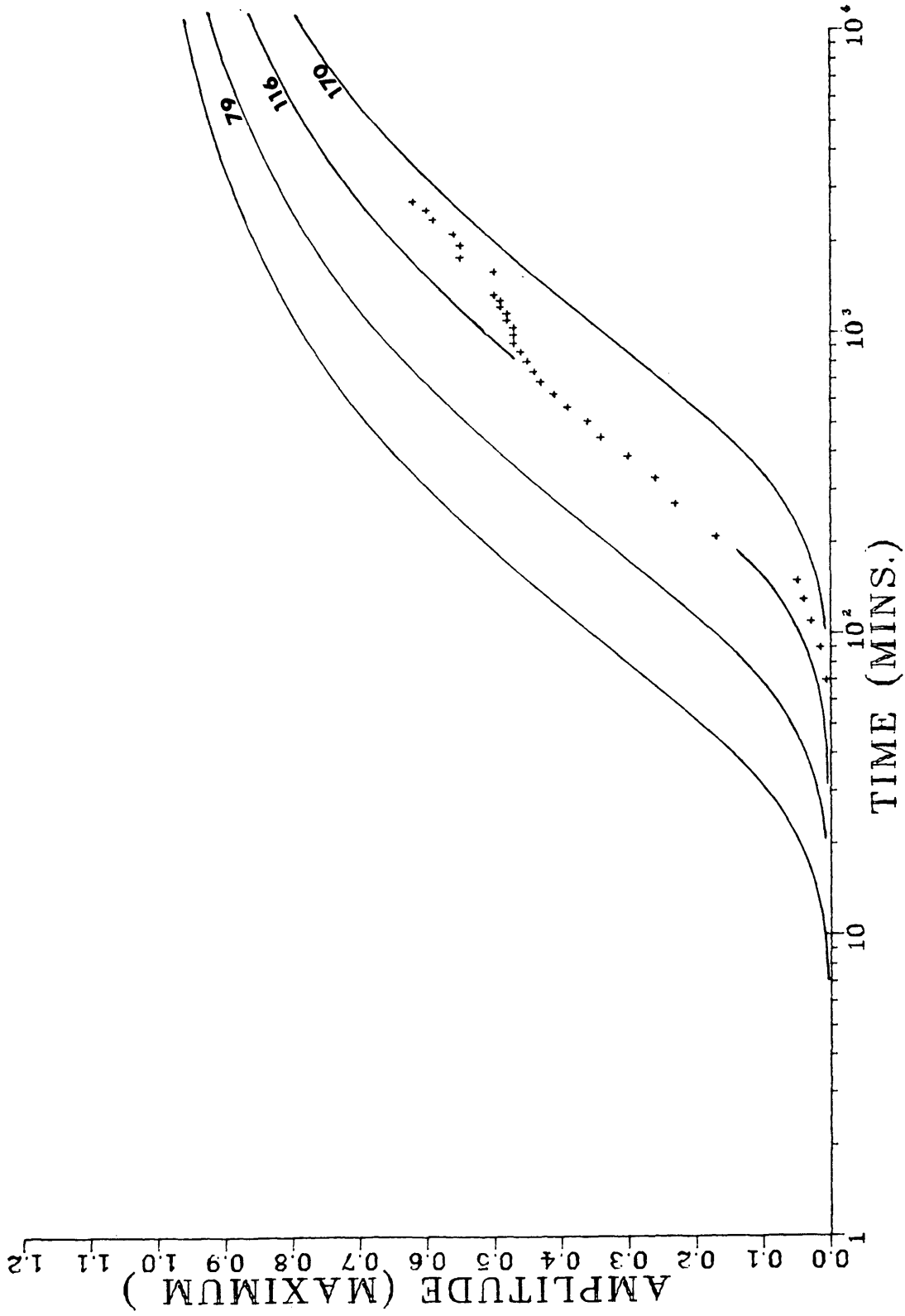


Figure 3-11a

Determination of the hydrologic parameter $\alpha [4\alpha]^{-1/2}$ for channel 1N.

NORMALIZED TILT DATA 28-29 AUG.
CHANNEL 3N

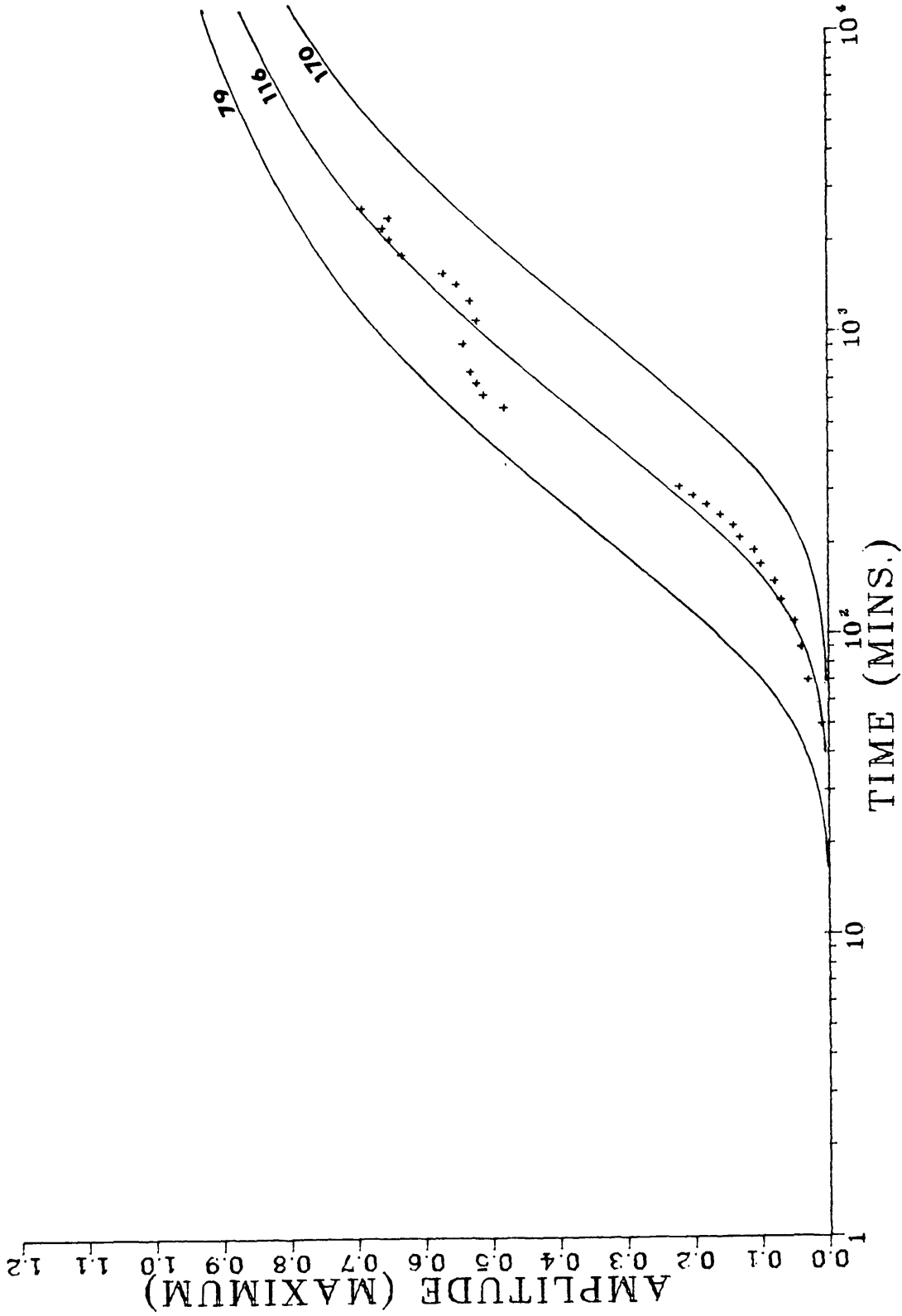


Figure 3-11b

Determination of the hydrologic parameter $\lambda [4Q]^{-1/2}$ for channel 3N.

NORMALIZED TILT DATA 28-29 AUG.
CHANNEL 3E

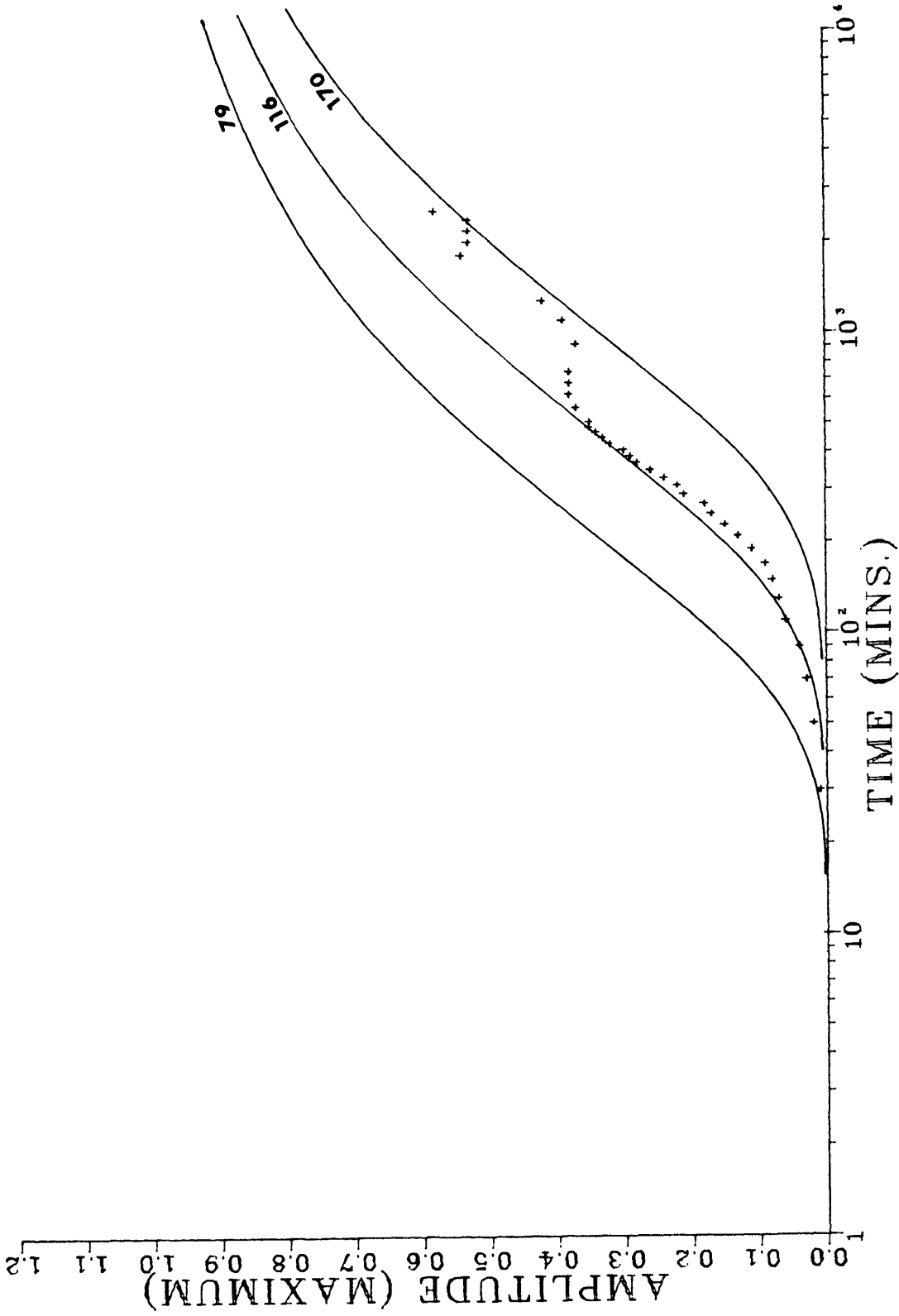


Figure 3-11c

Determination of the hydrologic parameter $\alpha [4\alpha]^{-1/2}$ for channel 3E.

doing so yields the residual curves shown in figure 3-12. Both the average day and the ditch transient have been removed from these curves, they represent the best possible estimate of the hydrofracture tilt of sites 1 and 3. Clearly the noise has been imperfectly removed from the records, and it is still not possible to attribute a particular deflection of the tilt record to the hydrofracture. However, now it is possible to put a meaningful upper limit on the hydrofracture tilt at these sites, something not possible before the ditch transients were estimated.

D.) RESULTS

A collection of the data from the pumping day with the noise processed out according to the schemes discussed above is shown in figure 3-13. The lower-most trace on this figure is a plot of the volume of fracturing fluid injected during the pumping operation as a function of time. This trace shows data obtained from the Amoco Production Company which gives the volume of material injected into the well during pumping and the volume of fluid recovered after pumping. The data provided by Amoco is reproduced in Appendix 3. Any tilt signature from the hydrofracture should have approximately this same shape. The residual signal on tract 4N has a remarkably similar

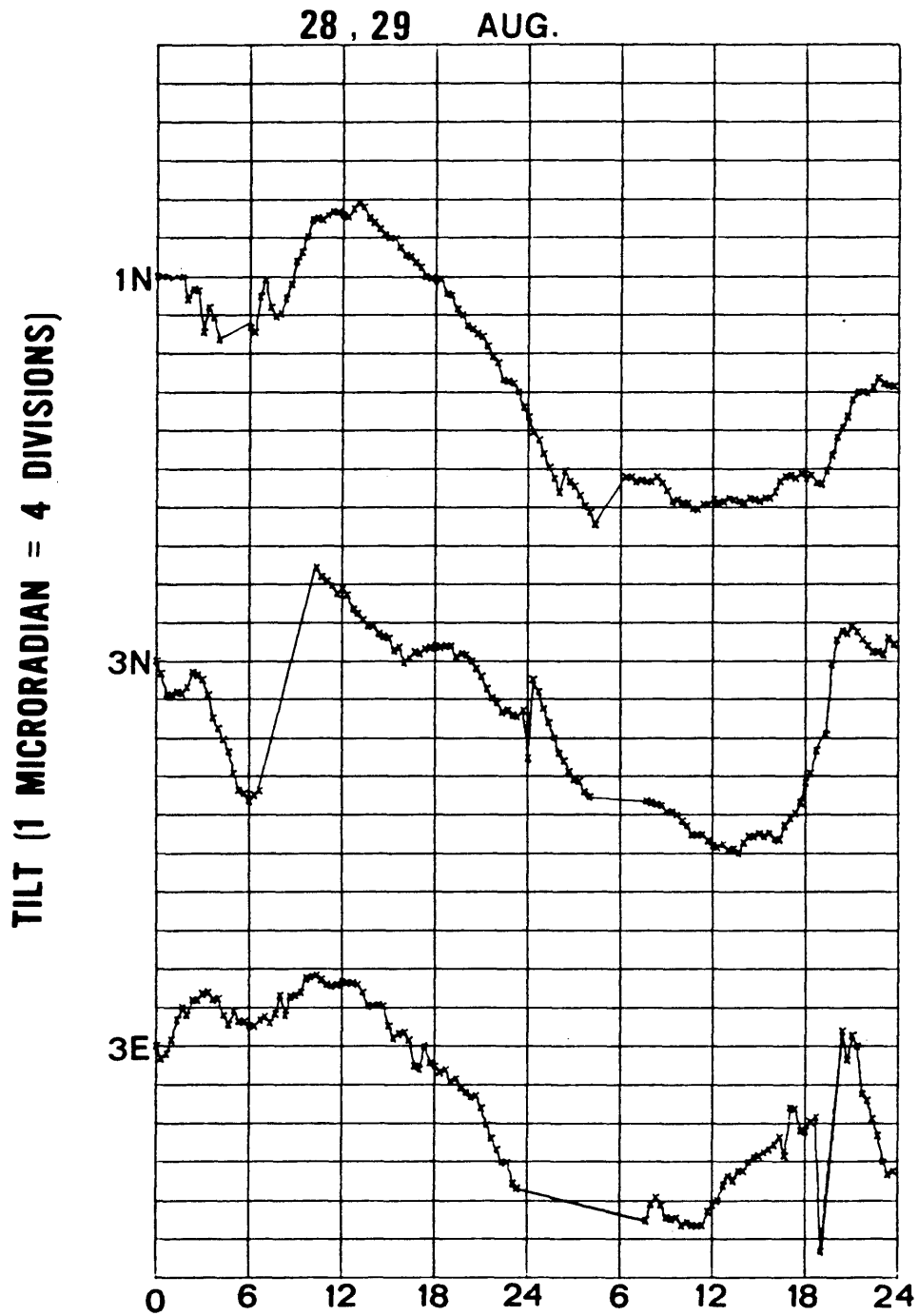


Figure 3-12

Residual curves for channels affected by the ditch tilt, after removal of the diurnal signal and the approximate ditch tilt.

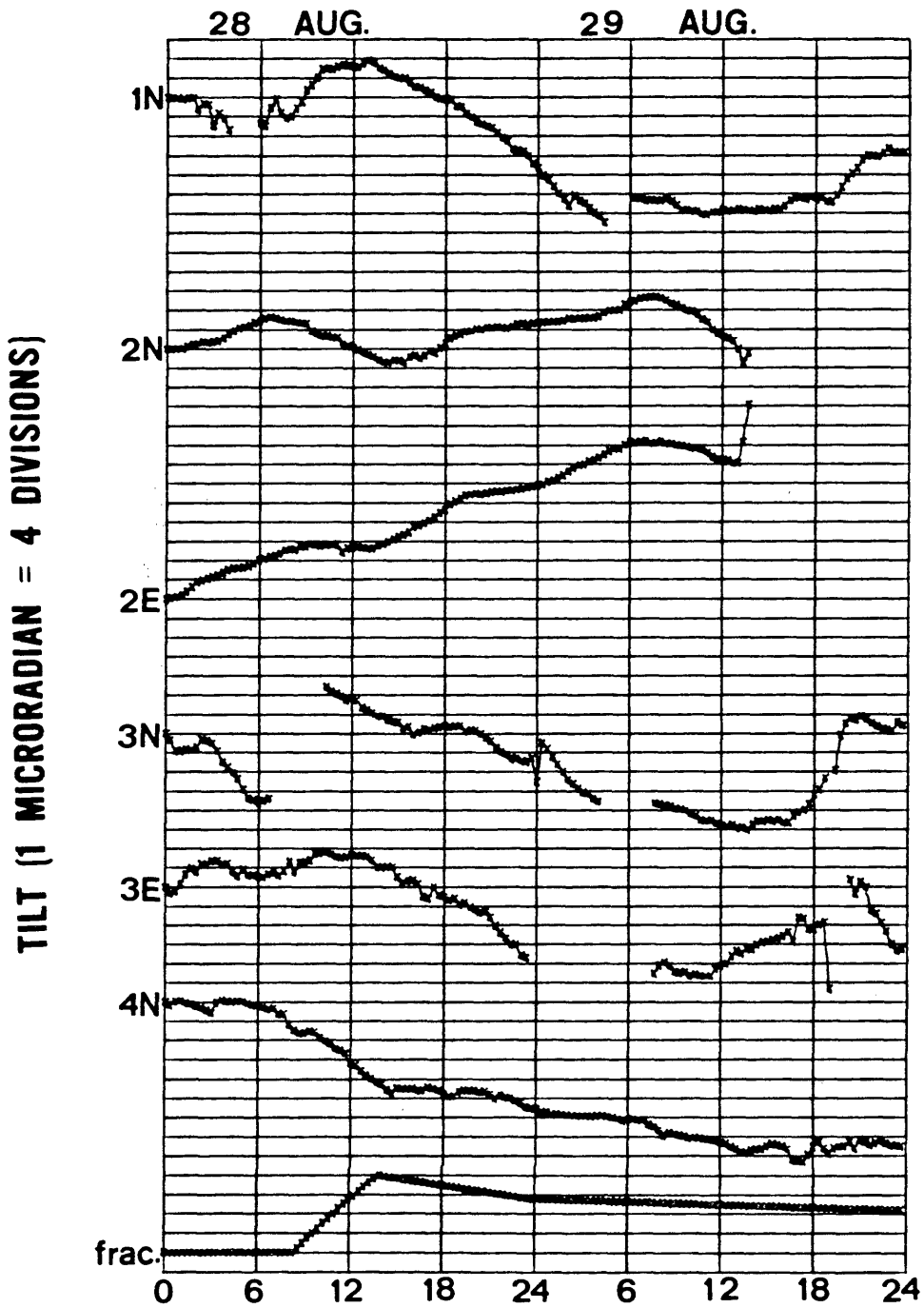


Figure 3-13

Collection of data from all channels during the pumping interval including a plot of the volume of fluid injected into and recovered from the fracture.

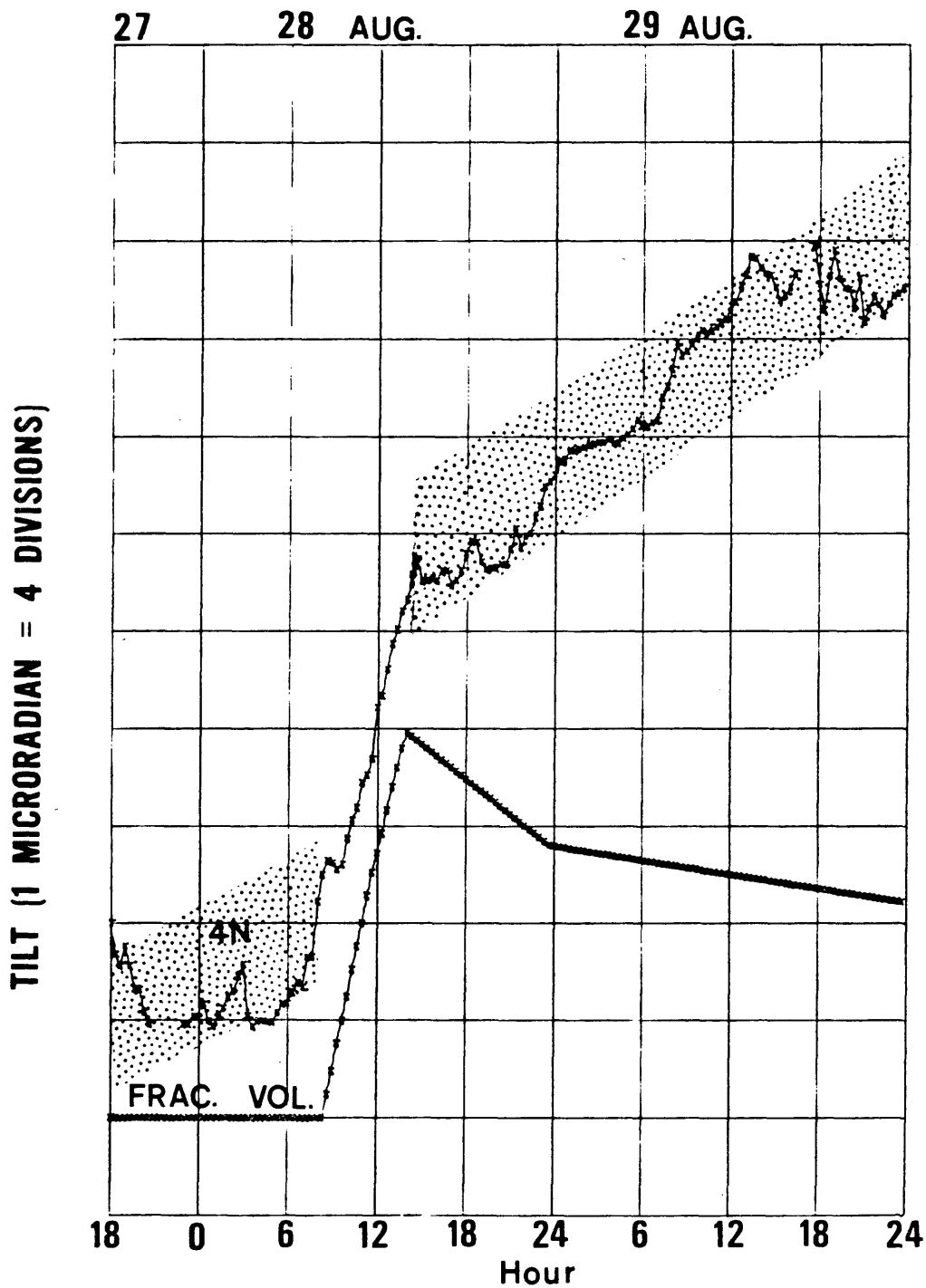


Figure 3-14

Channel 4N and the fracture volume as a function of time during the pumping operation. The high frequency noise on the tilt record is contained in the stippled envelope.

shape, which strongly suggests this tilt is due to the hydrofracture. No other channels show tilt which can realistically be attributed to the hydrofracture, but upper limits for the tilt due to the hydrofracture can be estimated for each remaining channel. An estimate of the hydrofracture tilt at site 4 and estimates for the upper limits for hydrofracture tilting at the other sites are given in table 3-2.

<u>Channel</u>	<u>Tilt (micro radians)</u>	<u>Upper Limit (micro radians)</u>
1N	--	0.75
2N	--	0.75
3E	--	0.5
3N	--	1.0
3E	--	0.5
4N	0.7	--

Table 3.2

SUGGESTIONS FOR FUTURE OPERATIONS

Although this experiment was not outstandingly successful from the standpoint of locating the hydrofracture, at least one signal proved encouraging, and a second attempt to determine a hydrofracture orientation with tiltmeters is probably justifiable. If such an attempt is to succeed, a fracture program just as large and just as shallow as the Hemple #2 program should be studied, and improvements must be made in the field technique to reduce the site noise to below the amplitude of the anticipated signal. If the following changes in experimental technique were to be implemented, this noise reduction may be realizable.

To obtain a more complete record set:

1.) Circuitry should be installed which will automatically actuate the micrometer motors when the output voltage approaches the saturation level of the amplifier. This measure should eliminate all loss of records from the output drifting off-scale.

2.) Two or more additional tiltmeters should be deployed in the field. This measure would improve the data density and would reduce the severity of the loss if a site were to prove to be unacceptably noisy.

T-2198

3.) A better mechanism should be provided for leveling and anchoring the recorder boxes to the ground; this should eliminate some of the record loss due to inking failures. Possible anchoring schemes are: a) mounting the boxes on short threaded rods, as the tiltmeters are mounted, or b) setting the boxes on leveled bricks and securing them to the ground with cord and tent pegs.

To Improve Tiltmeters:

Several modifications might be made to the tiltmeters which would make their initial setup and subsequent operation less troublesome.

1.) The positioning of the ligature wires with respect to the suspension wires should be improved so delicate adjustments are not required to keep these wires from interfering with one another.

2.) A port or tool should be included through which the capacitor air gaps could be viewed. This would allow the operator to be confident his initial adjustments of the pendulum position were correct.

3.) Higher quality tunable inductors should be used in the electronics boxes. This should eliminate the "skipping" sometimes experienced while tuning the circuits.

To Reduce Site Noise:

1.) Avoid irrigation ditches or other sources which might alter the groundwater table during the experiment.

2.) Arrange to rope off an area approximately 30 meters in radius around each site to prevent unwanted surface loads.

3.) The sites could be monitored with a small movie camera, equipped with a wide angle lens, exposing 1 or 2 frames per minute. This would allow positive identification of noise sources.

To Improve Data Analysis:

1.) The vault temperature should be recorded to 0.1°C in order to attempt to correlate temperature with the diurnal signal.

2.) If possible, the tiltmeters should be running and the vaults should not be entered for several days before the pumping operation.

CONCLUSIONS

By considering a hydrofracture to be a dislocation on a surface within an elastic half space, Volterra's method in elasticity theory can be used to model the displacement and tilt fields at the earth's surface which are caused by the hydrofracture. This method models a dislocation as a distribution of point force combinations, or nuclei of strain, over the dislocation surface. Different types of strain nuclei represent different types of dislocations; the strain nucleus which represents a hydrofracture dislocation consists of a double force without moment and a center of dilatation. An equation which describes the vertical component of displacement at a point on the earth's surface caused by this type of dislocation is given by Maruyama, but he neglects in his formulation of the equation to include the contribution made by the center of dilatation. Including the dilatation term and taking spatial derivatives of Maruyama's equation gives expressions for surface tilt, these expressions are used to make maps of the surface tilt field in the vicinity of the hypothetical hydrofracture.

These maps of the modelled tilt response show that:

- 1) Tilts as large as $\sim 3.0 \times 10^{-7}$ radians should be expected from a large, shallow (vol. = 10^3 m^3 , depth =

T-2198

1 km), hydrofracture, and 2) that the shape of the tilt field strongly reflects the fracture orientation. These modelling results were promising enough that a field experiment was carried out in August and September of 1978 at the site of an Amoco Production Company well in Weld County Colorado. The goal of this experiment was to sample the tilt field set up by the fracturing operation in hopes of determining the fracture orientation. The results of the field experiment are:

1.) One record channel showed a tilt of $\sim 7 \times 10^{-7}$ radians which was probably caused by the hydrofracture. This is greater than the largest magnitude of tilt predicted by the modelling study, and suggests that the method used to model surface tilts is probably valid.

2.) Six record channels produced records on which no hydrofracture tilt signal could be identified. This indicates that if a future experiment is to be successful, efforts must be made to eliminate much of the troublesome noise in the 1 to 24 hour period range which was present in this experiment.

Based on experience gained during this experiment, the following modifications of experimental parameters are suggested to improve the data quality in a second hydrofracture tilt field experiment.

T-2198

1.) To obtain a more complete record set: Automatic instrument rezeroing, deploying 2 more tiltmeters, and a simple mechanism for leveling and securing the recorder boxes to the ground.

2.) To simplify instrument adjustment: A slight change in ligature-suspension wire geometry, a method for viewing capacitor air gaps, and higher quality tuning slugs.

3.) To reduce site noise: Avoid locating near irrigation ditches, rope off 30 m radius area around vault, and use a movie camera with a wide angle lens to provide a visual record of noise sources.

4.) To improve field technique: monitor vault temperature and operate instruments a greater time before the fracture.

Two of the four sites selected in this experiment were within 50 m of an irrigation ditch. Tilt episodes with amplitudes as large as 2×10^{-5} radians were observed to coincide with flooding of the ditch. Assuming surface tilt to be proportional to groundwater table tilt allowed the observed tilt to be modelled with a hydrologic equation.

Three parameters in this equation must be determined in order to specify a particular tilt transient, these parameters involve the aquifer properties permeability,

T-2198

void ratio, thickness of water table, leakage rate, and flooding onset time.

If these properties are not known, the three hydraulic parameters t_o , A_{max} and $x[4\alpha]^{-1/2}$ can be determined graphically from the tilt records. Curves calculated using this technique fit the observed tilt transients to about 1 part in 20.

Possible applications of this hydraulic transient tilt modelling technique are: 1) approximately removing undesirable transients from tilt records, (as was done in this experiment), 2) evaluation of aquifer properties in the vicinity of leaky ditches, and 3) providing information helpful in choosing tiltmeter sites which will not be subject to hydraulic transient tilts.

APPENDIX 1 DISPLACEMENT MAP PROGRAM

This program is adapted from a program written by Dr. Yeatts. It produces a lineprinter map of vertical surface displacements. The program is written in the language basic. Two programs must be run to make a map: One program to build a displacement array, another program to contour and print the data.

A map can be made on the lineprinter by the following commands.

```
.R BASIC  
READY OLD HYDROF  
READY RUN  
READY OLD FRAPLT  
READY RUN  
READY SYS
```

The user can choose fracture dimensions, map dimensions, and relationship of map boundaries to the hydrofracture.

Suppose fracture dimensions of $L = 1.0$ km., $H = 2.0$ km., and $x = 1.0$ cm. are desired. (W always must be $0.2 \times L$). Suppose the map is to be 2.0 km. \times 1.5 km., starting 0.5 km. to the left of the fracture and starting at the center of the hydrofracture, like figure 1-8. To make such a map, do the following.

- 1) Normalize all values to the fracture

length. For this example,

$$L = .1.0$$

$$H = 2.0$$

$$x = 10^{-5}$$

$$\text{map length } x = 2.0$$

$$\text{map length } y = 1.5$$

$$\text{map start } x = -0.5$$

$$\text{map start } y = 0.0$$

2) Multiply the x and y starting values by 10, and subtract 0.25 from the x starting value, so map start $x = -4.75$, and map start $y = 0.0$

3) Multiply the map lengths by 10 and add to the starting values to get the final values, so map finish $x = 15.25$, and map finish $y = 15.0$.

4) Substitute the x start and finish values into line 160 and substitute the y start and finish values into line 170 in the program HYDROF.BAS giving

```
0160 FOR X9 = -4.75 TO 15.25 STEP 0.5
```

```
0170 FOR X9 = 0.0 TO 15.0 STEP 0.5
```

5) Multiply H by 10 and insert into line 190, giving

```
0190 FOR U = 20. + G TO .....
```

The programs can now be executed as outlined above, and will produce a lineprinter map of contoured vertical surface displacements. The contour values will be in values of x meters.

```
00010 FILES FRADAT
00020 SCRATCH #1
00040 P1=.314159/18
00050 N=4
00060 G=1/N
00070 K=5-G
00160 FOR X9=-6.25 TO 13.5 STEP .5
00170 FOR Y9=0 TO 14.5 STEP .5
00180 S=0
00190 FOR U=20+G TO 22-G STEP 2*G
00200 X5=0
00210 Z5=U
00220 X=(X9-X5)/Z5
00230 X2=X^2
00240 O=(2*G/Z5)^2
00250 FOR Y5=-K TO K STEP 2*G
00260 Y=(Y9-Y5)/Z5
00270 Y2=Y^2
00280 Z=X*Y
00290 R=SQR(X2+Y2+1)
00300 A=1/R
00310 A2=A*A
00320 A3=A2*A
00330 A5=A3*A2
00340 A7=A5*A2
00350 B=1/(R+1)
00360 B2=B*B
00370 B3=B2*B
00380 B4=B3*B
00390 F2=6*A5
00400 K0=-A*B
00410 L=A3-A*B2-F2
00500 E=K0+L*X2
00510 E=O*E
00520 S=S+E
00670 NEXT Y5
00680 NEXT U
00740 PRINT #1,S
00760 NEXT Y9,X9
00770 END
```

PROGRAM HYDROF.BAS

```
00010 FILES FRADAT
00030 DIM A(40,30), B(39,29), C(29,70)
00040 DIM D(3,5), E(57,39), F(3,3)
00050 DIM U(39,70), V(57,70)
00060 FOR I=1 TO 40
00070 FOR J=1 TO 30
00080 INPUT #1, A(I,J)
00100 NEXT J,I
00110 FOR I=1 TO 39
00120 FOR J=1 TO 29
00130 B(I,J)=A(I,J)
00150 NEXT J,I
00155 PRINT "CHECK AREAL (6,15)";B(6,15)
00156 PRINT
00157 PRINT
00158 PRINT
00160 MAT C=ZER
00170 MATREAD D
00180 DATA 4,2,0,0,0,1,3,5,3,1,0,0,0,2,4
00190 MAT D=(1/5)*D
00200 FOR I=1 TO 29
00210 FOR J=1 TO 70
00220 K=INT((J-1)/5)
00230 M=INT((I+K-1)/3)
00240 IF K<>M THEN 270
00250 L=J-5*K
00260 N=I-2*M
00265 C(I,J)=D(N,L)
00270 NEXT J,I
00280 MAT U=B*C
00290 MAT E=ZER
00300 MATREAD F
00310 DATA 2,1,0,0,3,0,0,1,2
00320 MAT F=(1/3)*F
00330 FOR I=1 TO 57
00340 P=INT((I-1)/3)
00345 FOR J=1 TO 39
00350 R=INT((J+P-1)/3)
00360 IF P<>R THEN 400
00370 Q=I-3*P
00380 S=J-2*P
00390 E(I,J)=F(Q,S)
00400 NEXT J,I
00410 MAT V=E*U
00420 FOR I=1 TO 57
00430 FOR J=1 TO 70
00440 V=V(I,J)

00450 IF V>-.384 THEN 471
00460 PRINT "6";
00470 GO TO 850
00471 IF V>-.352 THEN 480
```

PROGRAM FRAPLT.BAS

```
00472 PRINT ' ';
00473 GO TO 850
00480 IF V>-.320 THEN 501
00490 PRINT '5';
00500 GO TO 850
00501 IF V>-.288 THEN 510
00502 PRINT ' ';
00503 GO TO 850
00510 IF V>-.256 THEN 531
00520 PRINT '4';
00530 GO TO 850
00531 IF V>-.224 THEN 540
00532 PRINT ' ';
00533 GO TO 850
00540 IF V>-.192 THEN 561
00550 PRINT '3';
00560 GO TO 850
00561 IF V>-.160 THEN 570
00562 PRINT ' ';
00563 GO TO 850
00570 IF V>-.128 THEN 591
00580 PRINT '2';
00590 GO TO 850
00591 IF V>-.096 THEN 600
00592 PRINT ' ';
00593 GO TO 850
00600 IF V>-.064 THEN 621
00610 PRINT '1';
00620 GO TO 850
00621 IF V>-.032 THEN 630
00622 PRINT ' ';
00623 GO TO 850
00630 IF V>0 THEN 651
00640 PRINT '0';
00650 GO TO 850
00651 IF V>.032 THEN 660
00652 PRINT ' ';
00653 GO TO 850
00660 IF V>.064 THEN 681
00670 PRINT 'A';
00680 GO TO 850
00681 IF V>.096 THEN 690
00682 PRINT ' ';
00683 GO TO 850
00690 IF V>.128 THEN 711
00700 PRINT 'B';
00710 GO TO 850
00711 IF V>.160 THEN 720
00712 PRINT ' ';
00713 GO TO 850
00720 IF V>.192 THEN 741
```

```
00730 PRINT "C";
00740 GO TO 850
00741 IF V>.224 THEN 750
00742 PRINT " ";
00743 GO TO 850
00750 IF V>.256 THEN 771
00760 PRINT "D";
00770 GO TO 850
00771 IF V>.288 THEN 780
00772 PRINT " ";
00773 GO TO 850
00780 IF V>.320 THEN 801
00790 PRINT "E";
00800 GO TO 850
00801 IF V>.352 THEN 810
00802 PRINT " ";
00803 GO TO 850
00810 IF V>.384 THEN 840
00820 PRINT "F";
00830 GO TO 850
00840 PRINT " ";
00850 NEXT J
00860 PRINT
00870 NEXT I
00880 END
```

APPENDIX 2 TILT MAP PROGRAM

This program creates a tilt vector map similar to figure 1-8. The user can specify the fracture dimensions L, H, and Δx as shown in figure 1-2. The dimension W is fixed at $0.2 \times L$. The user can also specify the map dimensions and position with respect to the hydrofracture.

Suppose fracture dimensions $L=1.0$ km., $H=2.0$ km., map length $x = 2.0$ km. and map length $y = 1.5$ km. are desired. Suppose further the map is to start 0.5 km. to the left of the fracture and at the center of the fracture (as in figure 1-8). To create such a map, do the following.

First, normalize all variables to L, so $L = 1.0$, $H = 2.0$, $\Delta x = 10^{-5}$, map $x = 2.0$, map $y = 1.5$, map start $x = -0.5$, and map start $y = 0.0$.

Second, multiply x by 10^5 , so for this example,
 $\Delta x = 1.0$

Third, substitute these values into the correct variables in the program tilt, as follows. (These variables are the first six executable fortran statements.)

L: L always 1 (built into program).

H: H = 2.0

Δx : X = 1.0

map length x: MAPX =2.0

map length y: MAPY = 1.5
map start x: X9S = -0.5
map start y: Y9S = 0.0

The program can now be executed to generate a plot,
with the command

```
EX TILT,TLTPLT
```

No interaction is required, the program creates a plot file
during execution.

DISPLAY OPTIONS

If a denser sampling of the tilt field is desired,
increase the value of the variable NPTSX in TILT.

If a different size plot is desired, change the value
of the variable FACT in TLTPLT.

If the arrows are not of a convenient length, all
can be scaled up or down by changing the value of the den-
ominator in the fortran statement VECL=VECL/4.00 in TLTPLT.

The program will not plot vectors for tilts less than
 1.0×10^{-9} radians. This threshold can be changed by altering
the additive constant in the statement VECL=ALOG10(TMAGN)+4.
in TLTPLT.

```

DIMENSION XT(30,30),YT(30,30)
REAL K,MAPX,MAPY
C
H=2.0
X=1.0
MAPX=2.0
MAPY=1.5
X9S=-0.5
Y9S=0.0
C
N=4
G=1./N
K=5.-G
X9S=X9S*10.
X9F=X9S+(MAPX*10.)
NPTSX=10
XDIF=X9F-X9S
XINC=XDIF/FLOAT(NPTSX-1)
X9=X9S-XINC
  DO 400 I=1,NPTSX
    X9=X9+XINC
    Y9S=Y9S*10.
    Y9F=Y9S+(MAPY*10.)
    YDIF=Y9F-Y9S
    NPTSX=INT(NPTSX*(YDIF/XDIF))
    Y9=Y9S-XINC
    DO 300 J=1,NPTSX
      Y9=Y9+XINC
      TILTXT=0.
      TILTYT=0.
      UINC=2.*G
      TOP=H*10.+G
      U=TOP-UINC
      DO 200 L=1,4
        U=U+UINC
        O=((2.*G)/U)**2.
        X=X9/U
        X2=X*X
        Y5=-(K+UINC)
        DO 100 M=1,20
          Y5=Y5+UINC
          TILTX=0.
          TILTY=0.
          Y=(Y9-Y5)/U
          Y2=Y*Y
          R=(X2+Y2+1)**.5
          A=1./R
          A2=A*A
          A3=A2*A
          A5=A2*A3
          A7=A5*A2

```

*PROGRAM
TILT*

```

      B=1./(R+1.)
      B2=B*B
      B3=B2*B
      TXC=X9/(U**2.)
      TF1=((-3*A5)+(A3*B2)+(2*A2*B3)+(30*A7))
      TF2=(X9/U)**2.
      TX1=(A3*B)+(A2*B2)+(2*A3)-(2*A*B2)-(12*A5)
      TILTX=(TX1+(TF1*TF2))*TXC
      TILTX=TILTX*Q
      TYC=(Y9-Y5)/(U**2.)
      TY1=(A3*B)+(A2*B2)
      TILTY=(TY1+(TF1*TF2))*TYC
      TILTY=TILTY*Q
      TILTXT=TILTXT+TILTX
      TILTYT=TILTYT+TILTY
100      CONTINUE
200      CONTINUE
      XT(I,J)=TILTXT*X
      YT(I,J)=TILTYT*X
C      WRITE(4,999)X9,Y9,XT(I,J),YT(I,J)
C 999  FORMAT(4G)
300      CONTINUE
400      CONTINUE
101  FORMAT(2I20)
      CALL TLTPLT(XT,YT,NPTSX,NPTSY)
      STOP
      END

```

```

SUBROUTINE TLTPLT(XT,YT,NFTSX,NFTSY)
DIMENSION XT(30,30),YT(30,30)
DIMENSION XFLT(4),YFLT(4)
IF(NFTSX.LT.NFTSY)GOTO 20
NFTSM=NFTSX
GOTO 30
20 NFTSM=NFTSY
30 PINC=9.5/(NFTSM-1)
K=IFLOT(1)
C CALL SETWIN(14.,11.)
FACT=0.7
CALL FACTOR(FACT)
IF(K.NE.0.)STOP
CALL PLOT(1.5,1.5,-3)
X=0.
ANG=0.
DO 100 I=1,NFTSX
  Y=0.
  DO 90 J=1,NFTSY
    TMAGN=(XT(I,J)**2.+YT(I,J)**2.)**.5
    RATX=XT(I,J)/TMAGN
    RATY=YT(I,J)/TMAGN
    VECL=ALOG10(TMAGN)+4.
    IF(VECL.LE.0) GO TO 90
    VECL=VECL/4.00
    XT(I,J)=RATX*VECL
    YT(I,J)=RATY*VECL
    XFLT(1)=X
    XFLT(2)=X+XT(I,J)
    XFLT(3)=0.
    XFLT(4)=1.0
    YFLT(1)=Y
    YFLT(2)=Y+YT(I,J)
    YFLT(3)=0.
    YFLT(4)=1.0
    CALL LINE(XFLT,YFLT,2,0,0,0)
    IP=NEWPEN(3)
    IF(YT(I,J).LT.0.)GOTO 70
    YP=Y-.20
    GOTO 80
70 YP=Y+.1
80 XP=X-.22
    FNUM=TMAGN*1.0E2
    CALL NUMBER(XP,YP,.17,FNUM,0,1)
    ANG=ATAN(YT(I,J)/XT(I,J))
    ANG=ANG*57.29578
    IF(XT(I,J).LT.0.)ANG=ANG+180
    ANG=ANG-90
    IP=NEWPEN(1)
    CALL SYMBOL(XFLT(2),YFLT(2),.10,6,ANG,-1)
    Y=Y+PINC

```

*PROGRAM
TLTPLT*

```
90      CONTINUE
      X=X+FINC
100     CONTINUE
      RETURN
      END
```

APPENDIX 3

The following seven pages are copies of the fracturing program summary provided by the Amoco Production Company.

Drilling Wire Cumulative Report.

END OF WELL SUMMARY CO- GRL-DEV MONTBELLO PAGE 5

IDENT 974636-03-7. AUTH ID 4600. DRL-DEV.
P8TD 4606. WD FRAC. DAYS: SPUD 148. CPER 148

*** 08-29-78***

EDWARD HEMPLE UNIT NO.2, HAMBERT.
IDENT 974636-03-7. AUTH ID 4600. DRL-DEV.
RMKS: PREP TO FRAC

*** 08-30-78***

EDWARD HEMPLE UNIT NO.2, HAMBERT,
IDENT 974636-03-7. AUTH ID 4600. DRL-DEV.
RMKS: EMULSIFRAC 5094 BC X 237A BM 81900 LB 100 MESH - 537600#
20/40 - 115600# 10/20 - PMP 500 GAL 7-1/2X MCA - BRKDN 1400
FLUSH X 107 8W - ATR 22 BPM ATP 2950 PSI ISIP 1600 -
30 MIN SIP 1250 - FLM 14 HRS ICP 1250 - FCP 50 - REC
1086 BLC X 1019 BLW

Initial casing pressure
final casing pressure

*** 08-31-78***

EDWARD HEMPLE UNIT NO.2, HAMBERT,
IDENT 974636-03-7. AUTH ID 4600. DRL-DEV.
RMKS: FLW 24 HRS 48/64 CH 0 FCP - REC 631 BLC X 259 BLW

*** 09-01-78*** (Choke in "A" Flowing Casing Press)

EDWARD HEMPLE UNIT NO.2, HAMBERT,
IDENT 974636-03-7. AUTH ID 4600. DRL-DEV.
RMKS: FLW 24 HRS 48/64 CH 100 FCP - REC 172 BLC X 131 BLW

*** 09-05-78***

EDWARD HEMPLE UNIT NO.2, HAMBERT,
IDENT 974636-03-7. AUTH ID 4600. DRL-DEV.
RMKS: FLW 24 HRS. CP 200. 42/64 CH. REC 274 BLC X 223 BLW

*** 09-06-78***

EDWARD HEMPLE UNIT NO.2, HAMBERT,
IDENT 974636-03-7. AUTH ID 4600. DRL-DEV.
RMKS: 090278 - FLW 24 HRS 48/64 CH 200 FCP. REC 185 BLO X 92 BLW
X 0 MCFD 1000
090378 - FLW 24 HRS 48/64 CH 300 FCP. REC 92 BLO X 63 BLW
X 1275 MCFD
090478 - FLW 24 HRS 48/64 CH. 200 FCP. REC 103 BLO X 51 BLW
X 1275 MCFD
090578 - FLW 24 HRS 1/4 CH 275 FCP. REC 83 BLO X 42 BLW X
1200 MCFD

Oil

Oil

PSI at which
flow starts

Pressure
Choke pressure reset

SUMMARY

DATE: 8-28-78

198ac

PRESSURES IN PSI

CIRCULATING: 1400 DISPLACEMENT: 3000

HEAVE DOWN: 2950 MAXIMUM: 3000

AVL: 1600 FRACTURE GRADIENT: 10

SHUT IN INSTANT: 1591 HYDRAULIC HORSEPOWER: 4000 USED: 1591

ORDERED: 22 AVAILABLE: 24 OVERALL: 22

TREATING: 22 CEMENT LEFT IN PIPE

VOLUMES

PREFLUSH: 500 GAL. TYPE: MCA Acid

LOAD & BKDN: 285600 GAL. PAD: 29400 GAL.

TREATMENT: 4500 GAL. DISPL: 4500 GAL.

CEMENT SLURRY: 320000 GAL.

TOTAL VOLUME: 320000

REMARKS: APPROX. 5094 Bbls Oil used

2374 Bbls Water used

107 Bbls Water for flush

ALLIBURTON SERVICES

JOB LOG

WELL NO. 2 LEASE Edward Hemple TICKET NO. 441959

CUSTOMER Amoco Production Co PAGE NO. 1

JOB TYPE Super Emulsifrac DATE 8-28-78

CHART NO.	TIME	RATE (RPM)	VOLUME (GAL)	PUMPS		PRESSURE (PSI)		DESCRIPTION OF OPERATION AND MATERIALS
				T	C	TUBING	CASING	
	0430							Called out
	0630							On Location
	0745							Requested ready
	0745							Ready to pump
	0720							Safety Meeting
1	0744	2	500	1				Pump Acid
	0745	15		8				Start Pad
	0749			1				Test Lines
	0800	4		1		1400		Breakdown

2	0831	23	6300	6	2930	Start 100 mesh @ 2# (2 lbs/gal/m)
3	0838	22½	4200	6	2910	Spacer (Pumped 4200 gal emulsio, 405000)
4	0842	22½	6300	6	2970	Start 100 mesh @ 3#
5	0849	22	4200	6	2910	Spacer
6	0853	20½	6300	6	2970	Start 100 mesh @ 4#
	0901	21	4200	6	2960	Spacer
8	0905	20	6300	6	2910	Start 100 mesh @ 4#
9	0912	21½	4200	6	2960	Spacer
10	0916	23	6300	6	2970	Start 20/40 @ 4#
11	0923	20	4200	6	2970	Spacer
12	0928	19½	6300	6	2920	Start 20/40 @ 4#
13	0935	20	4200	6	2950	Spacer
14	0939	21	6300	6	2950	Start 20/40 @ 4#
15	0947	21½	4200	6	2920	Spacer
16	0951	22½	6300	6	2920	Start 20/40 @ 4#
17	0958	22	4200	6	2910	Spacer
18	1002	23	6300	6	2910	Start 20/40 @ 4#
19	1009	22	4200	6	2910	Spacer
20	1013	23	6300	6	2920	Start 20/40 @ 4#
21	1020	22	4200	6	2930	Spacer
22	1024	22½	6300	6	2920	Start 20/40 @ 4#
23	1031	22½	4200	6	2950	Spacer
24	1035	22½	6300	6	2950	Start 20/40 @ 4#
25	1042	22½	4200	6	2950	Spacer
26	1046	23	8400	6	2920	Start 20/40 @ 4#

HALLIBURTON SERVICES

JOB LOG

WELL NO. 2 LEASE Edward Hemple TICKET NO. 41122
 CUSTOMER Amoco Production Co PAGE NO. 2
 JOB TYPE Super Emulsifrac DATE 8-28-78

FORM 3013 R-2

CHART NO.	TIME	RATE (BPM)	VOLUME (BBL) (GAL)	PUMPS		PRESSURE (PSI)		DESCRIPTION OF OPERATION AND MATERIALS
				T	C	TUBING	CASING	
	1056	22½	4200		6		2930	Spacer
28	1100	23	8400		6		2920	Start 20/40 @ 4#
29	1110	18½	4200		6		2970	Spacer
30	1115	18½	8400		6		2920	Start 20/40 @ 4#
31	1126	19	4200		6		2960	Spacer
32	1130	19	8400		6		2970	Start 20/40 @ 4#
33	1142	19	4200		6		2930	Spacer
34	1147	20	8400		6		2980	Start 20/40 @ 4#
35	1158	20	4200		6		2950	Spacer
36	1202	23	8400		6		2530	Start 20/40 @ 4#
37	1213	19	4200		6		2950	Spacer
38	1218	18	8400		6		2930	Start 20/40 @ 4#
39	1229	19½	4200		6		2960	Spacer
40	1234	20	8400		6		2950	Start 20/40 @ 4#
41	1245	19	4200		6		2920	Spacer
42	1250	20	8400		6		2920	Start 20/40 @ 4#
43	1300	20	4200		6		2950	Spacer
44	1305	20½	8400		6		2920	Start 20/40 @ 4#
45	1316	19	4200		6		2960	Spacer

46	1321	19½	8400	6	2940	Start 10/20 @ 4#
47	1332	19	4200	6	2930	Spacer
48	1337	17½	8400	6	2870	Start 10/20 @ 4#
49	1348	20	4200	6	2990	Spacer
50	1353	19½	2016	6	2950	Start 10/20 @ 5#
51	1356	18	6384	6	2930	Start 10/20 @ 6#
						Finish Mix
52	1404	18	4500	6	2910	Start Flush (4500 gals ≈ 107 bbl/s)
	1410	24		6	2300	Finish
					1600	ISIP Instantaneous shut in pressure
					1450	5 Min (Press. for 5 min. shut in)
					1420	10 Min (" " 10 " " ")

FIELD OFFICE

REFERENCES

- Glover, R.E., 1974, Transient Ground Water Hydraulics: Dept. of Civil Engineering, Colo. St. Univ., Ft. Collins, Colo.
- Hubbert, M. King, 1957, Mechanics of Hydraulic Fracturing: Petroleum Transactions, Vol. 210, p. 153-166.
- Jones, A.H., Abou-Sayed, A.S., and Rodgers, L.A., Rock Mechanics Aspects of MHF Design in Eastern Devonian Shale Gas Reservoirs: Prepared for ERDA under Contract No. E(46-1)-8014.
- Komar, C.A., and Frohne, K-H., 1973, Factors Controlling Fracture Orientation in Sandstone: Soc. Pet. Eng. AIME, Paper No. SPE 4567.
- Komar, C.A., and Shuck, L.Z., 1974, Pressure Responses from Induced Hydraulic Fractures in Adjacent Wells Within a Petroleum Reservoir: An Experiment: Soc. Pet. Eng. AIME Paper No. 5006.
- Love, A.E.H., A Treatise on the Mathematical Theory of Elasticity: 4th edition, Dover Publications, N.Y.
- Major, M.W., 1976, Specialized Instrumentation and Analysis Support in the Vicinity of North Las Vegas, Nevada: Final Report on U.S.G.S. Project P.O. 56420.
- Maruyama, T., 1964, Statical Elastic Dislocations in an Infinite and Semi-Infinite Medium: Bull. Earthquake Res. Inst., Tokyo Univ. Vol. 42, p. 289-368.
- Mindlin, R.D., Cheng, D.H., 1950, Nuclei of Strain in the Semi-Infinite Solid: J. App. Phys., Vol. 21, p. 926-930.
- Power, D.V., Schuster, C.L., Hay, R., and Twombly, J., 1975, Detection of Hydraulic Fracture Orientation and Dimensions in Cased Wells: Soc. Pet. Eng. AIME, Paper No. 5626.
- Shuck, L.Z., 1974, The Determination of Direction and Length of Hydraulically Induced Fractures in Petroleum Reservoirs: A Field Experiment: Soc. Pet. Eng. AIME, Paper No. SPE 5160.

T-2198

- Stekettee, J.A., 1958a, On Volterra's Dislocations in a Semi-Infinite Elastic Medium: Can. J. Phys. Vol. 36, p. 192-205.
- Sokolnikoff, I.S., 1956, Mathematical Theory of Elasticity: McGraw-Hill Book Company, New York.
- Tyler, L.D., and Vollendorf, W.C., 1975, Physical Observations and Mapping of Cracks Resulting From Hydraulic Fracturing in Situ Stress Measurements: Soc. Pet. Eng. AIME, Paper No. SPE 5542.
- Tyler, L.D., Vollendorf, W.C. and Northrop, D.A., In Situ Examination of Hydraulic Fractures: Prepared for ERDA under Contract No. AT(29-1)789.
- White, J.E., 1965, Seismic Waves: Radiation, Transmission, and Attenuation: McGraw-Hill Book Company, New York.
- Wood, M.D., and King, N.E., 1976, Monitoring Massive Hydraulic Fractures with Tiltmeters: Implications for Earthquake Prediction: AGU Fall Annual Meeting Abstract T 99.
- Yeatts, F.R., 1973, A Multipole Representation of Earthquake Source Mechanisms: Bull. Seism. Soc. Am., Vol. 63, No. 1, p. 211-225.
- Yeatts, F.R., 1973, Deformation Near a Dislocation: an Atlas: Colo. School of Mines Publication 73-3-447.